Faculty of Science and Technology
Department of Geosciences

3D-seismic interpretation of the glacial deposits in the outer Ingøydjupet area, SW Barents Sea

Ice sheet dynamics reconstructed from glacial landforms

Kristine Strømme
Master thesis in Geology, GEO-3900
May 2019

UiT

THE ARCTIC
UNIVERSITY
OF NORWAY

In cooperation with Lundin Norway

Kristine Strømme

Abstract

The late Quaternary evolution of the outer Ingøydjupet area (SW Barents Sea) is studied using a merge of conventional 3D-seismic cubes and a new generation of high-resolution 3D-seismic (TopSeis). The glacigenic sequence is subdivided into five main seismic units: unit A_1 (oldest) to A_5. These are separated by six glacially eroded boundaries: the Upper Regional Unconformity (URU), intra-glacial horizons (Q1-Q4) and the seafloor. A correlation to established seismic stratigraphies suggests that the units A_1-A_3 were deposited during middle Pleistocene and A_4-A_5 during late Pleistocene.

The internal seismic signature of the units is described and the geomorphologies of the main surfaces are mapped. This forms the basis for a reconstruction of the ice-sheet dynamics and depositional environment during the late Quaternary evolution of the outer Ingøydjupet area. Mega-scale glacial lineations and troughs observed on the paleo-surfaces confirm that fast-flowing ice streams have occupied and eroded the outer Ingøydjupet area at least five times since the formation of the URU. The orientation of the lineations suggests that both the Ingøydjupet- and the Bjørnøyrenna Ice Streams have been active in the area during these glaciations. Buried sediment blocks, which are interpreted to have been entrained, transported and re-deposited by the paleo-ice streams indicate that the ice streams underwent phases of basal freezing.

The recessional features on the URU and the seafloor suggest complex and dynamic retreats of the ice sheet following glacial maxima, where repeated halts and re-advances characterized the deglaciation. The intra-glacial horizons on the other hand show evidence of rather rapid ice sheet retreats, where mega-scale glacial lineations are preserved on the paleo-surfaces.

Acknowledgement

Table of contents

1 Introduction

1.1 Objectives

The Barents Sea shelf covers an area of approximately 1.2 million km^2 and is one of the widest continental shelves in the world (Andreassen et al., 2008). During Late Pliocene and Pleistocene, the Barents Sea experienced multiple glaciations where ice sheets covered larger parts of the shelf. Due to this, the depositional environment and the morphology in this area have been strongly influenced by glacial activity (Laberg et al., 2010).

Previous studies of the Plio-Pleistocene evolution of the Barents Sea have been carried out by using sediment cores, multibeam bathymetric data and conventional 2D- and 3D-seismic data (e.g. Vorren et al., 1988, 1990; Sættem et al., 1992; Rafaelsen et al., 2002; Andreassen et al., 2004, 2007, 2008; Winsborrow et al., 2010, 2012; Rydningen et al., 2013). In this study, a merge of conventional 3D-seismic cubes covering approximately 14,000 km^2 in the outer Ingøydjupet and Bjørnøyrenna area will be analyzed on a regional scale. Furthermore, TopSeis-data, which is a new generation of 3D-seismic reflection data with a very high resolution, will be analyzed in detail in the western part of the outer Ingøydjupet. The focus will be on the stratigraphy between the Upper Regional Unconformity (URU) and the seafloor, which corresponds to the GIII unit in the literature (e.g. Laberg et al., 2012).

The overall objectives of this thesis is to:

   i)   Subdivide the glacigenic sediments in the outer Ingøydjupet area
   ii)   Generate volume attribute maps from the glacigenic units
   iii) Map the geomorphology of buried intra-glacial horizons and the seafloor
   iv)   Reconstruct the ice sheet dynamics within the GIII unit

1

1.2 Study area

The study area is situated on the continental shelf in the southwestern part of the Barents Sea, within the Bjørnøyrenna and Ingøydjupet troughs (Figure 1.1). Structurally, it is located at the Loppa High area (Figure 1.2). The study area covers approximately 14,000 km^2 and extends roughly from 71°44'N to 73°00'N and 19°20'E to 23°00'E (Figure 1.1 & 1.2). The water depths in the area are from less than 50 m to more than 300 m on the banks, and from 300 m to more than 500 m in the overdeepened troughs (Laberg et al., 2012).
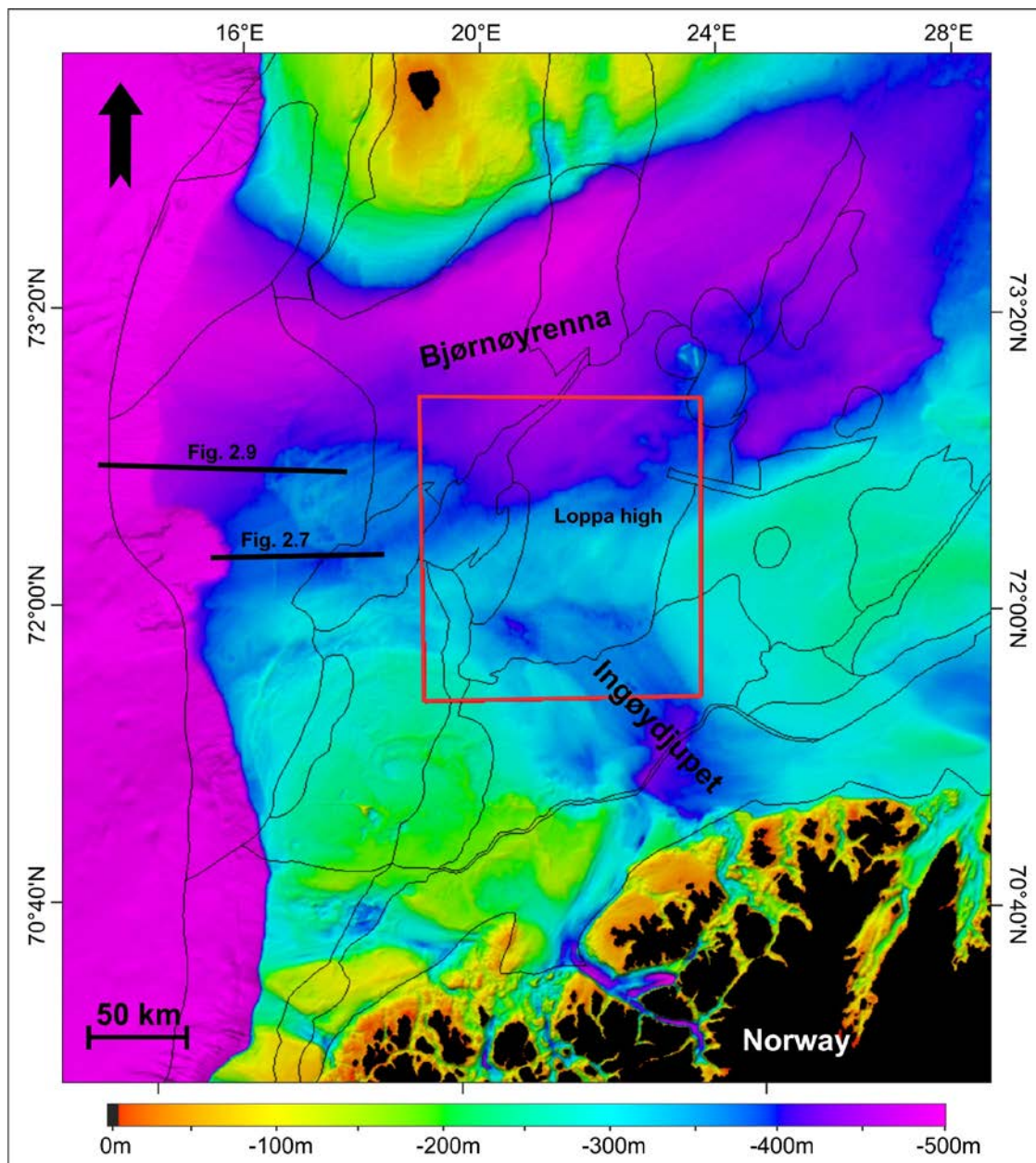
Figure 1.1 – *Bathymetric map of the southwestern part of the Barents Sea shelf, including structural elements from NPD. The study area is within the red box and the black lines indicate the locations of the seismic line in Fig.2.7 & 2.9. Bathymetric map from IBCAO version 3.0 (Jakobsson et al., 2012).*

The structural geology of the southwestern Barents Sea includes platform areas, structural highs and basins (Figure 1.2). The structural elements are the result of post-Caledonian extension as well as later rifting episodes, which ultimately led to continental breakup in early Cenozoic time. The 3D-seismic data applied for this study covers a large part of the Loppa High structure, as well as Polhem Sub-Platform, and parts of Bjørnøyrenna Fault Complex, Rigvassøy-Loppa Fault Complex and the Hammerfest Basin (Figure 1.2). The stratigraphic interval of interest have a varying thickness throughout the dataset, at some parts the thickness reach up to 200 ms (TWT) whilst it can nearly be absent other places. Generally, it has an interval of 100 ms (TWT) in the study area (Figure 1.3).
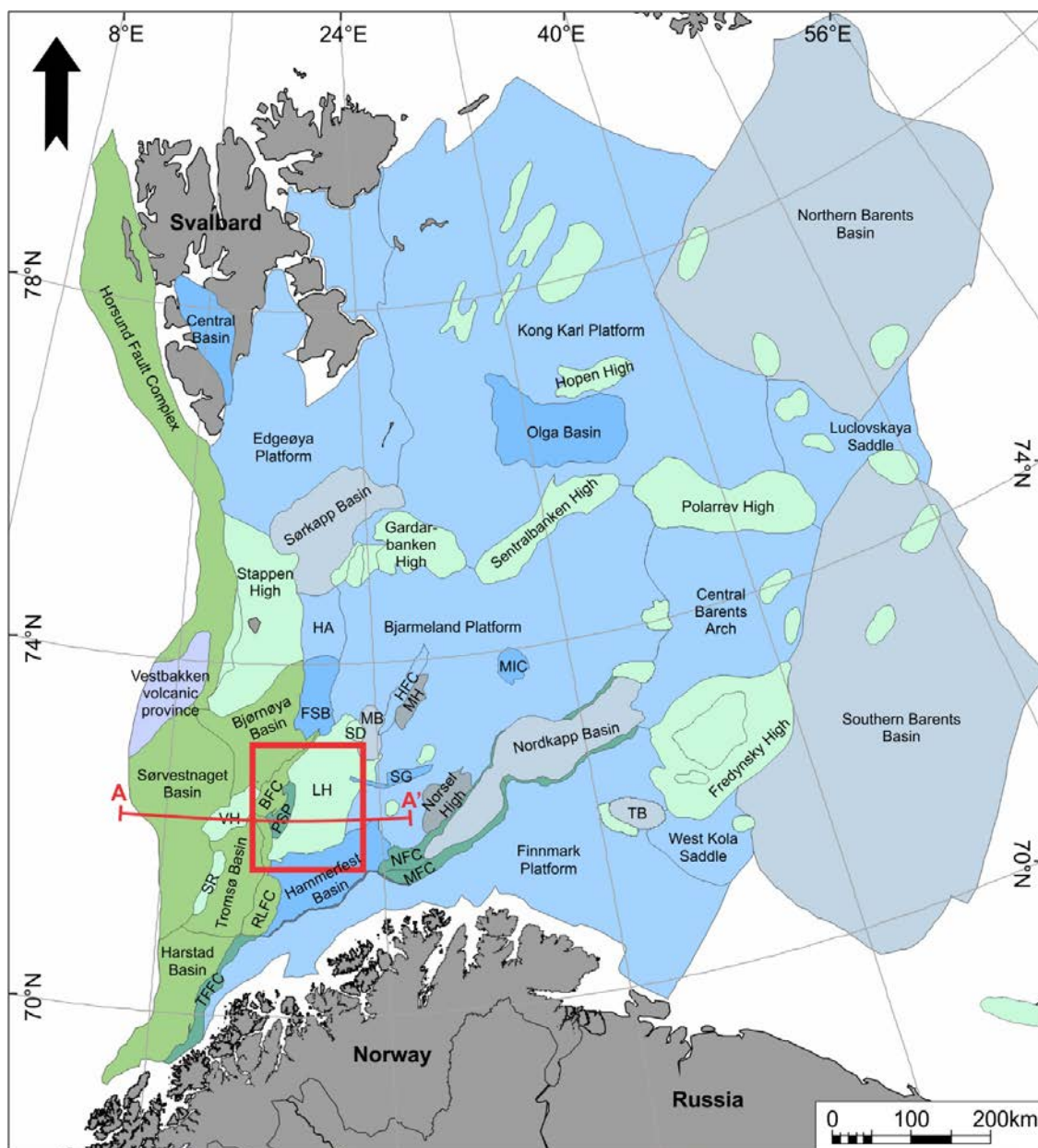
Figure 1.2 – *Structural elements of the Barents Sea. Study area is illustrated with a red box, and the red line (A-A')
indicates the position of the geoseismic profile (Figure 1.3). LH: Loppa High, PSP: Polhem Sub-platform, BFC:
Bjørnøyrenna Fault Complex, RLFC: Ringvassøy-Loppa Fault Complex. Modified from NPD-FactMaps (2019a).*

3
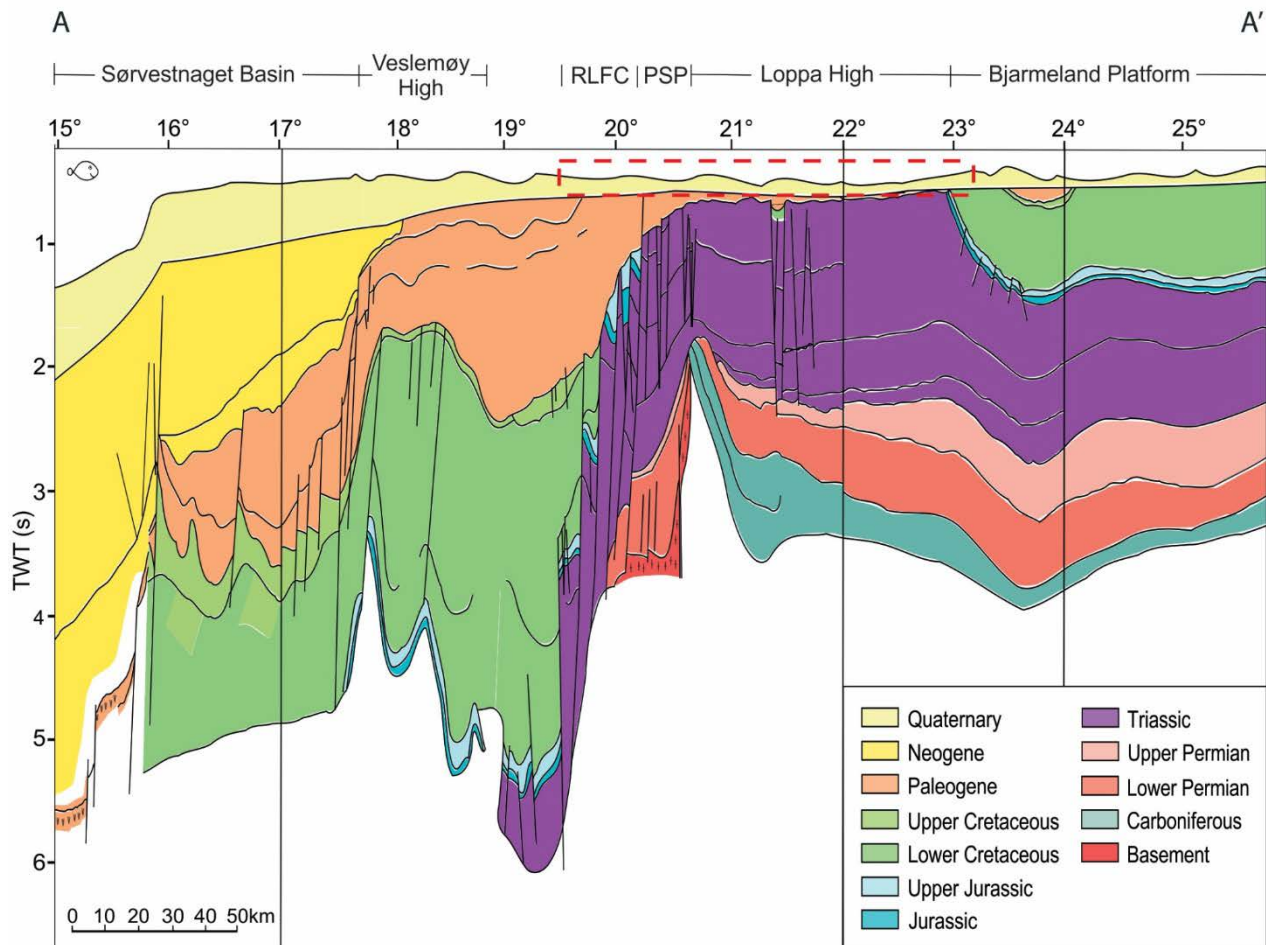
Figure 1.3 *– Geoseismic profile showing some of the structural elements in the SW Barents Sea. The location of the profile is shown in figure 1.2. The red box marks the study area and the sedimentary package of interest in this study. RLFC: Ringvassøy-Loppa Fault Complex, PSP: Polhem Sub-platform. Modified from Halland et al. (2014).*

2 Geological background

2.1 Tectonic development in the SW Barents Sea

2.1.1 Paleozoic

The basement history of the western Barents Sea mainly corresponds to the Scandinavian Caledonides. In the beginning of Devonian, the development of the Caledonian Orogeny culminated. At this time the Laurentian and Baltican plates consolidated into one continent called Laurussia (Smelror et al., 2009). Later, during Devonian and Carboniferous, most of the Barents Sea was affected by crustal extension, which led to reactivating of faults and evolution of rift basins along weakness zones in the Caledonian thrust sheet (Faleide et al., 1993). The most pronounced event is represented during mid-Carboniferous times, when a 300 km wide and 600 km long rift zone was formed. This was a direct continuation of the northeast Atlantic rift between Greenland and Norway, resulting in a fan-shaped array of northeast-southeast-trending rift basins and intrabasinal highs along the Caledonian basement (Faleide et al., 2015).

2.1.2 Mesozoic

The tectonic activity was relatively stable in the beginning of Mesozoic, but at the start of Middle Jurassic, the tectonic activity increased. The structural development in the southwestern parts of the Barents Sea during this period can be divided into two main tectonic regimes; (i) the Mid-Kimmerian tectonic phase, and (ii) the Late-Kimmerian tectonic phase (Faleide et al., 1993). The Mid-Kimmerian tectonic phase in Middle-Late Jurassic was dominated by rifting and opening in the central parts of the Atlantic Ocean. The regional extension accompanied by minor strike-slip adjustments along old structural lineaments resulted in formation of normal faults and development of deep rift basins such as the Harstad-, Bjørnøya- and Tromsø basins (Faleide et al., 1993). In the Late-Kimmerian tectonic regime (Late Jurassic to Early Cretaceous), a series of deep-seated normal faults were formed along the zones of weakness in the Caledonian basement. These movements resulted in development of the Ringvassøy-Loppa Fault Complex (Faleide et al., 1984). In addition to the Late Kimmerian rifting, subsidence increased. The main phase of subsidence occurred when the main phases of tectonic activity had ceased and continued in the Late Cretaceous–Early Paleogene, but at a slower rate (Faleide et al., 1984; Faleide et al., 1993).

2.1.3 Cenozoic

Late Cretaceous and Early Cenozoic rifting in the North Atlantic lead to breakup of the margins and opening of the Norwegian-Greenland Sea in the Paleocene-Eocene transition (Faleide et al., 2008; Smelror et al., 2009). These tectonic events led to reactivation of regional faults in the western parts of the Barents Sea, which resulted in subsidence and westward tilting of the Barents Sea shelf. This led again to the development of several basins and platforms in the area (Faleide et al., 1984). The tectonic trend during Cenozoic was interrupted by periods of uplift and subsequent erosion. Volumetric calculations show that the overall Cenozoic erosion varies both spatially and temporally, from approximately 3 km in the Svalbard area to 1.2 km in the southwestern Barents Sea (Vorren et al., 1991; Nyland et al., 1992). During Late Cenozoic (Late Pliocene and Pleistocene), the geological development of the Barents Sea was largely controlled by large glaciations (Smelror et al., 2009). The pre-glacial development of the margin and the onset of glaciations are summarized in Figure 2.1.
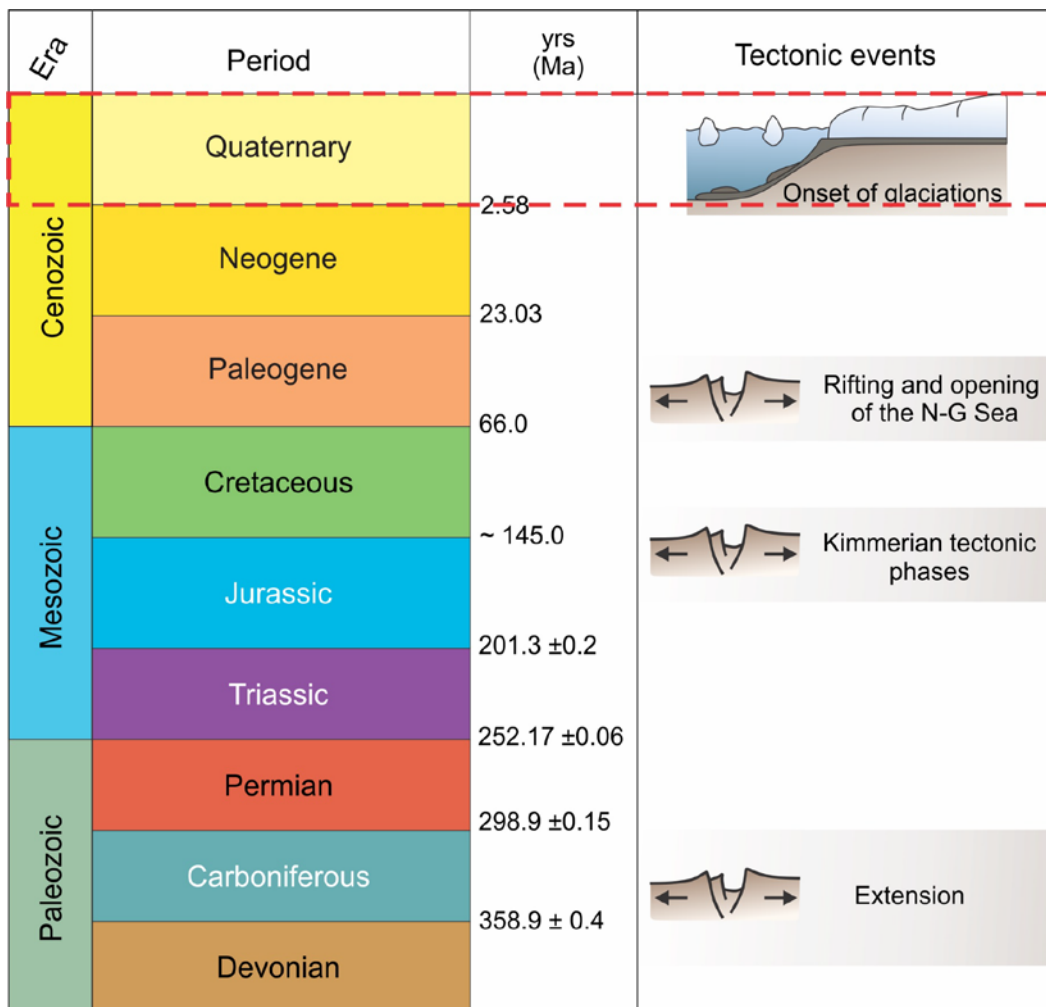
Figure 2.1 – Schematic overview of the main tectonic events from Paleozoic to Cenozoic in the Barents Sea. The period highlighted in red is the focus for this study.

2.2 Depositional environments in the SW Barents Sea

2.2.1 Paleozoic

In Devonian to Early Carboniferous times, the depositional environment in the western Barents Sea region was controlled by the formation and subsequent denudation of the Caledonian mountains (Smelror et al., 2009). Additionally, most of the Barents Sea was affected by crustal extension during Devonian and Carboniferous, resulting in several extensional basins that were filled with syn- and post-rift sediments (Worsley, 2008; Faleide et al., 2015). The rifting ceased in the Late Carboniferous and Early Permian times, and the environment changed, in combination with a transgression, to the formation of large areas of shallow marine settings with carbonate and evaporate depositions (Worsley, 2008). The climate during this period resulted in a warm water carbonate platform, but this changed to a cool water carbonate platform during the Middle to Late Permian due to the northward drift of the continent (Ahlborn & Stemmerik, 2015).

2.2.2 Mesozoic

During Early Mesozoic, large parts of the Barents Sea were covered by a regional deepwater basin, and the region received sediments from the Ural Mountains in the east, from the Fennoscandian Shield in the south, and from local exposed areas (Smelror et al., 2009; Faleide et al., 2015). This strata is thus dominated by coarser shallow marine and coastal-deposited sandstones, but the trend shifted to finer clastic sediment deposits due to a regional transgression that occurred during the Middle Jurassic (Smelror et al., 2009; Worsley, 2008). In the Later Jurassic times, there were fluctuations in the depositional environment, due to several periods of regression and transgression.

In the transition from Jurassic to Cretaceous, there was an overall regression, causing a change in the depositional environment on the Barents Shelf. Additionally, the northeastern part of the Barents Sea region was uplifted, causing sediments to prograde into the subsiding basins along the western margin, whereas the structural highs and platforms between the basins were dominated by thinner successions, with carbonates being the most prominent (Worsley, 2008; Smelror et al., 2009). This environment continued in the western Barents Shelf during the middle Lower Cretaceous. When it comes to the Upper Creataceous successions, they are more or less absent in the Barents Sea due to erosion (Faleide et al., 2015).

2.2.3 Cenozoic

During Cenozoic, the eastern and northern parts of the Barents Sea shelf were uplifted, due to the tectonic activity linked to the opening of the Norwegian-Greenland Sea. Consequently, the sediment deposition in the Barents Sea was restricted to the westernmost basins, as eroded material from the newly uplifted areas was transported towards the shelf edge in western parts (Smelror et al., 2009). During late Cenozoic, the depositional environment was generally controlled by the repeated glaciations. The glaciations led to removal of large amounts of sediments from the shelf, which was re-deposited as clastic wedges at the continental slope (Worsley, 2008; Smelror et al., 2009). Due to the sufficient glacial erosion during the latest Cenozoic, the base of the Quaternary deposits are recognized as an erosional boundary, i.e. Upper Regional Unconformity (URU), marking the transition to glacial sediment deposition (Vorren et al., 1988; Faleide et al., 2008).

2.3 Glacial history of the Barents Sea

During the Neogene, the climate changed dramatically and there were a significantly cooling at high latitudes, which led to extensive glaciations in both hemispheres. The cooling was associated with the northward continental drift as well as the tectonics affecting the ocean circulation pattern and exchange of air masses. The opening of the Norwegian Sea led to exchange of warm- and cold-water masses between the southern Atlantic Ocean and northern oceans. Additionally, the formation of large mountain ranges from Pyrenean and the Alps to Himalaya, prevented exchange of tropical and cold polar air masses. These factors affected the climate to change from warm and humid, to a cooling period (Martinsen & Nøttvedt, 2013).

2.3.1 Early glaciations

Due to glacial erosion, pre-Weichselian deposits are only found in a few sites, and the older glacial history has to be reviled from deposits of ice-rafted debris (IRD) along the continental margin and in the deep sea (Mangerud et al., 2011). The oldest IRD pulses indicates that the initial glaciations on the northern hemisphere occurred in Middle Miocene, approximately 12-14 Ma years ago (Thiede et al., 1998). However, the IRD pulses may have originated from the Greenland Ice Sheet, as it is suggested that the ice sheet extended beyond the coast of Greenland during this time (Helmke et al., 2003). Studies done by Knies et al. (2009) suggest that the onset of the glaciations in the Northern hemisphere occurred in Late Pliocene-Early Pleistocene, about ~3.6-2.4 Ma. This phase is implied to be the inception of the build-up phase of the Barents Sea ice sheet, where the ice covered the mountainous regions and reached the coastline/shelf edge in the northern Barents Sea (Figure 2.2a) (Knies et al., 2009).

2.3.2 Early- and mid-Quaternary glaciations

A coherent glaciation model for the Barents Sea ice sheet proposed from Knies et al. (2009) suggests that there was a more extensive growth phase during early- and mid-Quaternary (2.4-1.0 Ma) where the ice sheet expanded towards the southern Barents Sea and reached the northwestern Kara Sea (Figure 2.2b). This is based on a decrease in the sediment supply from the Siberian rivers into the Barents Sea, presumably caused by ice sheet blockade and glacigenic wedge growth. In addition, the sediment transport changed and led to an increased growth rate of the sedimentary wedge along the western shelf margin (Knies et al., 2009; Smelror et al., 2009).

The first glacial advance to the paleo-shelf break are likely to have occurred around 1.5 to 1.3 Ma (Butt et al., 2000; Andreassen et al., 2007). This is indicated by acoustic and sedimentological data, in addition to an increase of IRD along the western Barents Sea margin (Knies et al., 2009). After the first big glacial advance in the southwestern Barents Sea, there is suggested that the ice sheets have advanced to the shelf break at least eight times during Middle-Late Pleistocene (Andreassen et al., 2004; Laberg et al., 2010). This is, according to the studies of Knies et al. (2009), the third phase of ice growth in the Barents Sea region. This phase began at approximately 1 Ma, and is characterized by a dominant 100 000 year cyclicity in ice-volume fluctuations and more extensive glaciations in the Barents Sea and circum-Artic region (Figure 2.2c) (Smelror et al., 2009).
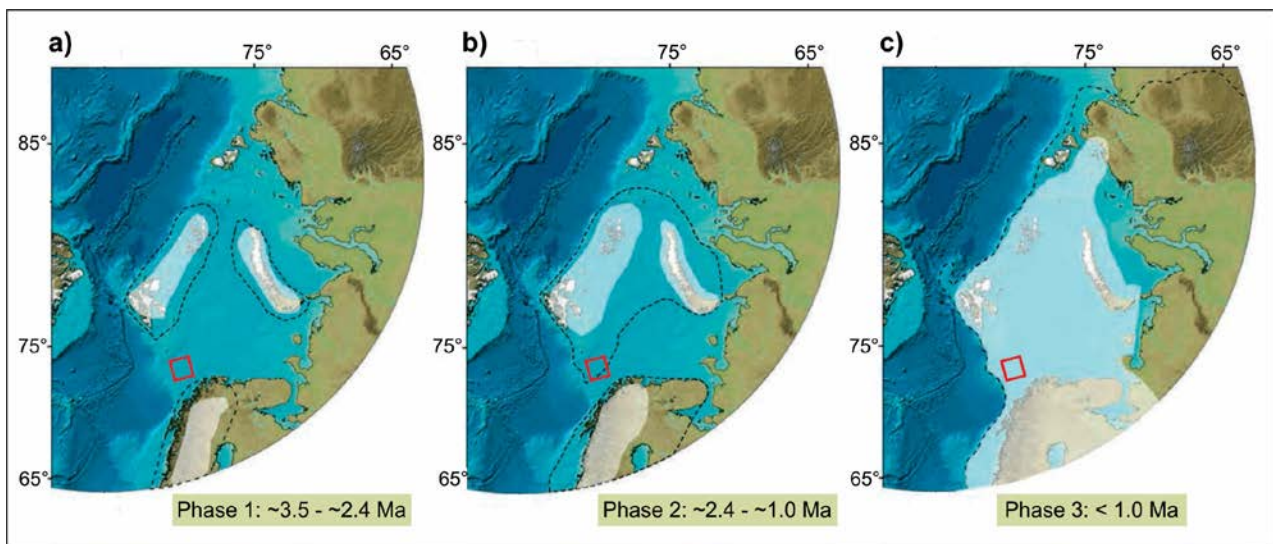
*Figure 2.2 – Coherent glaciation model for the Barents Sea ice sheet during the Late Plio-Pleistocene (black dotted lines = maximum; white transparent polygons = minimum). **a)** Phase 1: Late Pliocene (~3.6 - ~2.4 Ma), **b)** Phase 2: Early Pleistocene (~2.4 - ~1.0 Ma), **c)** Phase 3: Late Pleistocene (<1.0 Ma). The red boxes indicates the location of the study area. Modified from Smelror et al. (2009).*

2.3.3   The last ice age (Weichselian)

The last ice age, Weichselian, occurred in the period 100-15 ka (Svendsen et al., 2004). During this glaciation, Svendsen et al. (2004) have suggested three periods for the maximum limits of the Eurasian ice sheets: the Early Weichselian, the Middle Weichselian and the Late Weichselian. However, studies done by Larsen et al. (2006) indicate that there have been four glacial periods where the Middle Weichselian had two periods of larger glaciations. During the Early Weichselian (~100-90 ka), the glaciation was restricted to the eastern Kara Sea and parts of Scandinavia and the Barents Sea remained ice-free during this period (Figure 2.3a). During the first glaciation in Middle Weichselian (~70-65 ka), the Scandinavian-, Barents Sea- and

Kara Sea Ice Sheets was confluent (Figure 2.3b), while during the second glaciation in Middle Weichselian (~55-45 ka) the Barents Sea was again ice-free and the ice cover was restricted around the Kara Sea, Svalbard archipelago and Scandinavia (Figure 2.3c). Previous models suggest only one glaciation during the Middle Weichsel where the ice sheets extended across Scandinavia, the Barents- and Kara Sea (Mangerud et al., 1998; Svendsen et al., 2004).
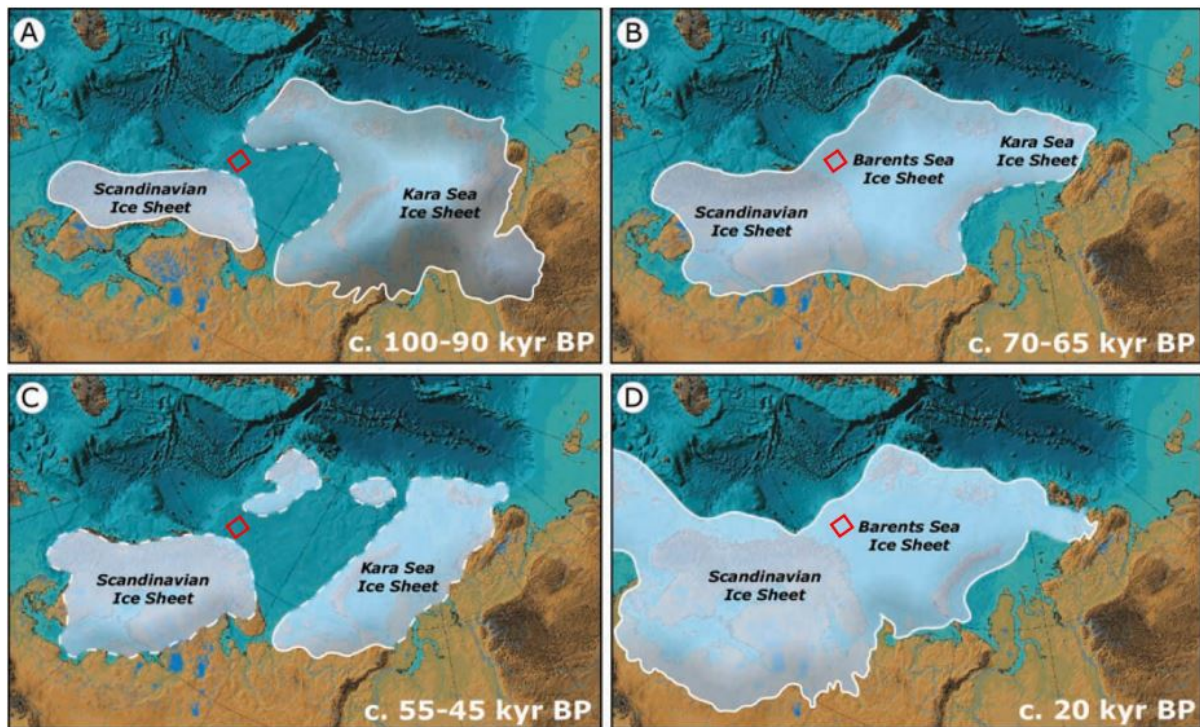
Figure 2.3 – *Reconstruction of the ice sheets extent during the last ice age (Weichselian).* ***a)*** *The Early Weichselian, ~100-90 ka,* ***b)*** *The Middle Weichselian I, ~70-65 ka,* ***c)*** *The Middle Weichselian II, ~44-45 ka, and* ***d)*** *The Late Weichselian ~20 ka. The red boxes indicate the location of the study area. Modified from Larsen et al. (2006).*

The Last Glacial Maximum (LGM) during Late Weichselian was the largest glaciation in the western part of the Barents Sea during the last ice age (Siegert et al., 2001). At this time, the Barents Sea- and Scandinavian- ice sheets were confluent to what is called the Eurasian ice sheets (Figure 2.3d), and the individual ice sheets reached their maximum limits asynchronously (Hughes et al., 2016). Stratigraphic records taken from three locations in the southern Barents Sea indicate two major ice advances to the outer shelf break during this period; one before 22 ka and one after 19 ka (Vorren & Laberg, 1996). During the maximum ice advances, the entire Barents Sea continental shelf was glaciated and large paleo-ice streams were located in the Bjørnøyrenna, Ingøydjupet and along the mainland coast. The Bjørnøyrenna Ice Stream was by far the largest of them, and worked as the main drainage outlet of the ice

sheet (Newton & Huuse, 2017). Beneath the ice-streams, large subglacial erosion took place and the material was transported and deposited in submarine fans on the continental slope (Winsborrow et al., 2010; Laberg et al., 2012).

The retreat after the last glacial maximum went quite rapidly with periods of standstill and re-advances (Winsborrow et al., 2010). The retreat started along the western Atlantic margin after 19 ka, and was probably triggered by rise in the global eustatic sea levels. The increase in sea level caused a major rise of icebergs calving in the deep troughs, especially in Bjørnøyrenna, causing a considerable loss of ice volume (Winsborrow et al., 2010). Reconstructions done by Andreassen et al. (2008) and Winsborrow et al. (2010) indicates that the retreat of the Bjørnøyrenna Ice Stream was characterized by at least four major re-advances when the ice margin was grounded. This is based on a series of grounding zone wedges located in the trough. By 15 ka most of the Barents Sea was ice-free and the ice margin was restricted onshore, causing the retreat to slow significantly since loss of ice volume by calving was no longer possible (Winsborrow et al., 2010).

2.3.4 Oceanic currents during the deglaciation and present-day

Atlantic water has flowed along the shelf break through the entire deglaciation (Figure 2.4). Present, three major ocean currents influence the Barents Sea: the Arctic Current coming from the north-northeast and dominate north of 74ºN as the East Spitsbergen Current (ESC) (Figure 2.4f). The Norwegian Atlantic Current (NwAC), which travels along the continental slope towards the north (Figure 2.4f), and the Norwegian Coastal Current (NCC) that follows the coast from the southwest (Bellec et al., 2008; Ślubowska-Woldengen et al., 2008). The NwAC splits into two branches in the southern Barents Sea (Figure 2.4f). One branch flows along the shelf break towards Svalbard as the West Spitsbergen Current (WSC) and another flows eastwards into the Barents Sea as the North Cape Current (NCaC) (Figure 2.4f), feeding the Barents Sea with relatively warm and saline Atlantic water (Steinsund & Hald, 1994; Ślubowska-Woldengen et al., 2008).
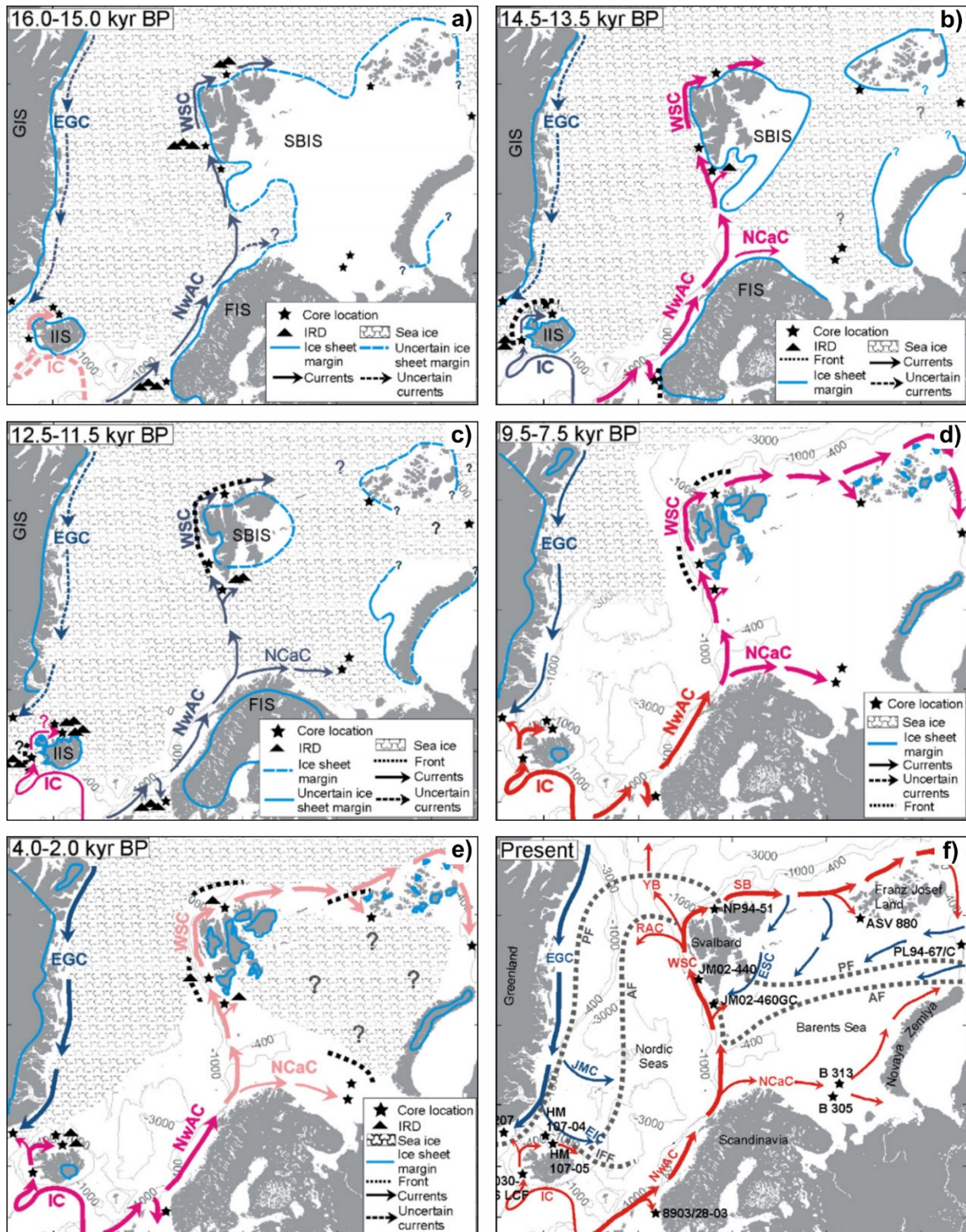
Figure 2.4 *– Reconstruction of coastal currents during the deglaciation and present time. Arrows: red - warm Atlantic Water, dark pink = chilled Atlantic Water, light pink = relatively cold Atlantic Water, dark blue = cold Atlantic Water or Polar Water.* ***a)*** *Late glacial,* ***b)*** *Bølling-Allerød interstadials,* ***c)*** *Younger Dryas,* ***d)*** *Early Holocene,* ***e)*** *Late Holocene,* ***f)*** *Present-day. Abbreviations: FIS, Fennoscandian Ice Sheet; SBIS, Svalbard Barents Ice Sheet; GIS, Greenland Ice Sheet; and IIC, Iceland Ice Sheet. Modified from Slubowska-Woldengen et al. (2008).*

2.4 Paleo-ice streams in the Barents Sea

Ice streams are narrow corridors of fast-flowing areas within an ice sheet, where the majority of ice, meltwater, and sediment is discharged (Bennet, 2003; Winsborrow et al., 2010). Consequently, the large ice flux of ice streams has a profound effect on ice sheet configurations, such as drainage basin and ice divide locations, and local and regional ice sheet topography. Thus, the understanding of their flow-pattern and extent are of importance when reconstructing the ice sheet histories (Stokes & Clark, 2001).

The presence of fast-flowing ice streams during the glaciations has been inferred from observations of large-scale streamlined features, e.g. mega-scale glacial lineations, using satellite imagery of the land surface and marine-geophysical observations on the seafloor (Ottesen et al., 2005). Within the study area of this thesis (red box in figure 2.5), two main ice streams dominated during the glaciations, draining through the Bjørnøyrenna and Ingøydjupet Troughs.
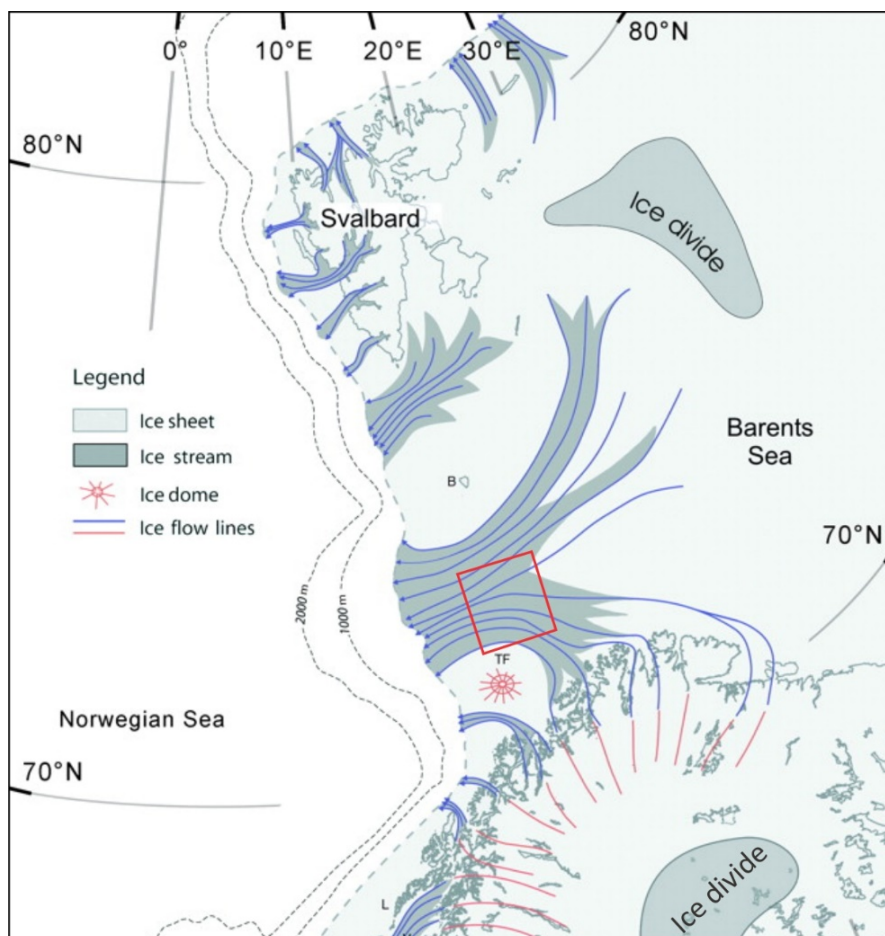
Figure 2.5 – Reconstruction of ice-sheet flow regime on the northwestern margin of the late Weichselian Eurasian and Barents/Svalbard ice sheets. The red box indicates the location of the study area. Modified from Ottesen et al. (2005).

During the glaciations, most of the erosion and sediment transport occurred in the troughs where the fast-flowing ice streams were located. A majority of the eroded material from the shelf was then transported and deposited as major depocenters at the mouth of the troughs (Figure 2.6) (Laberg et al. 2012). A more detailed description of these sediments will be given in the next sub-chapter.
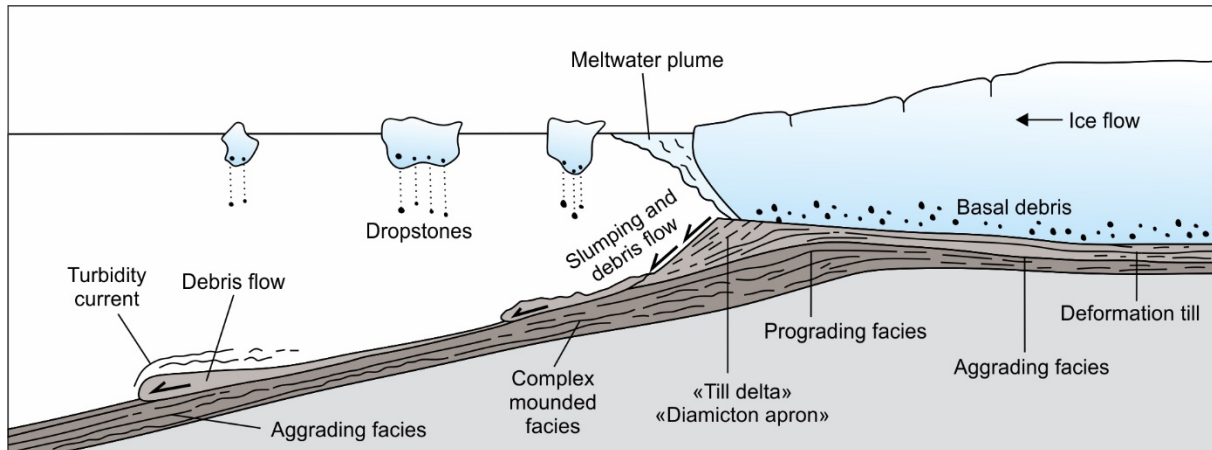
***Figure 2.6*** *– Schematic model showing the main sedimentary processes on the upper slope and shelf break during the presence of the ice sheet at the shelf break. Modified from Henriksen & Vorren (1996).*

2.5 Glacigenic sediments in the Barents Sea

Glacial deposits on the Barents Sea shelf are separated from the underlying bedrocks by the Upper Regional Unconformity (URU) (Vorren et al., 1991; Faleide et al., 1996; Fiedler & Faleide, 1996; Andreassen et al., 2008; Laberg et al., 2012). URU is likely to represent the erosion surface from several glaciations on the shelf, and was originally suggested to have formed in the mid-Oligocene as a fluvial surface before it was modified by glacial erosion during Plio-Pleistocene (Vorren et al., 1988). This unconformity extends over most of the continental shelf, and the glacigenic sequence above it varies in thickness. Generally, the thickness is less in the northern and central parts of the Barents Sea, from 10-15 m (Elverhøi & Solheim, 1983), compared to the southwestern parts where the thickness varies from 0-100 m (Faleide et al., 1996). Towards the shelf break, the URU splits into several unconformities where the glacigenic sequence reaches a thickness up to 3.5-4 km (Figure 2.7) (Laberg et al. 2012).

The Plio-Pleiostocene succession towards the shelf break in the western Barents Sea indicates several phases of erosion on the shelf and deposition on the slope during the last 2.7 million years (Andreassen et al., 2007; Laberg et al., 2012). The sequence has been subdivided into three main sediment packages (GI, GII and GIII) separated by regional unconformities, respectively R7, R5 and R1 (Figure 2.7) (Faleide et al., 1996). Ages of the different unconformities and sediment packages have been suggested from exploration wells and the Ocean Drilling Program (ODP) Site 986 (Andreassen et al., 2007). The age model from Laberg et al. (2012) suggest that GI was deposited in the period from approximately 2.7-1.5 Ma, GII from 1.5-0.7 Ma and GIII from <0.7 Ma.

The GI sediment package is characterized by distal glaciofluvial and fluvial depositions, the GII by a chaotic reflection pattern likely to represent sediments deposited from grounded ice, and the GIII by large debris flows deposited during full glacial conditions (Butt et al., 2000; Andreassen et al., 2007; Laberg et al., 2010; 2012). Whitin the GIII unit, eight subunits can be identified, representing eight periods where the glacier advanced and deposited shelf sediments to the shelf break (Figure 2.7) (Laberg et al., 2010).
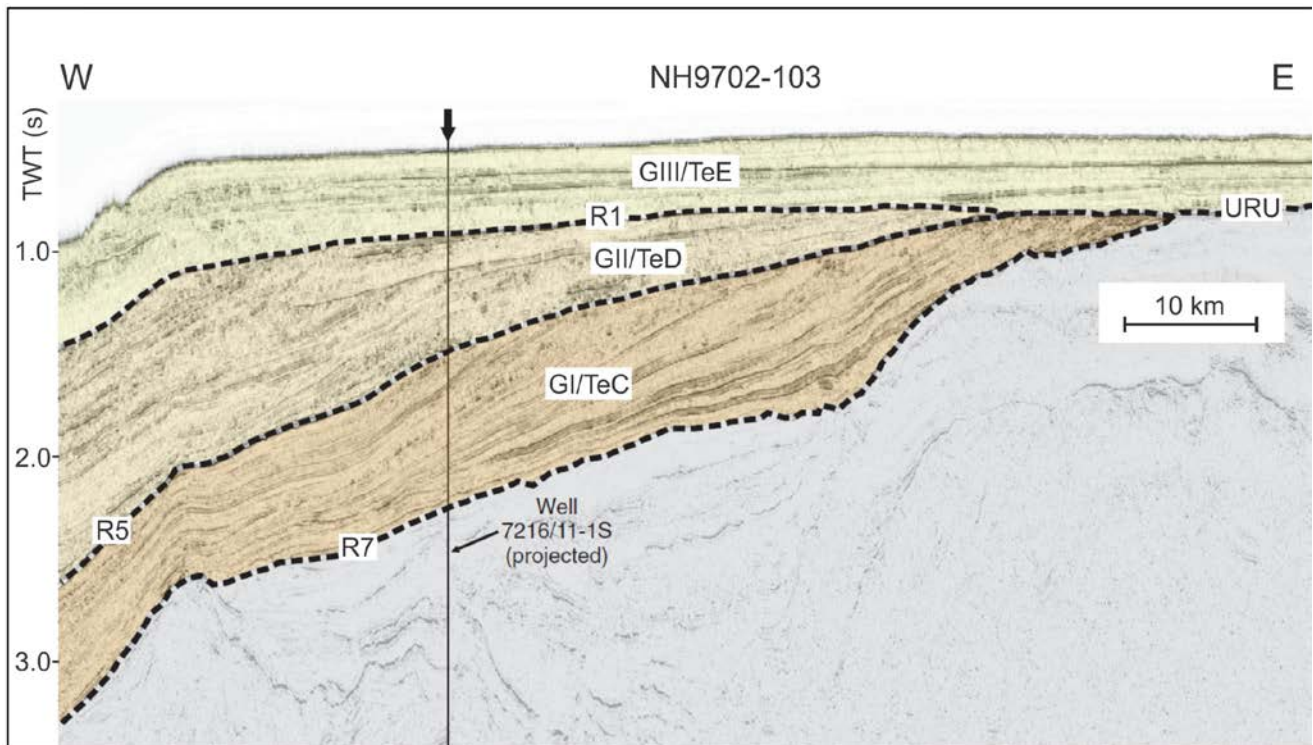
Figure 2.7 *– Interpreted seismic profile across the southwestern Barents Sea continental margin. The profile are interpreted as the Plio-Pleistocene succession with sediment packages GI, GII and GIII separated by the regional unconformities R7, R5 and R1. The location of the profile is indicated with a black line on fig.1.1. Modified from Laberg et al. (2012)*

Several authors have investigated the glacigenic sequence in the western parts of the Barents Sea shelf, which mostly corresponds to the seismic unit GIII, e.g. Vorren et al. (1990), Sættem et al. (1992) and Rafaelsen et al. (2002). The paleo-shelf sediments of GIII, characterized by chaotic seismic-reflection pattern, are inferred to consist mainly of sediments deposited by grounded glaciers (Andreassen et al., 2016). Vorren et al. (1990) subdivided the glacigenic sequence in the southern Barents Sea into four subunits (1W-4W) on the outer shelf and shelf break, and six subunits (1E-6E) on the inner shelf (Figure 2.8). They believe that a substantial part of the sediments were mainly deposited proglacially from turbid meltwater plumes and icebergs, and that syn- and post-depositional glacial erosion and till deposition has occurred both on the inner and outer shelf. The study done by Sættem et al. (1992) divided the succession in the outer Bjørnøyrenna into nine seismic units (A_0-G) (Figure 2.9), whereas units A_0-A was interpreted to consist of Plio-Pleistocene sediments, B-D_2 Middle Pleistocene sediments, and E-F Upper Pleistocene sediments, based on age estimates derived from magneto-, amino-, and bio-stratigraphy of sediments from shallow boreholes. They interpreted that most of the sediments represent glacial till deposited during major glacial advances, with exception of the unit E, which by the acoustically stratified configuration was interpreted to represent

17

glaciomarine sediments. Rafaelsen et al. (2002) were the first to study the glacigenic sequence of the southwestern Barents Sea shelf by using 3D-seismic data. They identified five glacigenic units (A-E) and mapped several generations of subglacial lineations observed on five buried seismic horizons (bA-bE) separating the units (Figure 2.10).
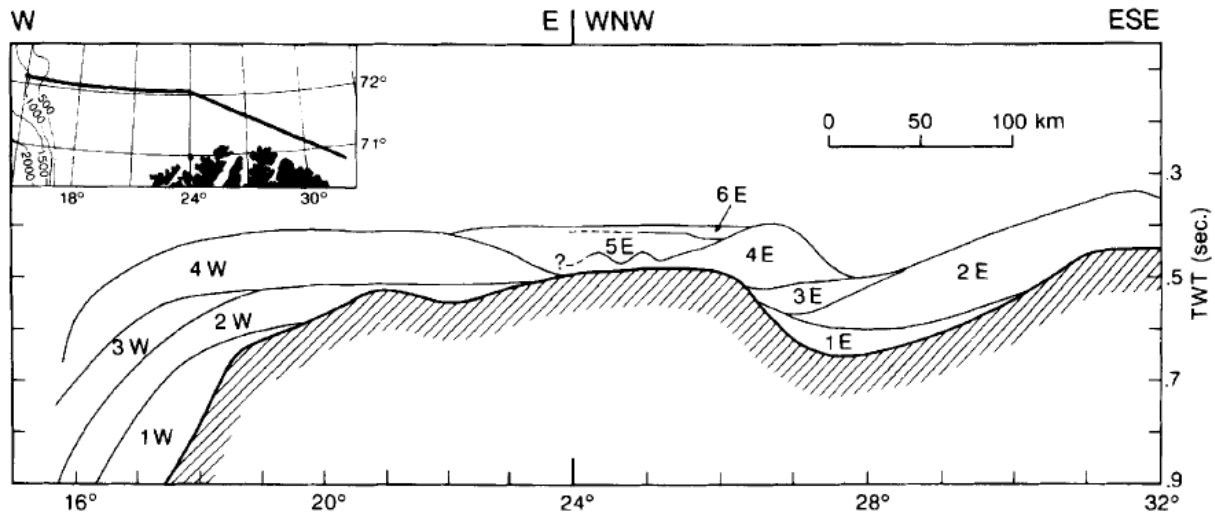
***Figure 2.8** – Geoseismic profile from the upper slope to the inner shelf showing the different seismostratigraphic units in the glacigenic sequence. Retrieved from Vorren et al. (1990).*
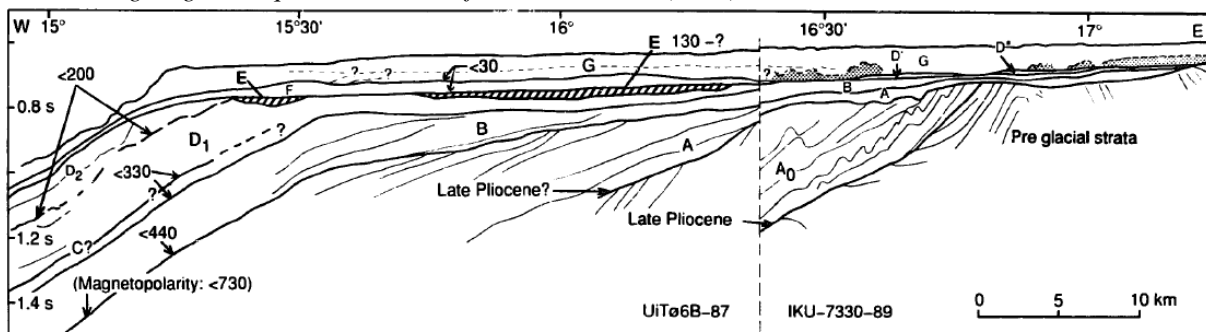
***Figure 2.9** – Geoseismic profile showing the development of the glacigenic sequence in outer Bjørnøyrenna and the top of the prograding clastic wedge deposited at the western Barents Sea shelf margin. The location of the profile is indicated with a black line on fig.1.1. Retrieved from Sættem et al. (1992).*
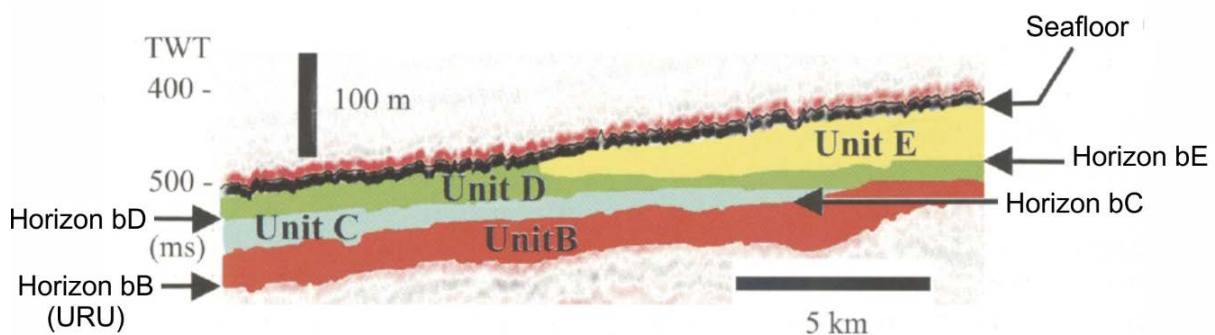
***Figure 2.10** – Geoseismic profile from one of the 3D-surveys (located in Bjørnøyrenna) used in the study by Rafaelsen et al. (2002) showing their interpreted glacigenic units and horizons. Modified from Rafaelsen et al. (2002).*

2.6 Geomorphology of the SW Barents Sea

The present-day morphology of the Barents Sea is a result of several episodes of uplift and erosion in addition to several major glaciations during the Cenozoic (Laberg et al., 2010). These processes have left characteristic imprints on the shelf. The geomorphology of the southwestern Barents Sea is dominated by glacial troughs separated by shallower banks (Figure 2.11).

The most prominent geomorphological feature in the southwestern Barents Sea is the Bjørnøyrenna cross-shelf trough, which extends from Storbanken in the northeast to the shelf break in the southwest (Figure 2.11a). It is 750 km long, 150-200 km wide and 300-500 m deep (Andreassen et al., 2008). Bjørnøyrenna is flanked by shallow bank areas (<300m), Spitsbergenbanken and Sentralbanken to the north and east, as well as Tromsøflaket and Nordkappbanken to the south (Rüther et al., 2011). The latter is separated by a northeast to northwest trending trough, Ingøydjupet, which reach water depths of 450 m (Figure 2.11b).

In the outer Bjørnøyrenna, there is a 280 km wide glacigenic sediment accumulation (Figure 2.11b). It was explored in detail by Rüther et al. (2011) who termed it as the outer Bjørnøyrenna sediment wedge (OBSW). Previous studies done by e.g. Andreassen et al. (2008) and Winsborrow et al. (2010) refer to the sediment system as *Bjørnøyrenna end moraine zone* and *Bjørnøyrenna grounding zone*, respectively. The OBSW is interpreted to be deposited during a rapid re-advance where the ice front pushed and bulldozed predominantly soft, diluted proglacial sediments (Rüther et al., 2011).
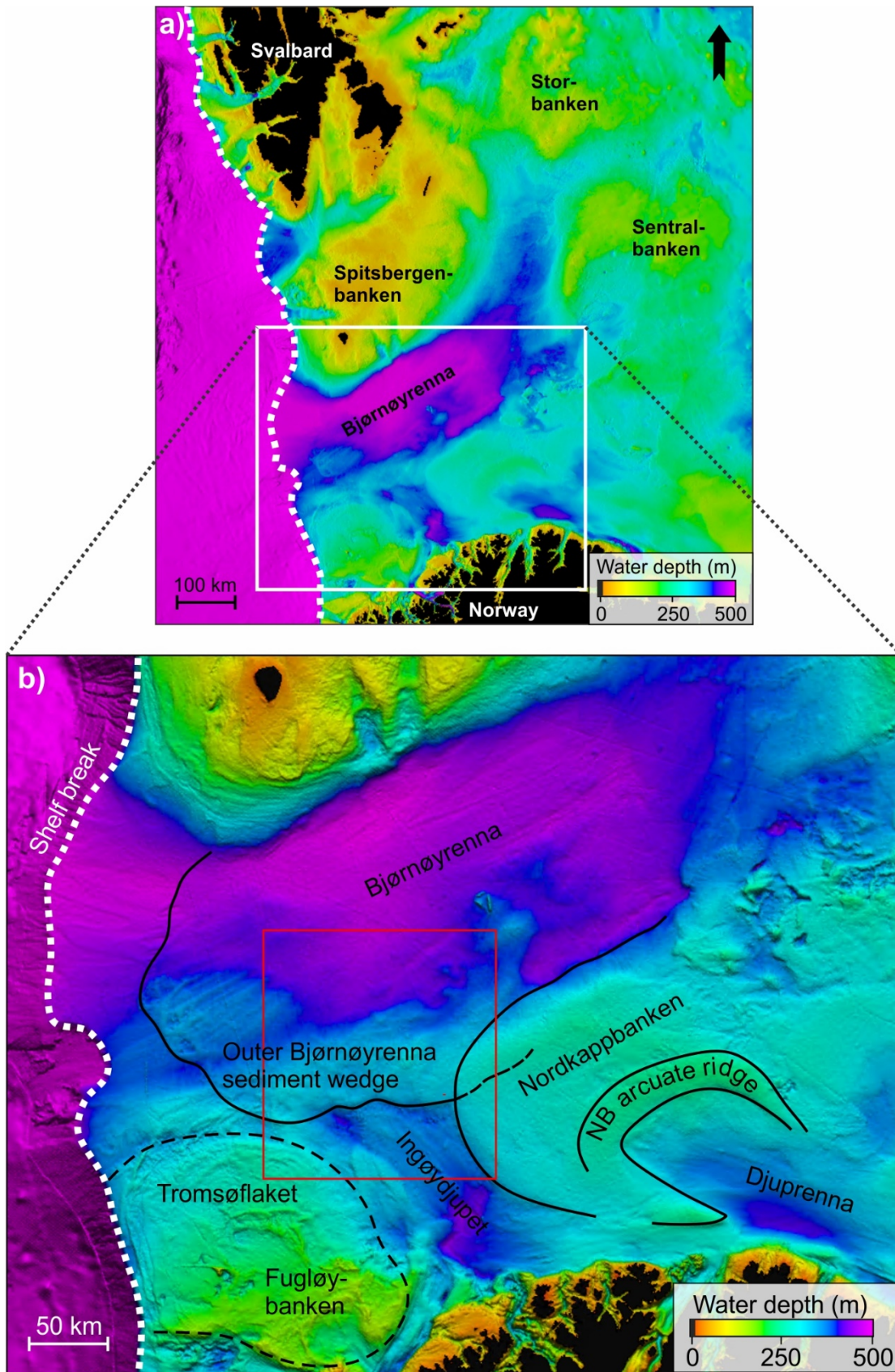
Figure 2.11 – ***a)*** *Bathymetric map of the western Barents Sea. White rectangle indicate the zoomed in area in b.*
b) *Bathymetric map including large-scale morphological features (NB= Nordkappbanken). The study area are within the red box.*

3 Data and methods

3.1 Datasets

The study is based on a merge of conventional 3D-datasets and a dataset of TopSeis, which is a new generation of 3D-seismic reflection data with a very high resolution, located in the southwestern Barents Sea (Figure 3.1 & 3.2). The data is covering an area of approximately 14 000 km^2, where the TopSeis overlaps an area of ~2000 km^2 in the southwestern corner of the merge (Figure 3.1 & 3.2). General information about the different 3D seismic surveys, including total planned area, company responsible, and year of acquisition are listed in Table 3.1.
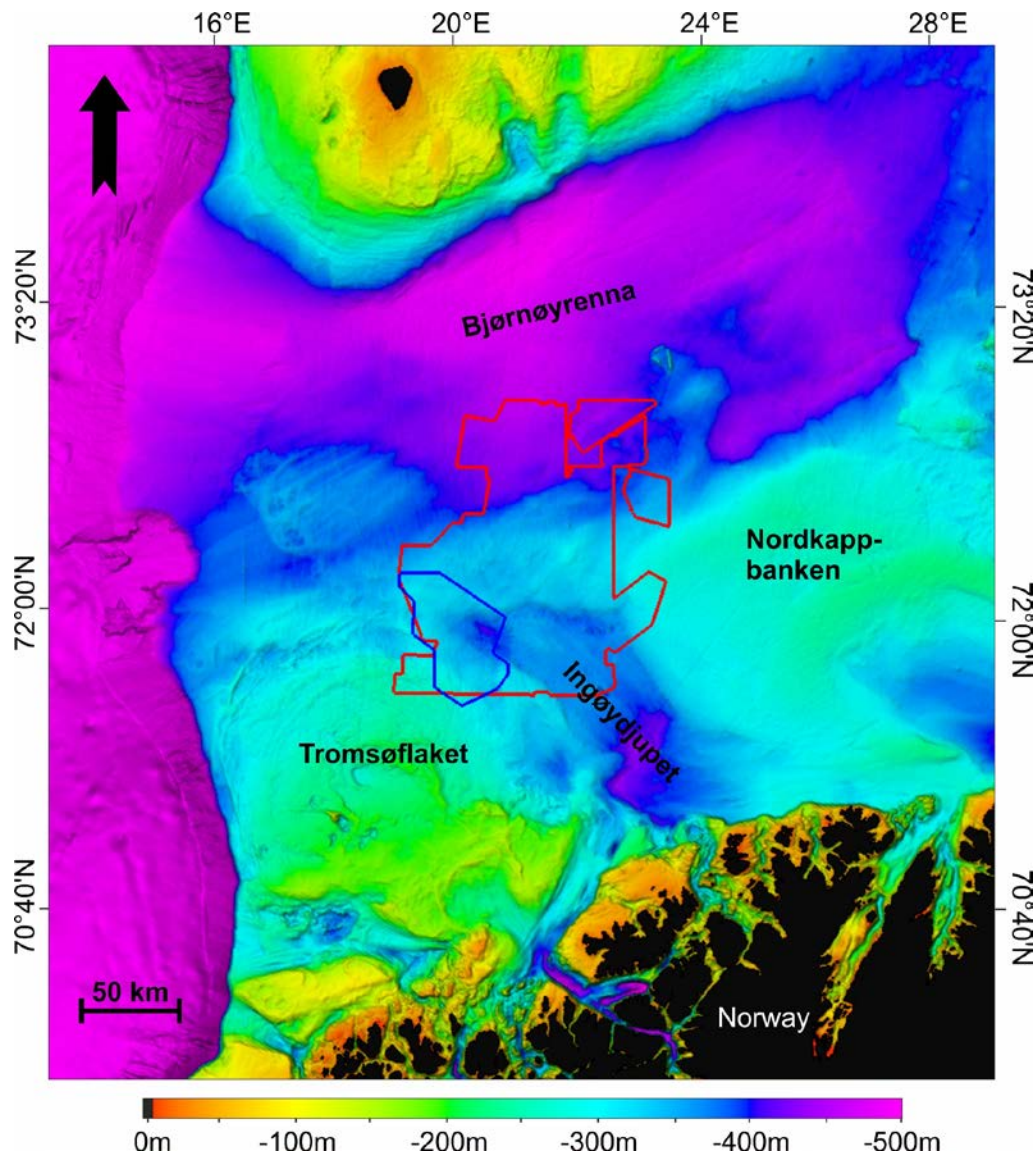
Figure 3.1 *– Bathymetric map of the southwestern part of the Barents Sea shelf, including 3D seismic data coverage of the study area. The red polygon represents LN17M01 (3D-merge), and the blue polygon represents LN17001 (TopSeis).*

21
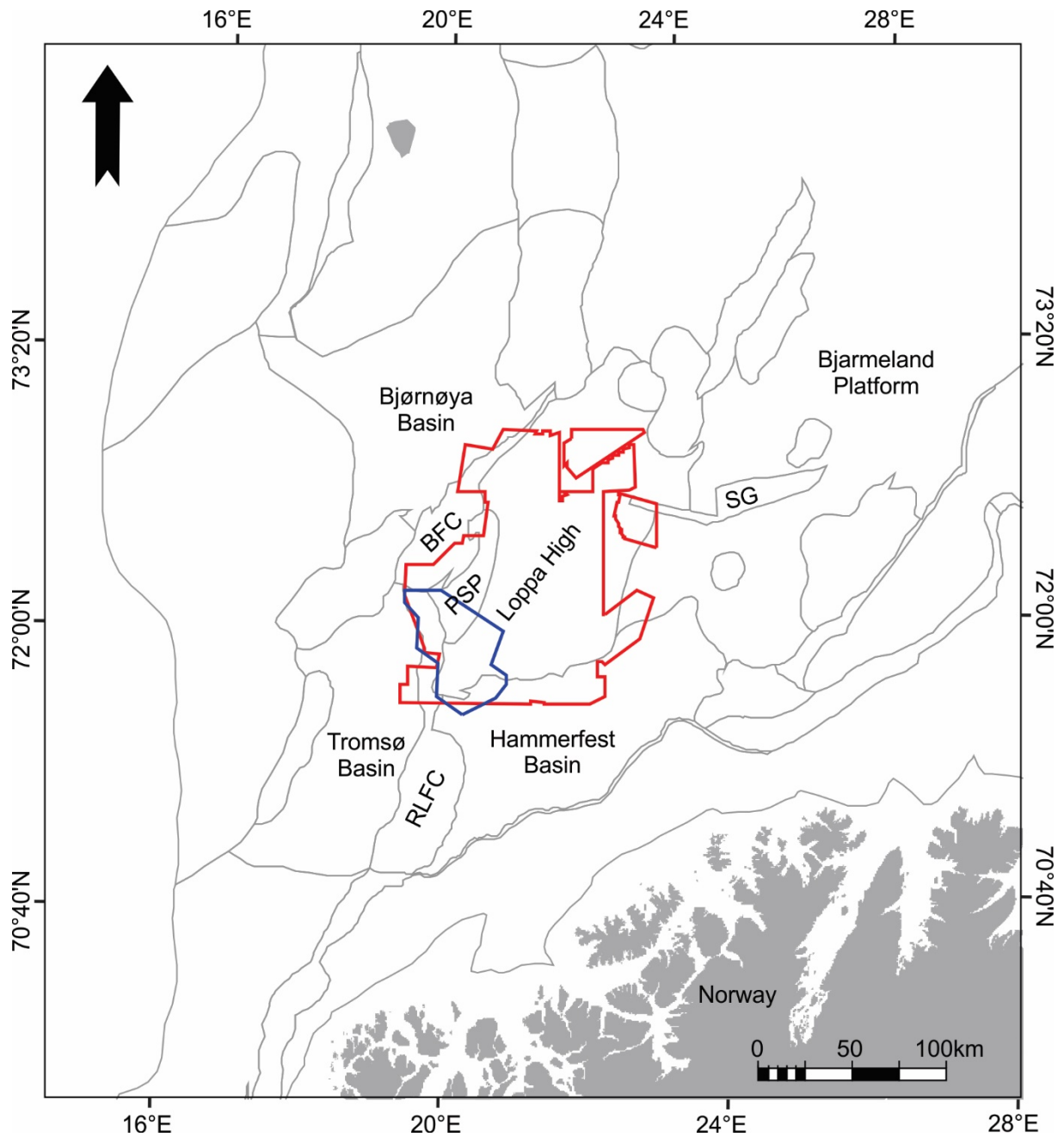
Figure 3.2 *– Location of the 3D seismic datasets, where LN17M01 (3D-merge) is illustrated with a red polygon and LN17001 (TopSeis) with a blue polygon. Selected structural elements are included as well (BFC = Bjørnøyrenna Fault Complex, PSP = Polheim Sub-platform, RLFC = Ringvassøy-Loppa Fault Complex, SG = Swaen Graben).*

Table 3.1 – *Overview of seismic surveys used in the study. Obtained from Lundin Norway AS and NPD-Factpages (2019b).*

Survey name	Sub type	Company responsible	Year completed	Size
LN17M01	**3D-merge**	**Lundin Norway AS**	**2017**	**~14 000 km²**
WG14001	3D	WesternGeco AS	2014	11894 km²
LN10M03	3D	Lundin Norway AS	2010	?
OMV09M01	3D	OMV (Norge) AS	2009	?
DOL14001	3D	Dolphin Geophysical AS	2014	5948.86 km²
LN11M07	3D	Lundin Norway AS	2011	?
SG9804	3D	Saga Petroleum AS	1998	~990 km²
LN11M04	3D	Lundin Norway AS	2011	?
LN0801R14	3D	Lundin Norway AS	2008	?
DN14001	3D	Det norske oljeselskap ASA	2014	2044.68 km²
WG1003	3D	WesternGeco AS	2010	?
LN15M02_ HELLEMOB	3D	Lundin Norway AS	2015	?
LN15M02	3D	Lundin Norway AS	2015	?
EASTLOPPA_ SG9803STR09	3D	Saga Petroleum AS/StatoilHydro Petroleum AS	1998/2009	?

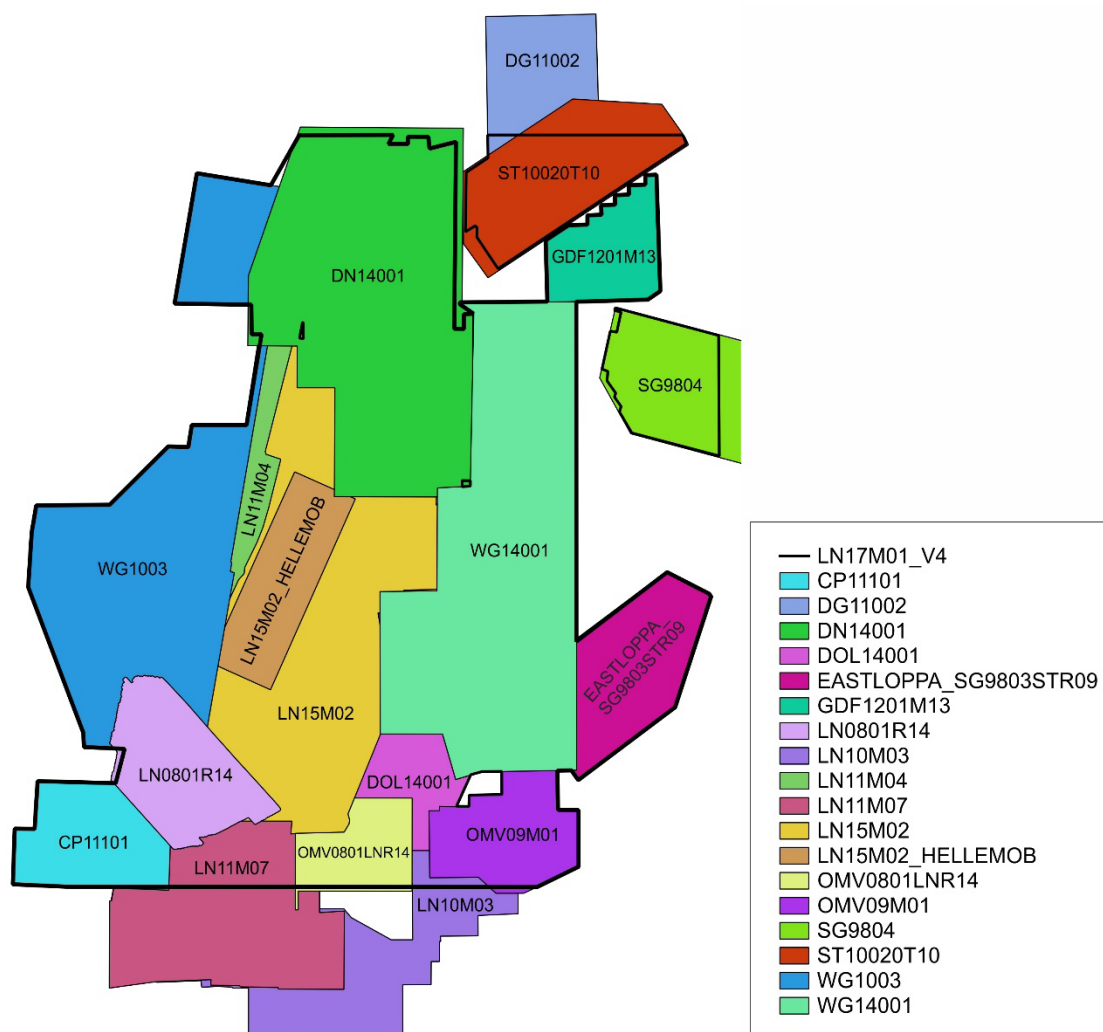| CP11101	3D	ConocoPhillips Skandinavia AS	2011	519.61 km^2
OMV0801LNR14	3D	OMV (Norge) AS/Lundin Norway AS	2008/2014	?
GDF1201M13	3D	GDF SUEZ E&P Norge AS	2012	949.96 km^2
ST10020T10	3D	Statoil ASA	2010	681.80 km^2
DG11002	3D	DONG E&P Norge AS	2011	?
LN17001	**3D (TopSeis)**	**Lundin Norway AS**	**2017**	**~2000 km^2**

Figure 3.3 – *Overview of the surveys used in LN17M01 (3D-merge). Retrieved from Lundin Norway AS.*

Phase and polarity

To determine the phase and polarity of the seismic data, the wiggle display trace across the seafloor was investigated, as this boundary represents a positive acoustic impedance contrast. Central troughs are represented at this boundary (Figure 3.4b), hence the survey is processed to a zero-phase reversed polarity signal according to the SEG (Society of Exploration Geophysicists) standard of Sheriff (2002), or to a zero-phase signal with normal polarity following the convention from Badley (1985) (Figure 3.4a). This applies to all of the surveys used in this study.
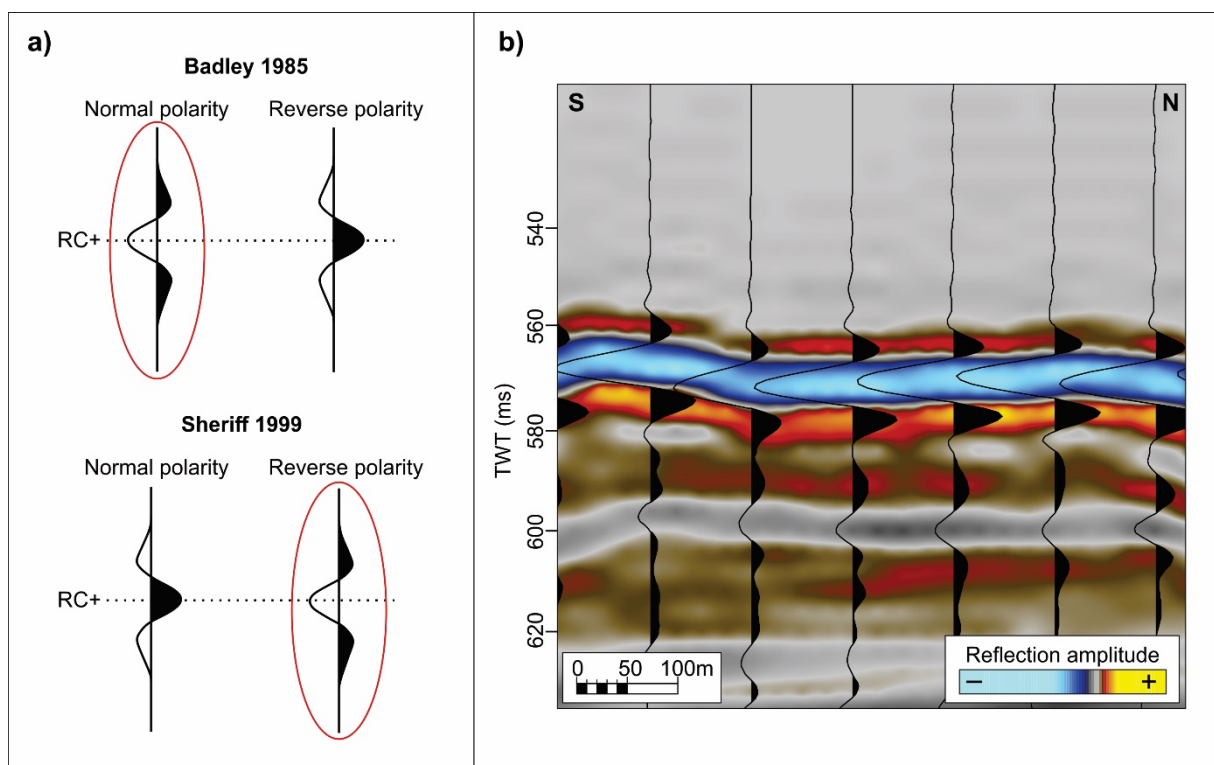
Figure 3.4 – ***a****) Badley and SEG polarity conventions for plotting seismic signals. The seismic data used in this study is zero-phase normal polarity according to the Badley convention, and zero-phase reverse polarity according to the SEG convention (outlined with red circles). Modified from Badley (1985) and Sheriff (2002). **b****) Seafloor wiggle reflection from the LN17M01 dataset. The central troughs represents a positive acoustic impedance contrast.*

3.1.1 Conventional 3D-seismic data

Several conventional 3D-datasets are merged together in a 3D-merge (LN17M01) on the Loppa High area. This is an internal merge done by the processing-team in Lundin. The different surveys included in LN17M01 are summarized in Table 3.1 and Figure 3.3.
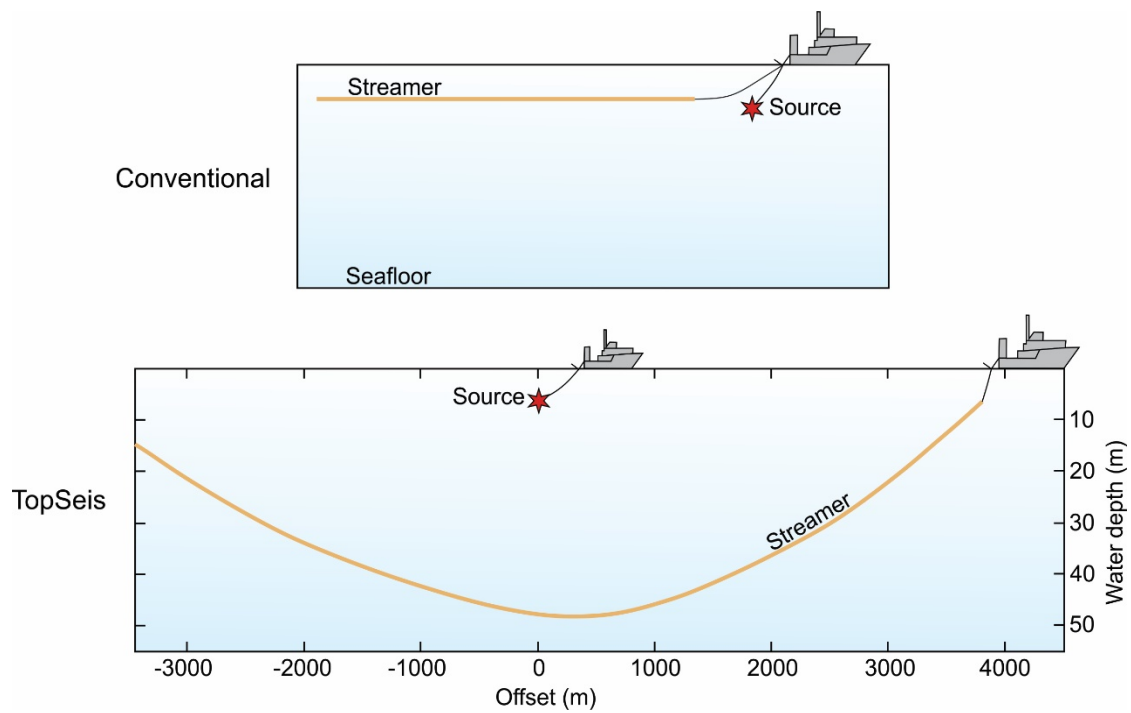
3.1.2 TopSeis data

In addition to the 3D-merge, TopSeis data have been utilized for the study. TopSeis is a new seismic acquisition method, and it is developed in co-operation between Lundin Norway and CGG (Compagnie Générale de Géophysique) (Vinje et al., 2017).

The conventional marine seismic surveys typically operate with one vessel towing two source arrays in front of a spread of ten or more streamers (Figure 3.5). This method gives a narrow-azimuth, meaning that the angle between the source and a particular receiver is narrow, and lack near offsets due to the wide distance between the sources and streamers (often 100 to 200 m for the inner cables, and up to 500 m for the outer cables). The method of TopSeis-acquisition improves these factors, and increase the amount of near offset data to significantly improve the resolution. TopSeis operates with a source vessel and a streamer vessel that operate in tandem, with the source vessel deployed above the streamers (Figure 3.5 & 3.6). To make this possible, the streamers have to be towed at a depth (40-50 m) so that the source vessel can move across the streamers without problems (Figure 3.6). Other features that differ from the conventional method is that TopSeis operates with smaller spacing between the streamers, a shorter shot distance and optionally deploys more than two sources. These solutions result in an exceptionally high subsurface imaging, as the TopSeis gives a much larger signal reflection since the subsurface achieve 10-15 times more energy form the source (Figure 3.7). In addition, the method improves the signal-to-noise ratio (S/N) which is beneficial for most processing steps, record near- and zero-offset data which is critical for imaging shallow targets and a great benefit for multiple attenuation and to achieve a semi-wide-azimuth coverage (Lundin, 2016; Vinje et al., 2017).

For the acquisition of the TopSeis survey on Loppa High, 14 densely spaced streamers and three sources were used (Figure 3.5). This resulted in a maximum of 17 times higher illumination density (number of times a specific depth point is recorded) in the shallow part of the section than achieved by a conventional configuration (Figure 3.7) (Firth & Vinje, 2018).
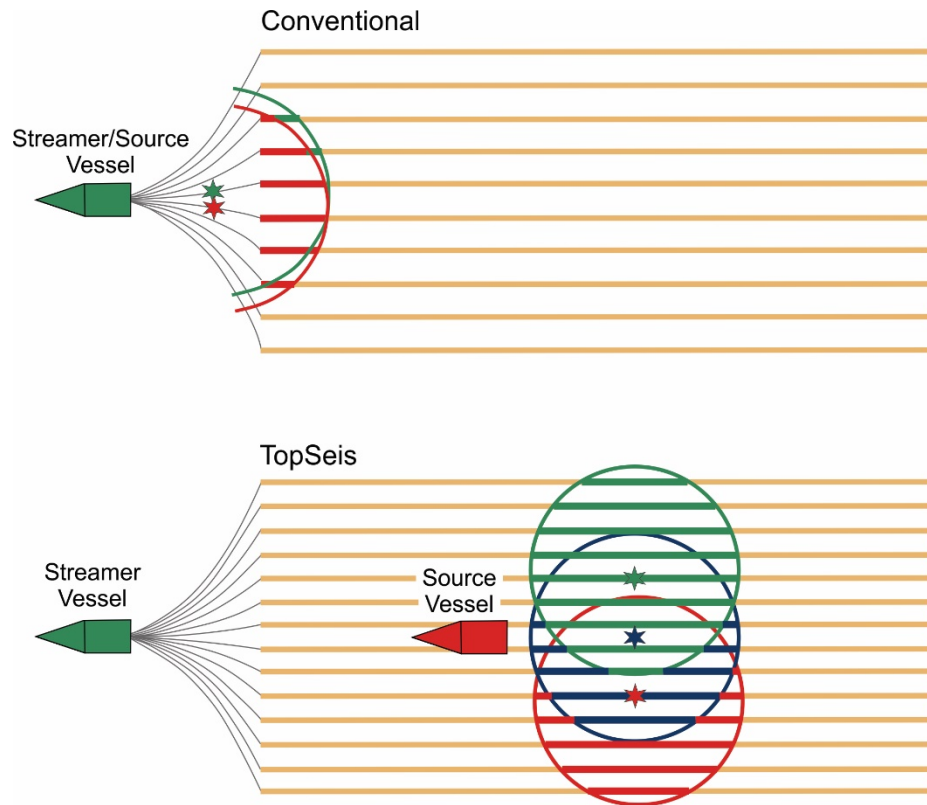
Figure 3.5 *– Conventional and TopSeis marine acquisition. The highlighted circles show near-offset data surrounding the airgun source arrays. Modified from Vinje et al.(2017) and Firth & Vinje (2018).*

Figure 3.6 *– Illustrations of conventional and TopSeis streamer profiles. Modified from Vinje et al., (2017).*
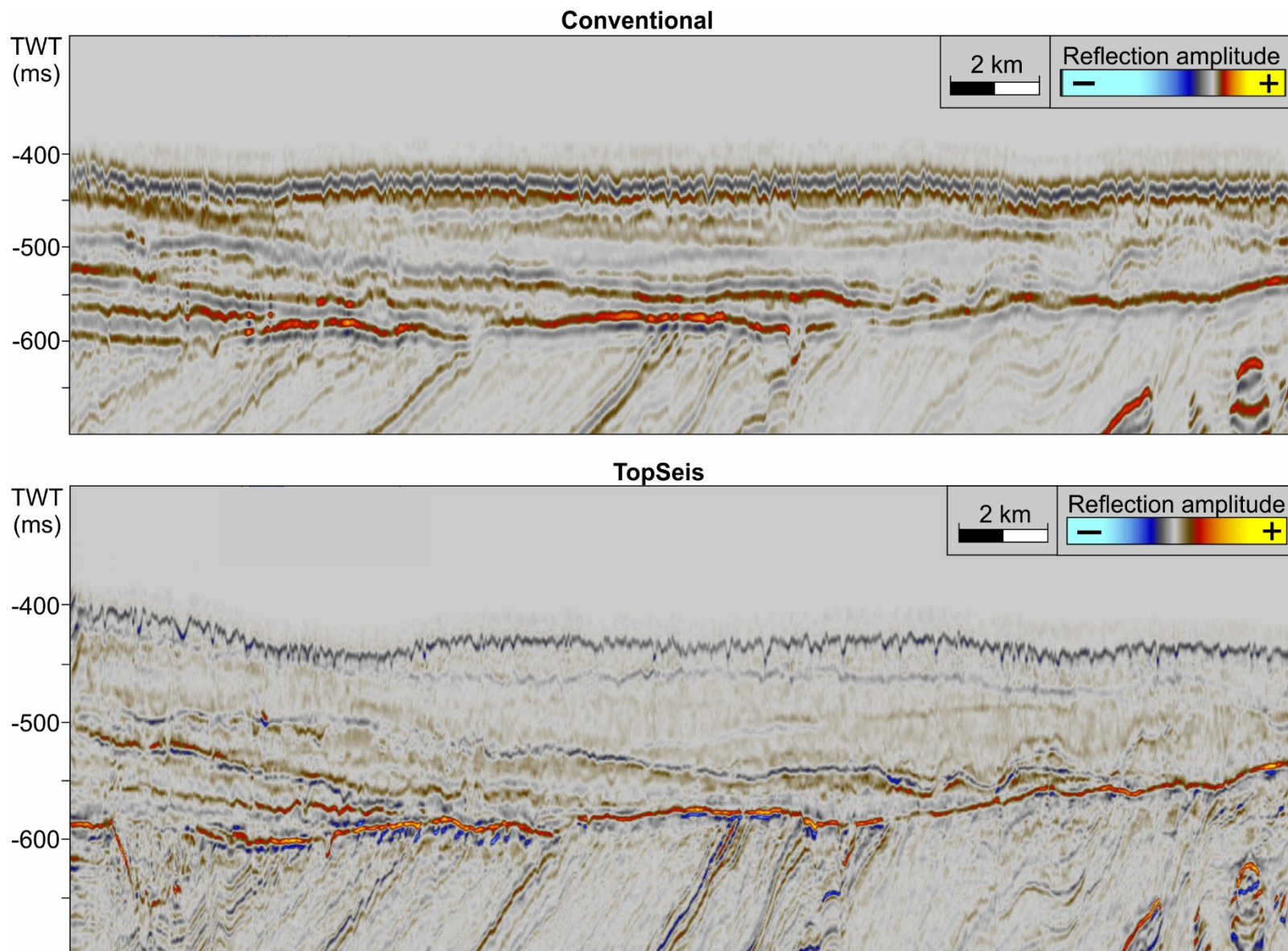
Figure 3.7 – *A crossline comparison between the Conventional- and TopSeis datasets used in this study.*

3.2 Seismic reflection theory

Seismic reflection is a geophysical method used to investigate the properties of the Earth's subsurface from reflected seismic pulses. The method is based on emitting seismic pulses from a source near the ocean surface and down into the subsurface. When the seismic pulses encounter interfaces in the subsurface, some of the energy is reflected back to the surface where seismic receivers detect the travel time. In order for a seismic pulse to be reflected back to the surface, there has to be an interface (reflector) representing a sufficient acoustic impedance contrast between the adjacent layers (Badley, 1985; Veeken, 2007). The acoustic impedance is defined as the product of density (ρ) and sound velocity (V) (Equation 3.1).

Equation 3.1 – Acoustic impedance

$$Z = \rho V,$$

Where ρ = density (kg/m^3) and V = velocity.

The strength of a reflection generated at an interface depends among other factors on the reflection coefficient (R) (Equation 3.2), which is determined by the difference in acoustic impedance between two layers. The reflection coefficient can either be positive ($Z_2 > Z_1$) indicating that "softer" rocks overlie "harder" rocks, or negative ($Z_1 > Z_2$) indicating that "harder" rocks overlie "softer" rocks (Badley, 1985).

Equation 3.2 – Reflection Coefficient

$$R = \frac{(Z_2 - Z_1)}{(Z_2 + Z_1)} = \frac{(\rho_2 V_2 - \rho_1 V_1)}{(\rho_2 V_2 + \rho_1 V_1)}$$

Where Z_1, ρ_1 and V_1 are acoustic impedance, density and velocity of the uppermost layer, while Z_2, ρ_2 and V_2 are acoustic impedance, density and velocity of the underlying layer.

3.3 Seismic resolution

Seismic resolution is a measure of how large an object needs to be in order to be identified in the seismic data, or the minimum distance two individual reflectors can have in order to be separated in the seismic data (Sheriff, 2002). There are two dimensions of seismic resolution, vertical and horizontal, and they are both dependent on the dominant seismic wavelength (λ) which is given by:

Equation 3.3 – Seismic wavelength

$$\lambda = \frac{v}{f}$$

Where λ = wavelength (m), v = seismic velocity (m/s) and f = frequency (Hz).

The ratio between the wavelength, seismic velocity and frequencies are shown in Figure 3.8. The frequency decreases with depth, as the higher frequencies in the seismic signal are attenuated more rapidly than the lower frequencies, while the seismic velocity increases with depth because the sediments are gradually more compacted deeper in the subsurface. Consequently, the wavelength increases with depth, as it is dependent on the velocity-frequency ratio, resulting in a poorer seismic resolution (Badley, 1985; Brown, 1999).
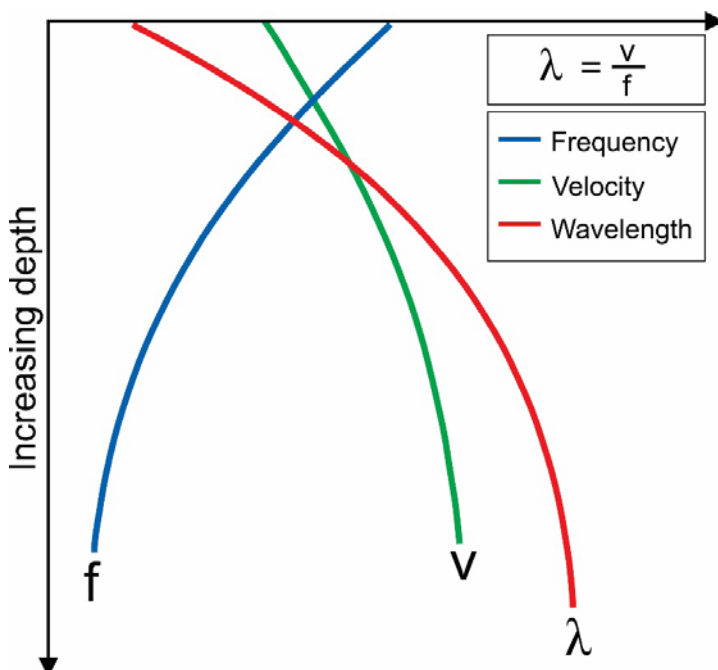
Figure 3.8 – The ratio between wavelength, velocity and frequency. The wavelength increases considerably with depth, while the frequency decreases, resulting in a poorer resolution of the data. Modified from Brown (1999).

3.3.1 Vertical resolution

Vertical resolution is a measure of the ability to recognize and separate individual, closely-spaced reflectors in the seismic data, and is given by the following equation:

Equation 3.4 – Vertical resolution

$$Vr = \frac{\lambda}{4}$$

Where Vr = vertical resolution (m) and λ = wavelength (m)

According to Brown (1999), the vertical resolution has two limits; (1) the limit of separability and (2) the limit of visibility. Generally, the limit of separability is defined as one-quarter of a wavelength, or half a period, which is the point where there is maximum interference (Figure 3.9). This means that when the space between two reflections approaches one-quarter of the wavelength, the seismic reflections will overlap and interfere. The interference can be either constructive, resulting in increasing amplitude wavelet (Figure 3.9), or destructive, resulting in a cancellation of the amplitudes, hence a lower-amplitude wavelet. However, identification of the top- and bottom-boundaries of layers can be identified in the seismic data as long as the thickness of the layer is equal to, or greater than, half the wavelength of the seismic wavelet (Figure 3.9) (Badley, 1985; Sheriff, 1985; Brown, 1999).

For layers thinner than a quarter of the wavelength, the amplitude is progressively attenuated by destructive interference until the limit of visibility is reached, which is down to one-thirtieth of the wavelength (Figure 3.9). This happens because the reflected signal becomes obscured by the background noise. However, the limit of visibility is affected by several factors and depend on how the acoustic contrast of a geological layer is relative to the surrounding material, random and systematic noise and the phase of the seismic wavelet (Sheriff 1985; Brown, 1999).
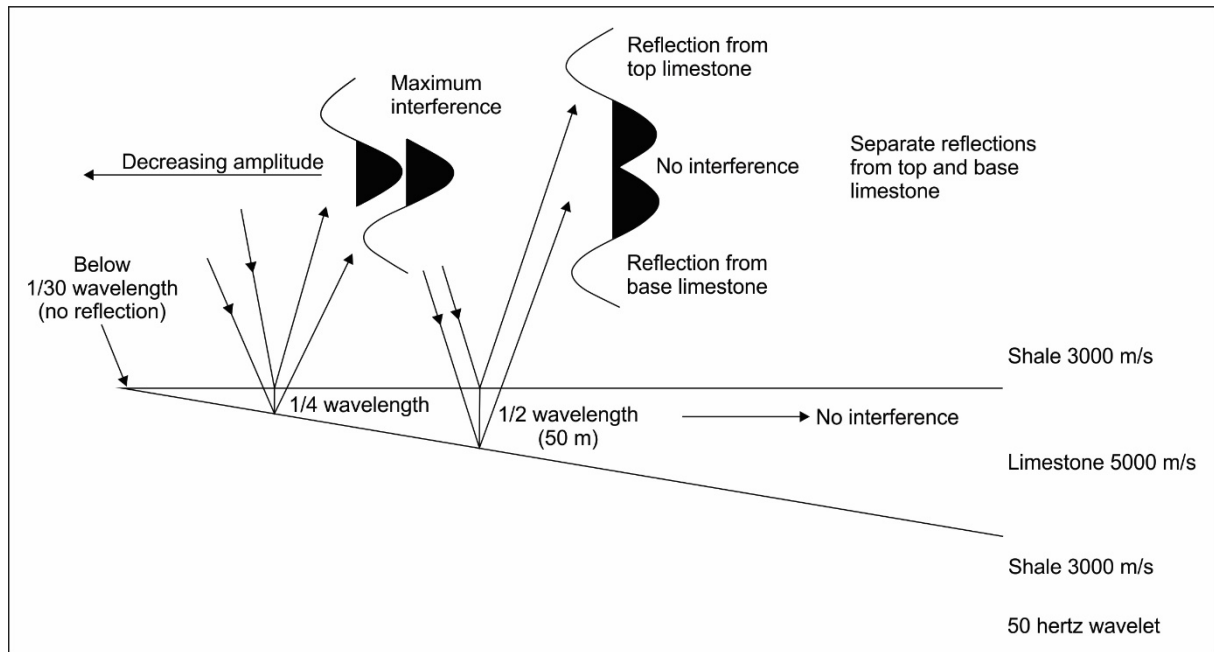
Figure 3.9 *– Interference effects associated with a high AI wedge surrounded by shale with lower AI. Modified from Badley (1985).*

### 3.3.2 Horizontal resolution

The horizontal resolution can be defined as the minimum horizontal distance two features can have and still be separated as two features in the seismic data. The reflected signals from a reflector do not come from single points, but a considerable area of the reflectors surface, defined as the Fresnel Zone (Figure 3.10a). This is due to the spherical propagation of the soundwaves down into the subsurface (Brown, 1999; Kearey et al., 2002). The horizontal resolution of unmigrated seismic data is given by the radius of the Fresnel zone, which is the portion of the reflector that contributes with energy back to the receivers. This means that features with a lateral extent exceeding the Fresnel zone will be visible in the seismic data, while features with a smaller extent than the Fresnel zone will not be visible (Sheriff, 1985; Brown, 1999). The magnitude of the Fresnel zone can be approximated from the equation:

Equation 3.5 – Horizontal resolution

$$rf = \frac{v}{2}\sqrt{\frac{t}{f}}$$

Where rf = the radius of the Fresnel zone (m), v = average seismic velocity (m/s), t = Two-way travel time (s) and f = dominant frequency (Hz).

32

Based on the equation, the radius of the Fresnel zone increases with depth, increasing velocity and lower frequencies (Figure 3.10b). The horizontal resolution is hence decreasing with increased depths, velocities and lower frequencies. To improve the horizontal resolution, seismic migration is a processing step that can be applied to reduce the Fresnel zone to a small circle (for 3D migration) (Figure 3.10c), resulting in a more concentrated seismic signal, hence a better horizontal resolution. If the migration of the data is ideal, the horizontal resolution equals one quarter of a wavelength ($\lambda/4$) (Brown, 1999).
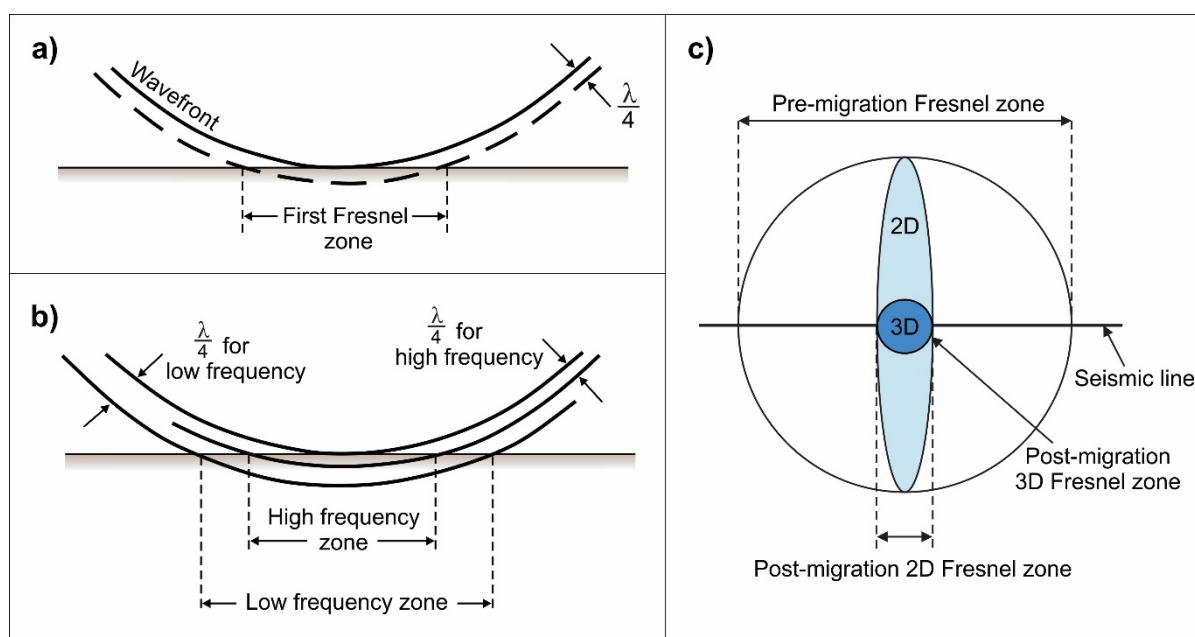
Figure 3.10 *– **a**) Illustration of the first Fresnel zone, **b**) displays how increasing frequencies decreases the Fresnel zone. **c**) Illustrates the Fresnel zone size and shape before and after migration. Figure a and b are modified from Sheriff (1985) and figure c is modified from Brown (1999).*

Table 3.2 *– Calculated wavelengths and resolutions for different 3D-seismic surveys.*

Survey	Average interval velocity	Average peak frequency	Wavelength (v/f)	Vertical resolution ($\lambda/4$)	Horizontal resolution (unmigrated)
SG9804	1970 m/s	26.33 Hz	74.82 m	18.71 m	147.45 m
LN15M02	1970 m/s	33.24 Hz	59.27 m	14.82 m	120.81 m
LN17001	1970 m/s	60.11 Hz	32.77 m	8.19 m	91.61 m

The vertical and horizontal resolutions have been calculated for the Quaternary sequence within different 3D-seismic surveys, including the oldest (SG9804) and newest (LN15M02) surveys in the 3D-merge (LN17M01), and the TopSeis survey (LN17001). In order to calculate the resolutions, the average peak frequencies were determined by using the inspector tool in Petrel to get information about the frequency spectrum of the seismic data. The average interval velocity for glacial sediments in the GIII sequence have been set to be 1970 m/s, extracted from Table 3 in Fiedler & Faleide (1996). The calculated values summarized in Table 3.2 show that the frequency increase for the newest data, consequently the wavelength decrease and the vertical and horizontal resolutions are improved. The same interval velocity has been used to determine the magnitude of the glacial landforms in the seismic (in chapter 4), using the equation:

$$\frac{TWT\ (s) \times 1970\ m/s}{2}$$

3.4 Software

3.4.1 Petrel

The interpretation and visualization of the 3D seismic data in this thesis have been carried out by using the Schlumberger produced software, Petrel, version 2017.3. This is an interpretation program commonly used in the exploration and production sector in the petroleum industry.

3.4.1.1   Seismic attributes

Seismic attributes are quantitative measurements of seismic characteristics used to enhance information about geological features and trends leading to a better interpretation of the seismic data (Sheriff, 2002). The seismic attributes applied in this study are isochore (true vertical thickness TWT) attributes and root-mean-square (RMS) amplitude attributes:

The isochore attribute calculate the two-way travel time thickness between two surfaces. In this study, it was useful to determine the thickness trends of the glacigenic succession to reveal areas of sediment accumulation as well as displaying the thickness variations between the interpreted glacigenic units.

The RMS amplitude attribute calculates the root mean square amplitudes divided by the number of samples (Veeken, 2007). This highlights strong amplitudes, both positive and negative, for a chosen stratigraphic volume. The RMS amplitude maps were used to recognize amplitude anomalies within the glacigenic units in the study area.

3.5 Artefacts and noise

Artefacts and noise influence the interpretation of seismic data, as they are not related to the geology and may contribute to misinterpretations. It is thus important to recognize and disregard these phenomena (Badley, 1985). In the datasets used in this study, artefacts and noise resulted from seismic acquisition and processing e.g. acquisition footprints and terracing, have been identified.

Acquisition footprints is defined as noise related to the geometric distribution of the sources and receivers of the acquisition (Figure 3.11a) (Marfurt et al., 1998). Acquisition footprints is seen as minor time shifts between lines giving rise to a corrugated effect. In marine data, feathering (the receiver cables have a certain amount of sideways drift, and are not straight and parallel to one another) appears to be the main source of acquisition footprint (Marfurt et al., 1998; Bulat, 2005).

Terracing appears as a step-like topography, similar to river terraces (Figure 3.11b). When the seismic data is loaded, it is common to truncate or clip the largest amplitudes to ensure that the deeper reflections with (normally) smaller amplitudes are properly visualized. As the seafloor often have the greatest acoustic impedance contrast, it is commonly clipped. This makes the creation of seismic horizons difficult, as several adjacent samples have been truncated or clipped. The software is thus forced to snap to the nearest sample. This results in the production of a stepped terrace effect that follows the TWT or depth contours, and destruction of visual continuity (Figure 3.11b) (Bulat, 2005).
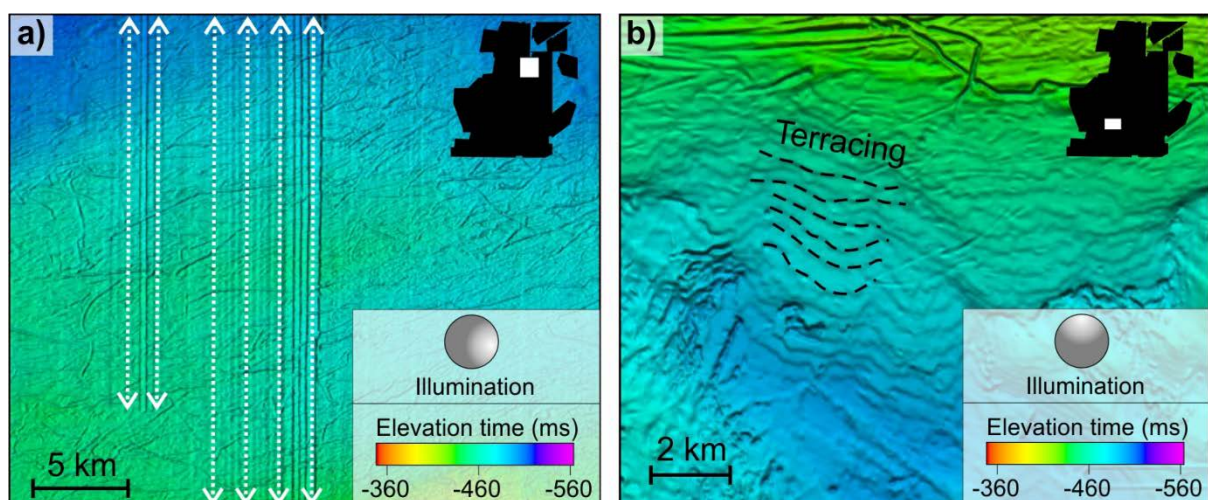
Figure 3.11 – *Display of the LN17M01 seafloor showing **a)** acquisition footprints (white stippled arrows) and **b)** terracing (black stippled lines).*

3.6 Seismic interpretation method

3.6.1 Seismic stratigraphic analysis

Mitchum et al. (1977) defines seismic stratigraphy analysis as the study of stratigraphy and depositional facies interpreted from seismic data. This technique is used to identify and correlate depositional sequences, as well as interpretation of the environmental setting and lithofacies (Mitchum et al., 1977; Vail, 1987). In this study this has been important in order to establish the stratigraphic framework for the Quaternary sediments i.e. interpret the URU and consequently the glacigenic sequence, in addition to interpretation of intra-glacial horizons.

Seismic stratigraphic analysis can be divided in two main steps: (1) seismic sequence analysis – where the seismic section is subdivided into packages of concordant reflections bounded by surfaces or discontinuities, and (2) seismic facies analysis – where different facies within the interpreted sequences are mapped out and studied (Mitchum et al., 1977).

3.6.1.1 Seismic sequence analysis

Seismic sequence analysis involves interpretation of depositional sequences and system tracts on seismic sections by subdividing the seismic section based on different reflection terminations, i.e. erosional truncation, toplap, onlap and downlap (Mitchum et al., 1977; Vekeen, 2007). The types of reflection terminations are characterized based on their geometric relationship between the strata and the stratigraphic surface where they terminate (Veeken, 2007). Figure 3.12 illustrates the main seismic stratigraphic reflection terminations within an idealized seismic sequence.
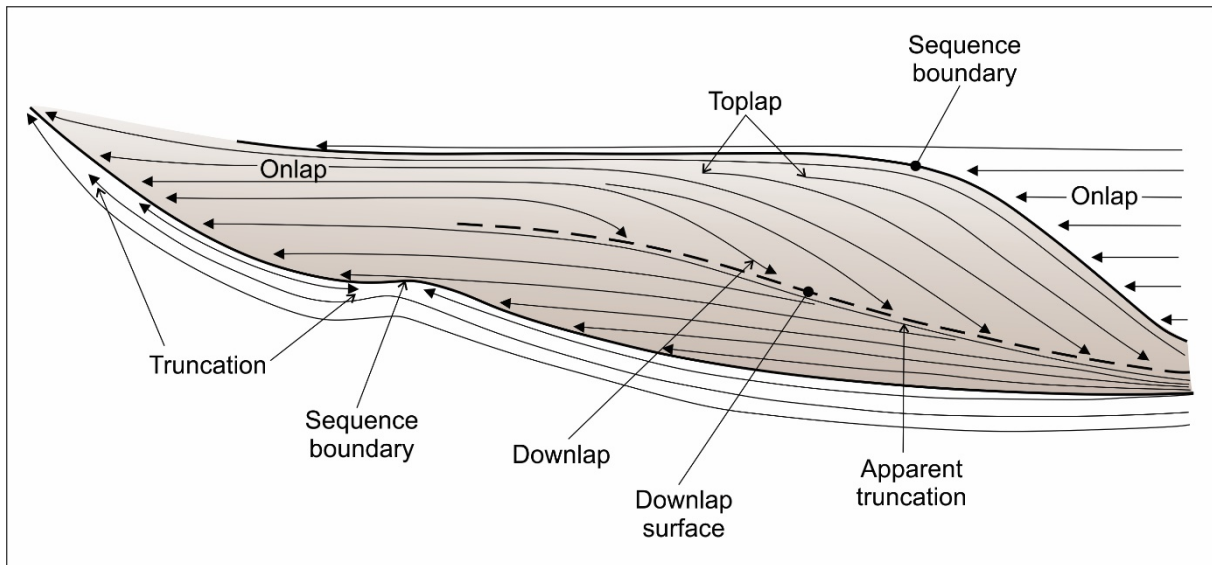
Figure 3.12 *– Idealized seismic sequence illustrating the main seismic reflection terminations. Modified from Vail (1987).*

Top-discordant relations, i.e. terminations occurring above a surface, include erosional truncation and toplap (Figure 3.12) (Mitchum et al., 1977; Catuneanu et al., 2009). Erosional truncation is characterized by termination of strata against an overlying erosional surface. This type of termination indicates that there has been deposition and subsequent removal of sediments along an unconformity. In some cases, erosional truncations can produce a seismic reflection itself, but this may not always occur. In that case, underlying reflections may define the surface. Toplap is mainly a result of nondeposition (sedimentary bypass), and is characterized as termination of strata against an overlying surface (Mitchum et al., 1977).

Base-discordant reflection patterns, i.e. terminations occurring below a surface, include onlap and downlap (Figure 3.12) (Mitchum et al., 1977; Catuneanu et al., 2009). Onlap is represented by termination of initially horizontal strata against an initially inclined surface, or as strata terminating progressively updip against a surface with a steeper inclination. Downlap is recognized as initially inclined strata terminate downdip against an initially inclined or horizontal surface (Mitchum et al., 1977).
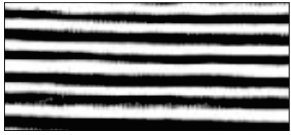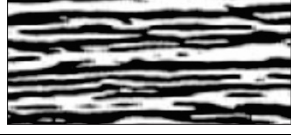
3.6.1.2 Seismic facies analysis

When the seismic sequences are defined, environmental setting and lithofacies within the sequences are interpreted by using the theory of seismic facies analysis. Seismic facies analysis is the description and interpretation of different seismic reflection parameters, including configuration, continuity, amplitude, frequency and interval velocity (Table 3.3 & 3.4). These different parameters provide information about the geology in the subsurface, thus are of importance regarding the interpretation of seismic data (Mitchum et al., 1977).

Table 3.3 *– Overview of seismic reflection parameters used in seismic stratigraphy and their geologic significance. Modified from Mitchum et al. (1977)*

Reflection parameter	Geological interpretation
Reflection configuration	• Bedding patterns • Depositional processes • Erosion and paleotopography • Fluid contacts
Reflection continuity	• Bedding continuity • Depositional processes
Reflection amplitude	• Velocity-density contrast • Bed spacing • Fluid content
Reflection frequency	• Bed thickness • Fluid content
Interval velocity	• Estimation of lithology • Estimation of porosity • Fluid content
External form and areal association of seismic facies units	• Gross depositional environment • Sediment source • Geologic setting

The different reflection parameters are listed in Table 3.3. Reflection configuration reveals the gross stratification patterns, which is related to the depositional processes, erosion and paleotopography. Additionally, fluid contacts (e.g. flat spots) are recognized by using the reflection configuration (Mitchum et al., 1977). Reflection continuity describes the continuity of the strata, and is directly related to the sedimentary processes, thus the depositional environment. Continuous reflections suggests extensive and uniform stratified deposits (Mitchum et al., 1977; Veeken, 2007). Reflection amplitude provides information about the acoustic impedance, i.e. velocity and density, contrasts of individual interfaces and the spacing between them, and is used to predict changes within the lateral bedding in addition to occurrence of hydrocarbons (Mitchum et al., 1997). Reflection frequency describes the nature of a seismic pulse, and can relate to geological factors such as the spacing of reflectors or lateral changes in interval velocity, as associated with existence of gas (Mitchum et al., 1997).
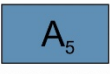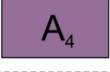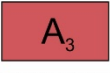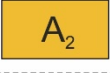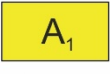
Table 3.4 – Examples of seismic facies units based on amplitude, frequency, continuity and configuration. Modified from Veeken (2007).

Seismic facies	Reflection configuration	Reflection amplitude	Seismic facies after Veeken (2007)
A	Parallel continuous	Medium amplitude	
B	Parallel continuous	High amplitude	
C	Parallel continuous	High amplitude	
D	Subparallel discontinuous	High amplitude	
E	Chaotic	Medium amplitude	

4 Results

The seismic stratigraphic framework for the glacigenic deposits in the outer Ingøydjupet area is here described in chronological order. This description includes seismic unit boundaries and seismic units, i.e. horizons and isochore maps.

The base Quaternary and seafloor horizons are regionally mapped in the 3D-merge (Figure 4.2 & 4.3) and the TopSeis dataset. Furthermore, four intra Quaternary horizons are mapped in the TopSeis dataset (Figure 4.4-4.7). Figure 4.1 summarizes the color codes assigned for the interpreted unit boundaries and the associated units, and it shows the correlation between the unit boundaries in the 3D-merge and TopSeis dataset. Due to time constrains, the 3D-merge has not been investigated in detail, thus the focus has been on the TopSeis dataset.

Figure 4.1 – *Color codes and names assigned for the interpreted unit boundaries and seismic units in the 3D-merge and TopSeis datasets. The black lines represent correlation between the different datasets.*
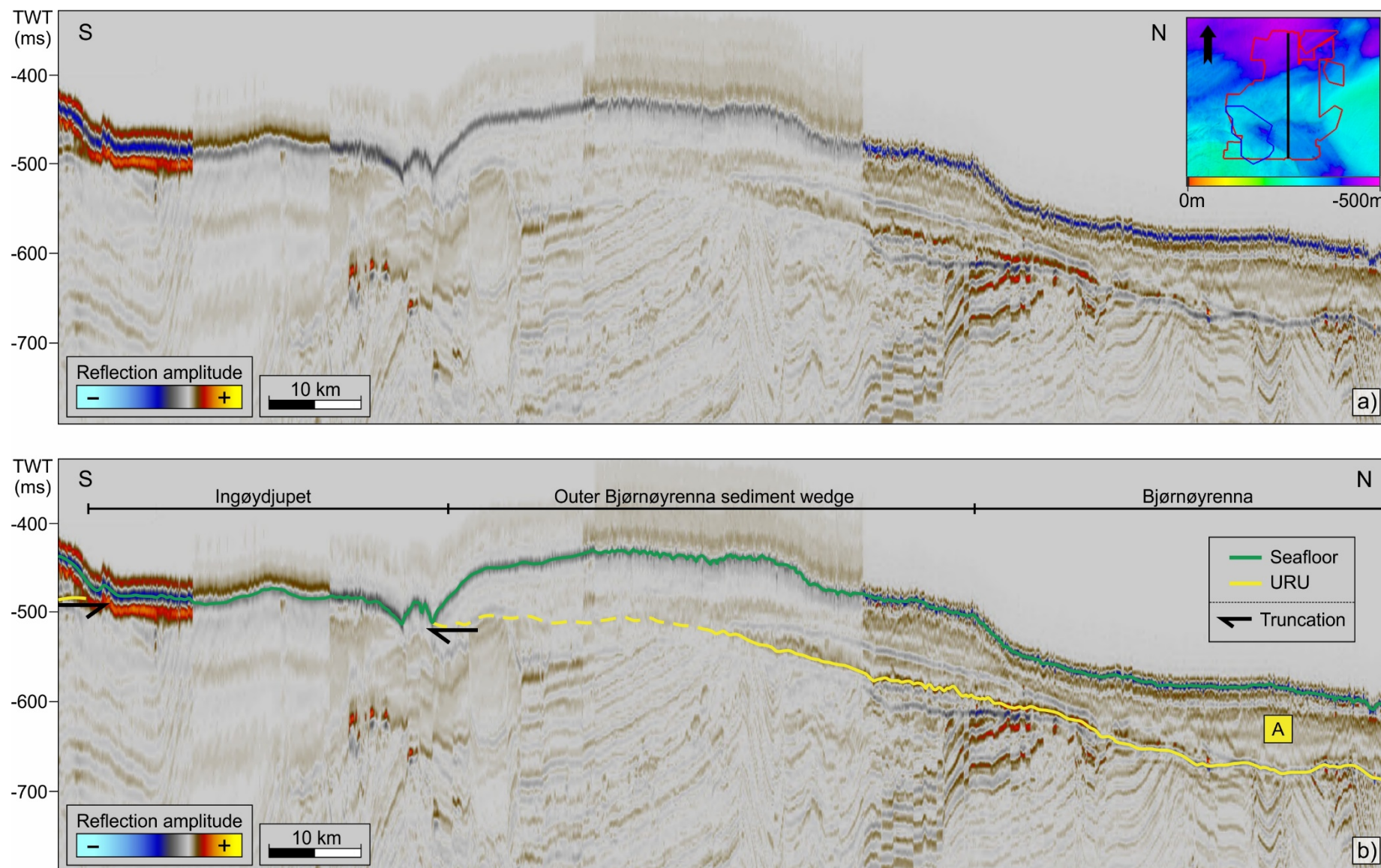
Figure 4.2 – a) Regional seismic line from LN17M01 (3D-merge) across the outer Bjørnøyrenna sediment wedge and Ingøydjupet in the central part of the study area without interpretation. The black line on the inset map indicates the location of the seismic line. b) Interpreted seismic profile showing the seismic unit boundaries and unit of the glacigenic succession in the area.
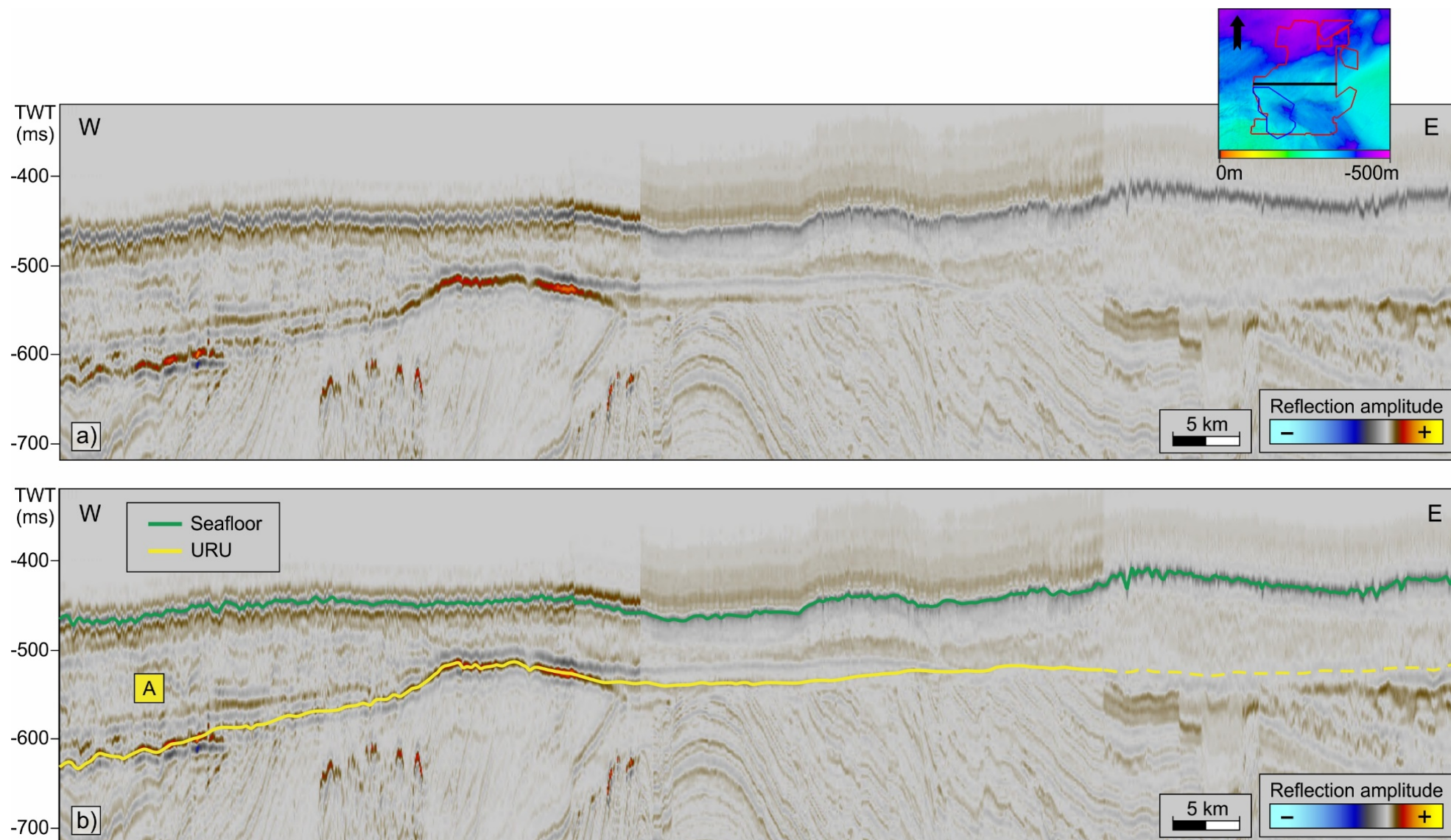
Figure 4.3 *– **a**) Regional seismic line from LN17M01 (3D-merge) across the outer Bjørnøyrenna sediment wedge in the central part of the study area without interpretation. The white line on the inset map indicates the location of the seismic line. **b**) Interpreted seismic profile showing the seismic unit boundaries and unit of the glacigenic succession in the area.*
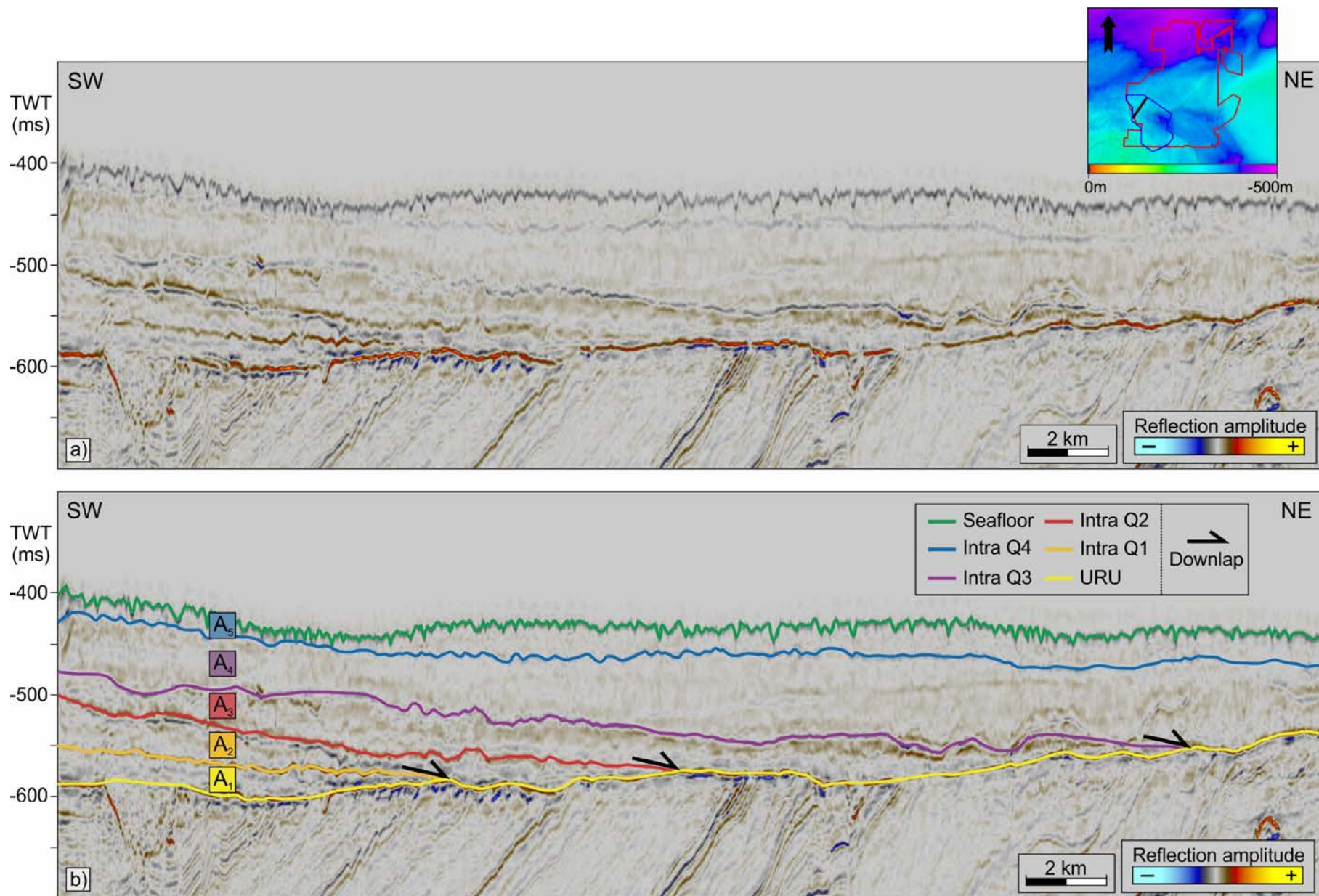
Figure 4.4 – a) Regional seismic line from LN17001 (TopSeis) from the outer Bjørnøyrenna sediment wedge without interpretation. The black line on the inset map indicates the location of the seismic line. b) Interpreted seismic profile showing the seismic unit boundaries and units of the glacigenic succession in the area.
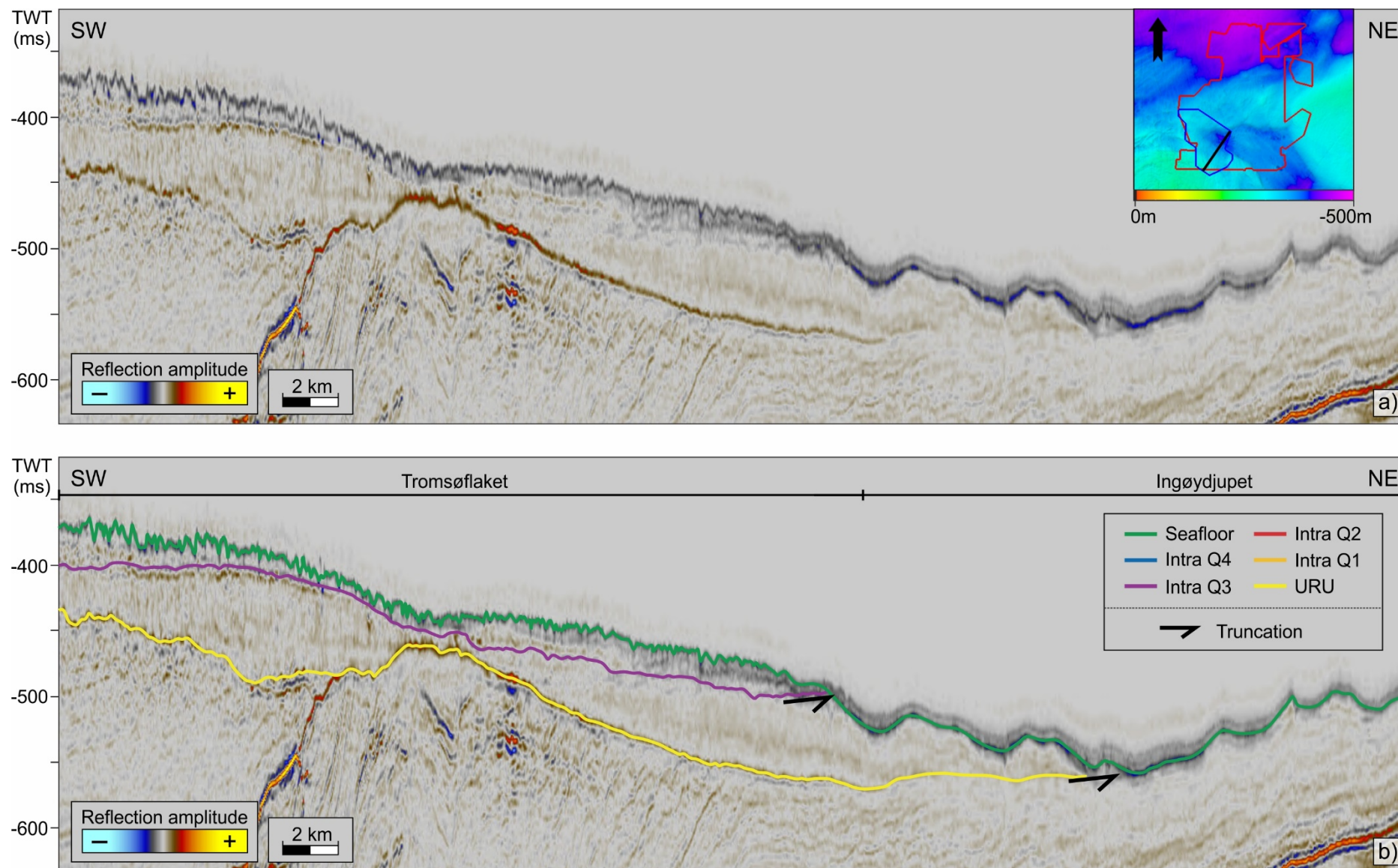
Figure 4.5 – **a)** *Regional seismic line from LN17001 (TopSeis) from Tromsøflaket and Ingøydjupet without interpretation. The black line on the inset map indicates the location of the seismic line.* **b)** *Interpreted seismic profile showing unit boundaries (URU and intra Q3) of the glacigenic succession in the area.*
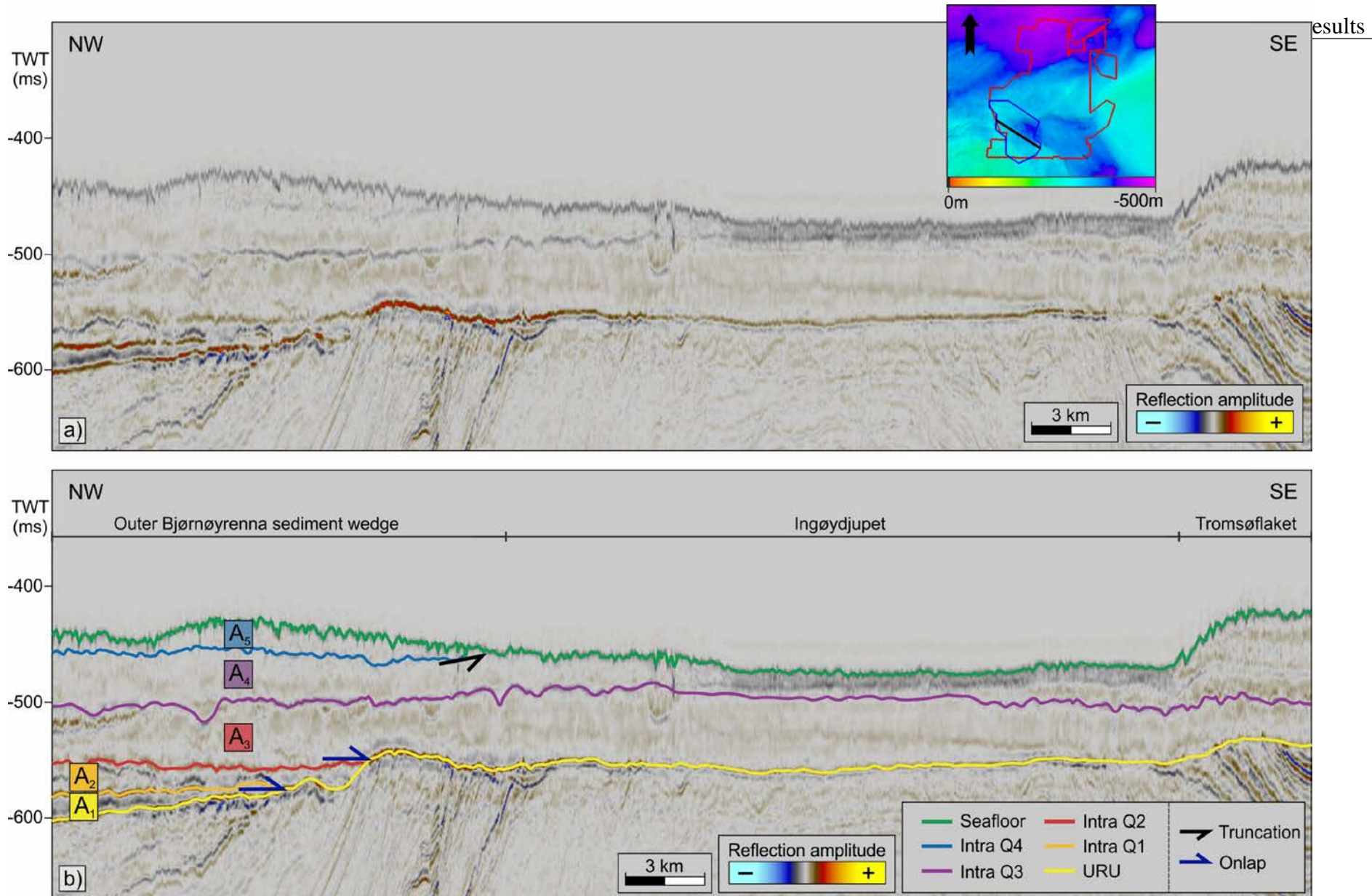
***Figure 4.6** – **a)** Regional seismic line from LN17001 (TopSeis) from the outer Bjørnøyrenna sediment wedge, Ingøydjupet and Tromsøflaket without interpretation. The black line on the inset map indicates the location of the seismic line. **b)** Interpreted seismic profile showing the seismic unit boundaries and units of the glacigenic succession in the area.*

46
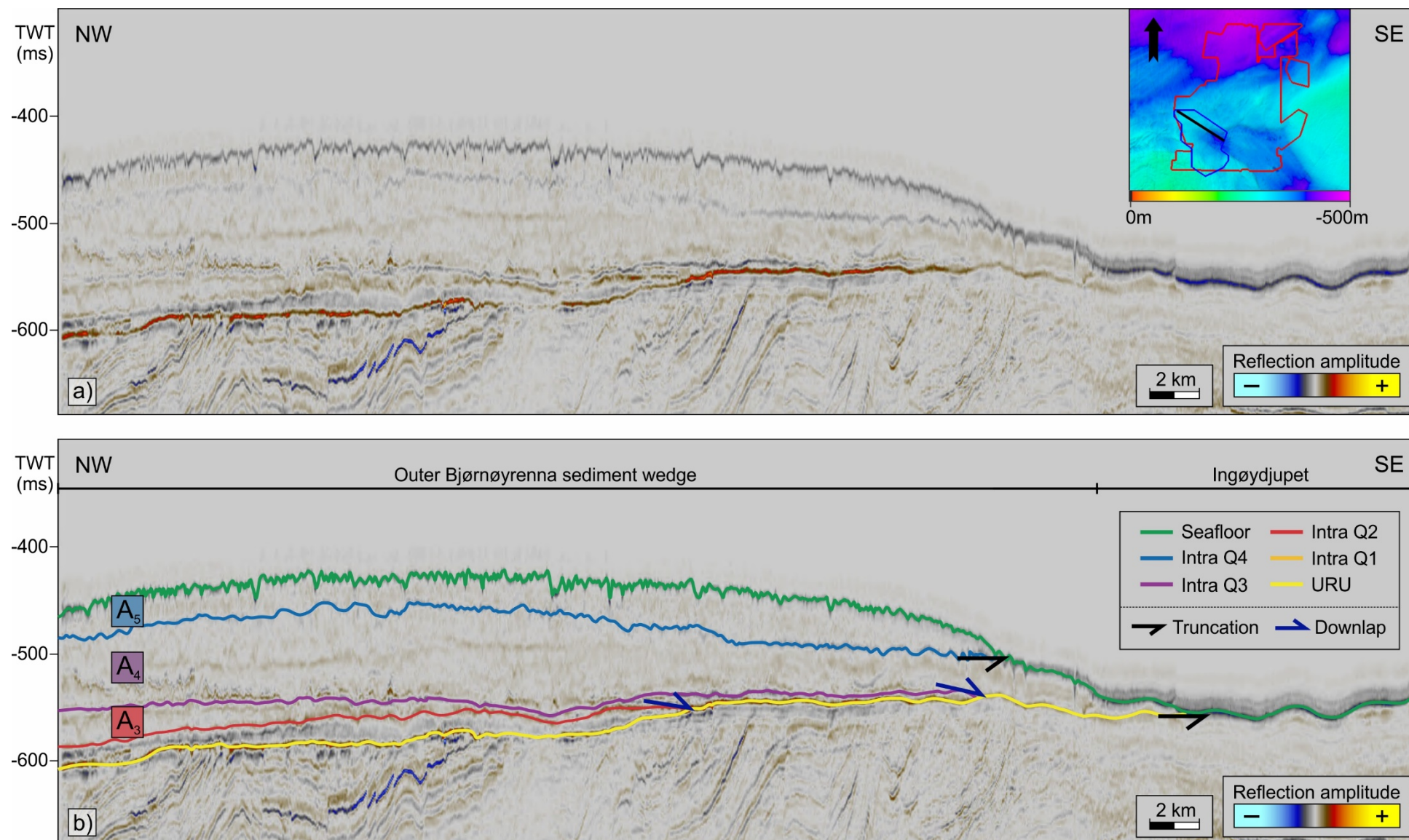
Figure 4.7 – *a) Regional seismic line from LN17001 (TopSeis) from the outer Bjørnøyrenna sediment wedge and Ingøydjupet without interpretation. The black line on the inset map indicates the location of the seismic line. b) Interpreted seismic profile showing the seismic unit boundaries and units of the glacigenic succession in the area.*

4.1 Regional seismic horizons and the Quaternary sediments in Ingøydjupet and Bjørnøyrenna (LN17M01)

4.1.1 Base Quaternary horizon: URU

The Base Quaternary (URU; Upper Regional Unconformity) horizon represents the boundary between glacigenic deposits and the underlying sedimentary bedrocks, and is the lowest stratigraphic level studied in this work (Figure 4.2 & 4.3). The horizon is mapped in most parts of the study area, with exceptions in the Ingøydjupet Trough where the URU horizon is truncated by the seafloor (Figure 4.2). It is generally interpreted on a peak, but in some parts of the 3D-merge it is interpreted on a trough due to greater continuity (Figure 4.2). The amplitudes of the horizon varies from low to high, and its continuity is ranging from continuous to discontinuous (Figure 4.2 & 4.3). Generally, the horizon is continuous with a high amplitude in the southwestern and northern parts of the 3D-merge, while it is characterized by a discontinuous reflection with low amplitudes in the southern to central parts of the study area. The differences in the reflections are mostly caused by the variability in seismic resolution between the different datasets included in the 3D-merge.

The URU horizon generally mirrors the seafloor morphology, i.e. deeper parts are located in the area of the Bjørnøyrenna Trough, with depths between 700 and 650 ms, respectively, and shallower parts are observed on the surrounding bank areas, i.e. Nordkappbanken, Tromsøflaket and the outer Bjørnøyrenna sediment wedge. The depths are here around 440-500 ms (Figure 4.8).
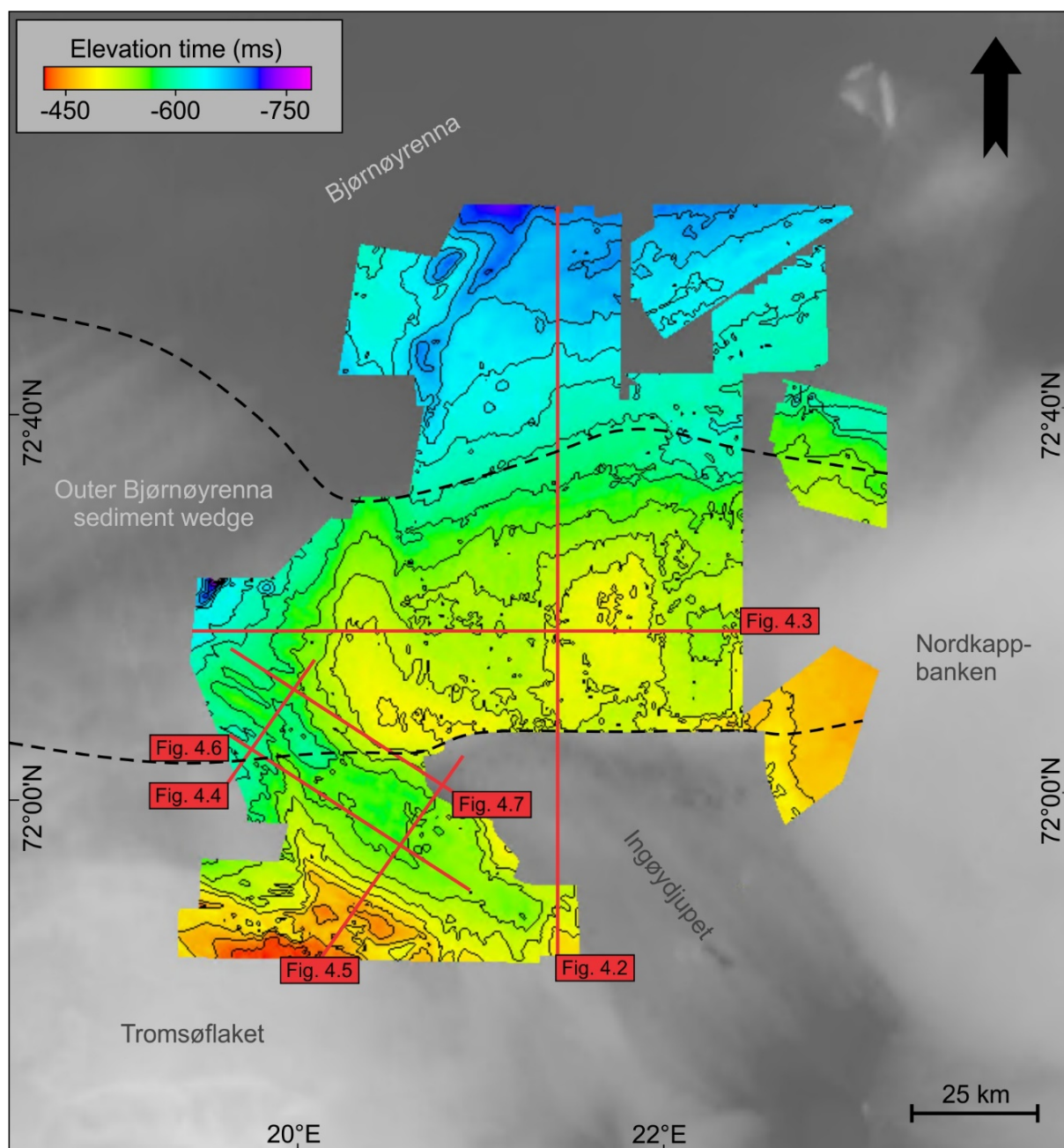
Figure 4.8 *– URU horizon with depths in milliseconds two-way travel time. Contour intervals are 20 milliseconds. Bathymetric map (grey shading) in the background where the black stippled lines indicate the outer Bjørnøyrenna sediment wedge.*

4.1.2 Seismic unit A

Seismic unit A is bounded by the base Quaternary and the seafloor horizon (Figure 4.2 & 4.3). Overall, the sediment distribution coincides with the seafloor morphology i.e. the unit has a greater thickness at the sediment accumulations on Tromsøflaket, Nordkappbanken and the outer Bjørnøyrenna sediment wedge, and a thinner sediment cover in the Ingøydjupet and Bjørnøyrenna Troughs (Figure 4.9).

A prominent depocenter is situated at the southeastern part of the Bjørnøyrenna Trough, where the thickness reaches 175 ms to 250 ms (Figure 4.9). This accumulation corresponds to the southeastern part of the outer Bjørnøyrenna sediment wedge. The thinnest sediment cover is found at the margins of the Ingøydjupet Trough and in the central parts of the Bjørnøyrenna Trough (between 20-50 ms) (Figure 4.9).

The internal seismic signature of unit A varies from medium- to low-amplitude reflections to a transparent configuration, and the continuity of the reflections vary from continuous to semi-continuous (Figure 4.2 & 4.3). Generally, the northern and western part of the 3D-merge has a seismic signature of medium- to low-amplitude reflections that are continuous to semi-continuous, while the southern central parts have a more transparent seismic signature (Figure 4.2 & 4.3).
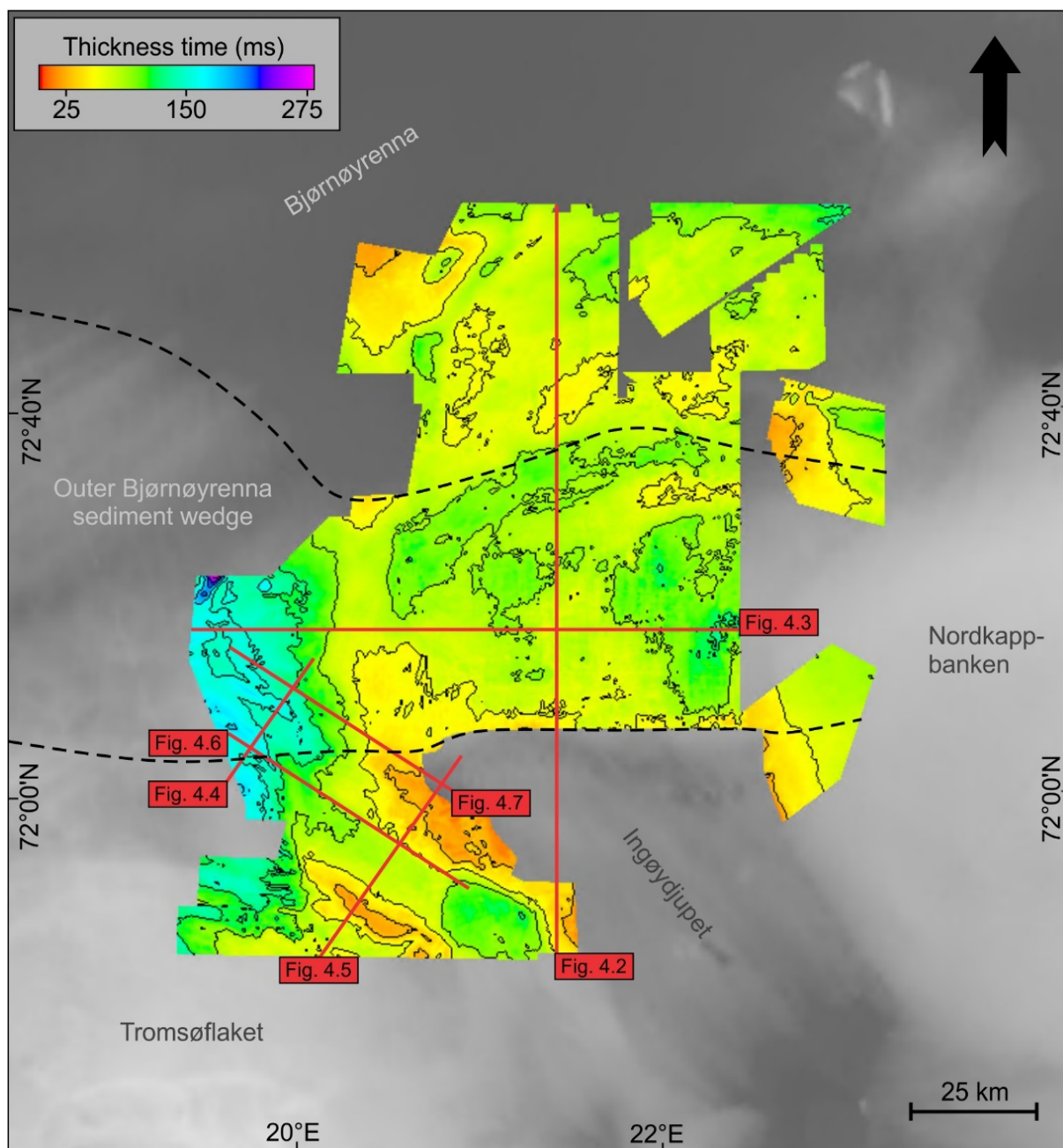
Figure 4.9 *– Isochore (thickness) map of seismic unit A, defined between the base Quaternary (URU) and the seafloor horizons. Sediment thickness is given in milliseconds two-way travel time. Contour intervals are 30 ms. Bathymetric map (grey shading) in the background where the black stippled lines indicate the outer Bjørnøyrenna sediment wedge.*

4.1.3 Seafloor horizon

The seafloor horizon is defined by a continuous trough reflection with high-to medium-amplitude (Figure 3.4b, 4.2 & 4.3). The depth in the Bjørnøyrenna and Ingøydjupet Troughs is between 625 and 500 ms. The surrounding bank areas and the sediment wedge are shallower, i.e. between 450 and 350 ms, respectively (Figure 4.10).
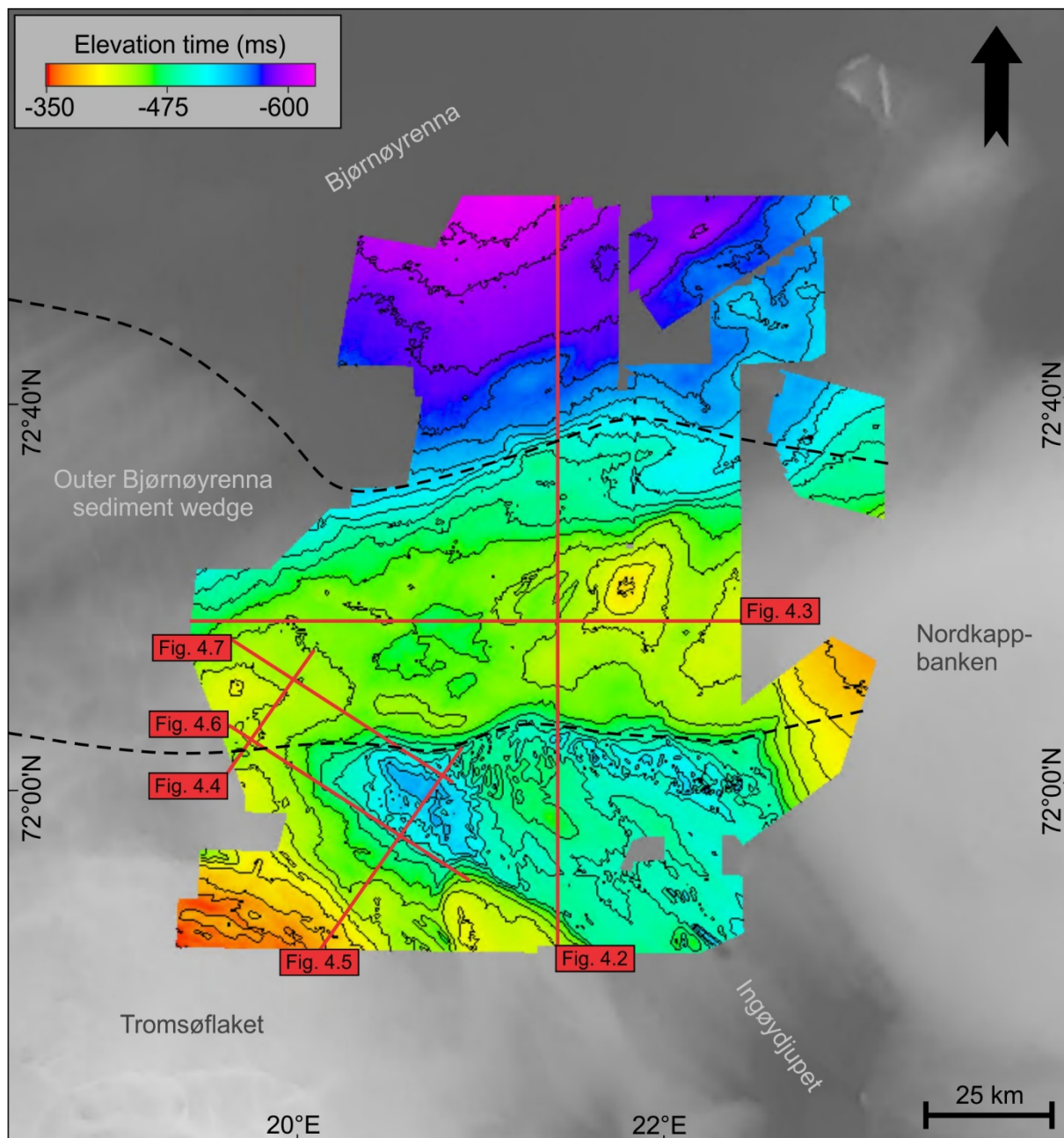
Figure 4.10 *– Seafloor horizon with depths in milliseconds two-way travel time. Contour intervals are 15 milliseconds. Bathymetric map (grey shading) in the background where the black stippled lines indicate the outer Bjørnøyrenna sediment wedge.*

52

4.2 Horizons and seismic units in Ingøydjupet (LN17001)

The TopSeis dataset (LN17001) is analyzed in the following chapters. The description includes seismic unit boundaries and seismic units, i.e. horizons and isochore maps. Furthermore, the morphology of the horizons is described in detail and their genesis is interpreted. Figure 4.11 & 4.12 summarizes the horizons and units interpreted in LN17001 and their extent in the study area.
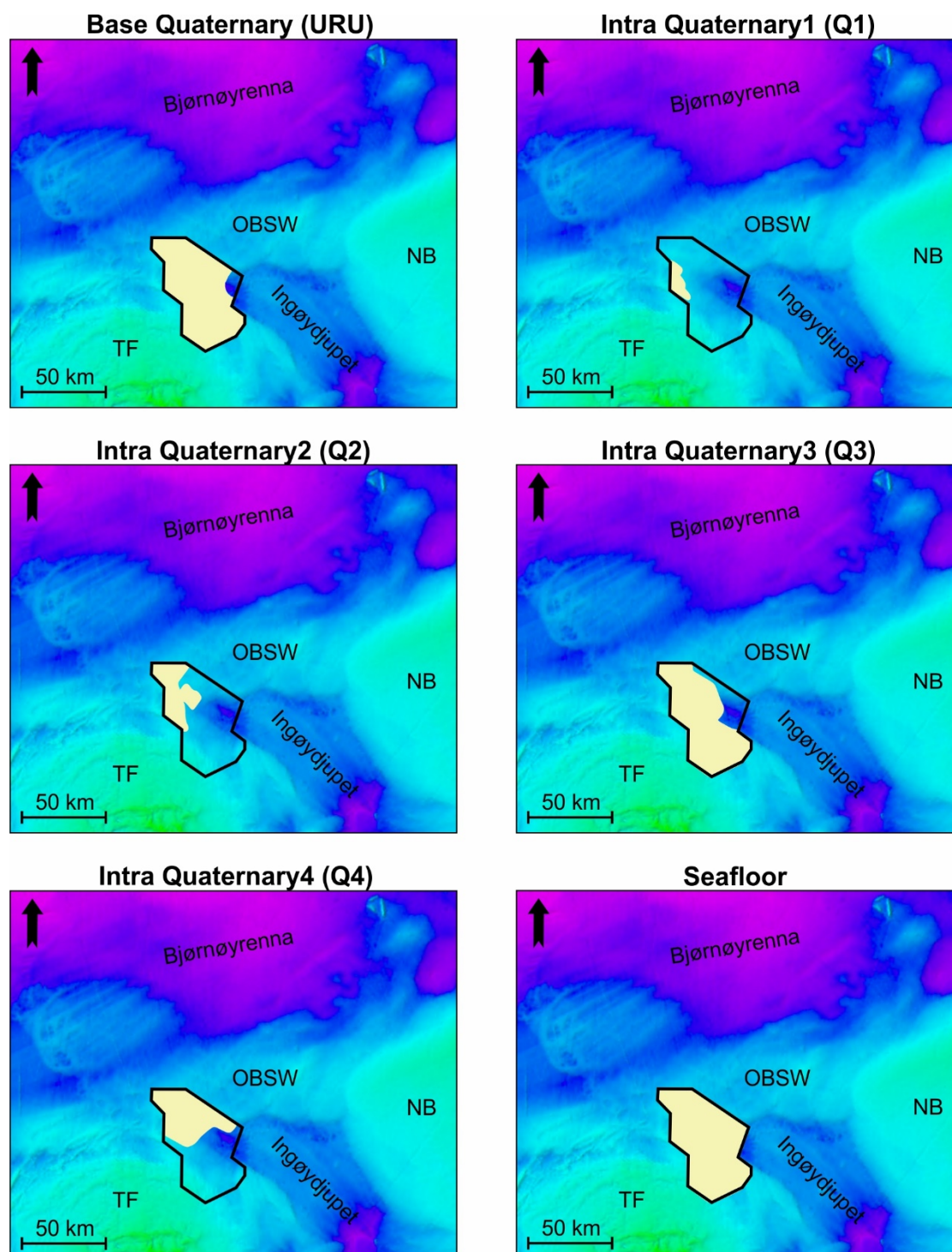
Figure 4.11 – (Page 53) Overview maps of the interpreted horizons in LN17001 (TopSeis) (Figure 4.1). Yellow color represents area of interpretation. Bathymetric map in the background.
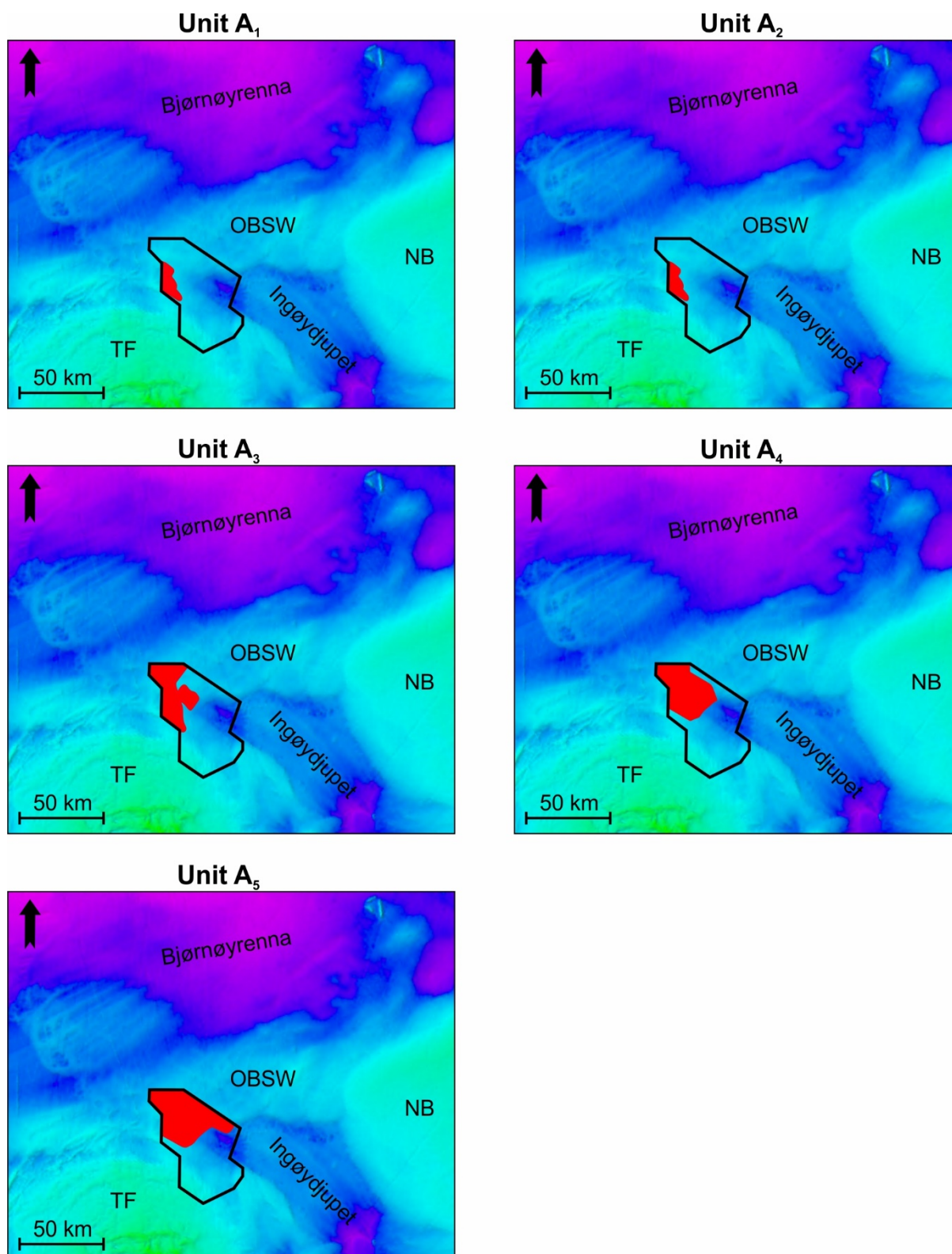
Figure 4.12 – Overview maps of the interpreted units in LN17001 (TopSeis) (Figure 4.1). Red color represents area of units. Bathymetric map in the background.

54

4.2.1 Base Quaternary horizon: URU

The Base Quaternary (URU) horizon is mapped in most parts of the dataset, except for in the northwestern part of the Ingøydjupet Trough where it is truncated by the seafloor (Figure 4.5, 4.7 & 4.11). The horizon is represented by a continuous peak reflection with high- to medium-amplitude (Figure 4.4-4.7).

The horizon is deepest in the northwest (between 620 and 580 ms), and shallower in the northeast and in the southern parts (between 500 and 440 ms) (Figure 4.13). The most prominent morphological features on the URU surface are the NW-SE trending paleo-trough, and the surrounding bank in the southwestern part of the surface (Figure 4.14a). These large-scale geomorphological features imply that fast-and slower-moving ice was present when URU formed, and that the paleo-ice flow direction was directed towards NW.

Lineations

Several sets of NW-SE trending lineations are observed in the paleo-trough (Figure 4.14b, 4.15a-b, 4.16a and c & 4.17a-c). The lineations can typically be followed 5 km, and the longest up to 15 km. They have widths between 300 and 500 m, and an elevation difference of 5 to 18 m. The spacing between them varies from 300 m to 3 km, where the lineations situated in the northern part of the paleo-trough have the largest spacing and elevation difference (Figure 4.15a-b).

Interpretation

The sets of lineations observed in the paleo-trough have the same orientation as the trough, supporting the indicated ice-flow direction towards NW (Figure 4.14). Based on their shape and geomorphology, these landforms are interpreted to be glacial bedforms produced by fast-flowing grounded glaciers, i.e. mega-scale glacial lineations (MSGL). MSGLs are typically identified within troughs where rapid ice-flow has been present. Similar features on buried horizons in the SW Barents Sea have been described and interpreted by several others (e.g. Rafaelsen et al., 2002; Andreassen et al., 2004; Bellwald et al., 2018).

Transverse ridges

Three transverse ridges trending in an NE-SW direction are situated in the southeastern part of the paleo-trough (Figure 4.14 & 4.17d). They have lengths varying between 3 and 5 km, widths of 1 to 1.5 km and a positive relief of 10 m. The ridges are relatively symmetrical in cross section (Figure 4.17e), and the spacing between them is approximately 1 km. Several transverse ridges also occur in the northeastern part of the paleo-trough (Figure 4.14 & 4.15a and c). They have the same orientation and are of similar size as the transverse ridges in the southeastern part of the trough.

Interpretation

The small transverse ridges in the southeastern and northeastern part of the trough have an orientation perpendicular to the glacial lineations, indicating that the ridges are deposited at the glacier front (Figure 4.14). These ridges are therefore interpreted to be moraines deposited at the glacier front, possibly during several small re-advances and/or stillstands during the deglaciation.

Linear depressions

Linear features with an NE-SW trend are found on the southern bank and in the southern part of the paleo-trough (Figure 4.14b & Figure 4.16a). They have a negative relief of 17 m, and they truncate underlying strata (Figure 4.16b). The depressions are up to 6 km long, 200 m wide and the spacing between them are from 100 to 500 m.

Interpretation

The linear depressions observed in the southern part of the paleo-trough and on the southern bank area are interpreted as linear iceberg plough-marks based on their geometry, orientation and extent (Figure 4.14). They are restricted to bank area and the shallower parts of the trough, possibly because of the increase in depth towards the trough and the increasing relief towards the bank area. Iceberg plough-marks often have a more or less random orientation, however, parallel sets may occur, formed by larger icebergs or by a set of icebergs trapped in a sea-ice floe which provides a uniform pattern of drift. Dowdeswell & Hogan (2016) have found similar sets of iceberg plough-marks on the northern Svalbard shelf, but of larger dimensions than the ones found in this study.
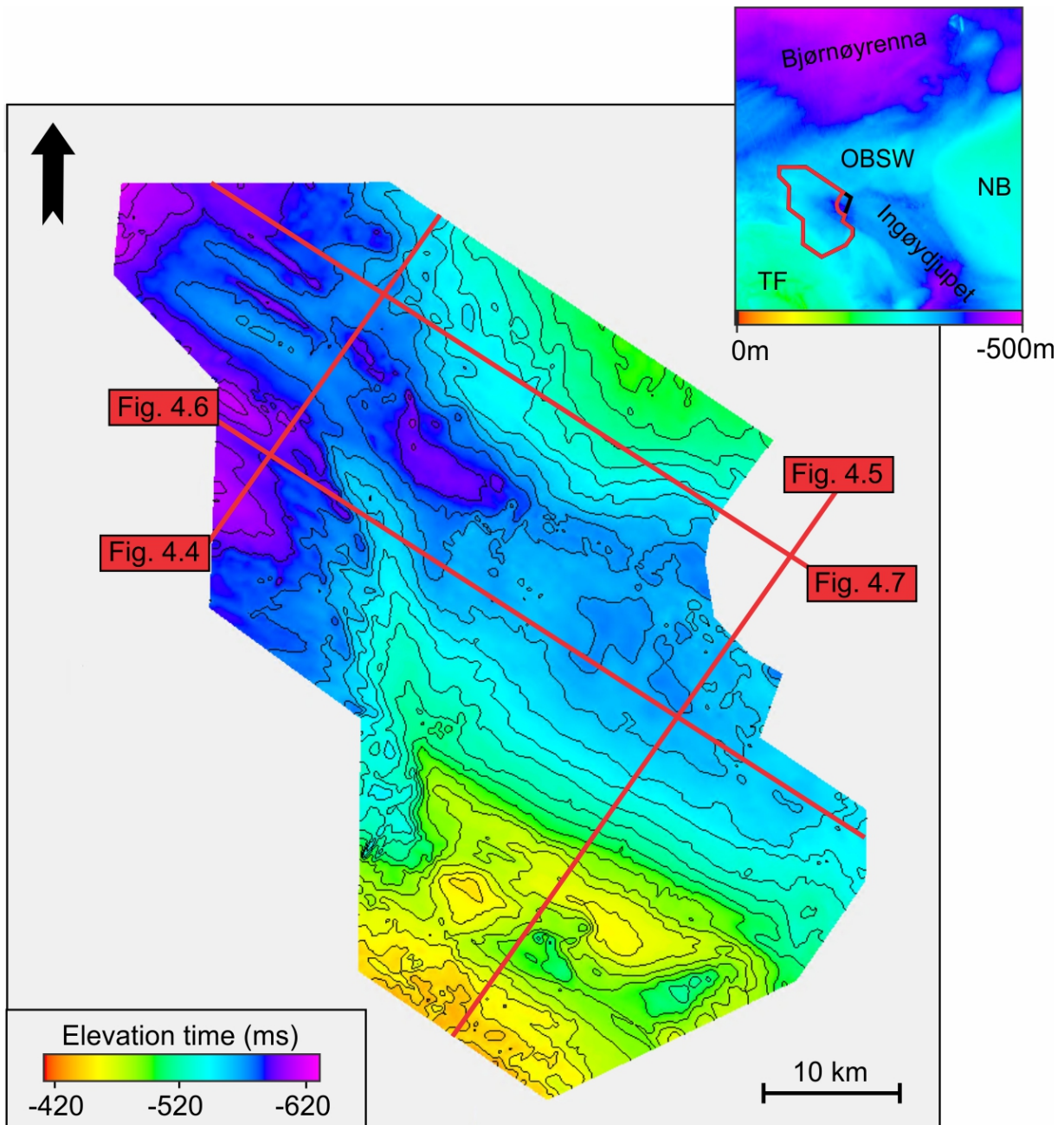
Figure 4.13 *– URU horizon with depths in milliseconds two-way travel time. The red polygon on the inset maps indicates the location of the horizon. Contour intervals are 10 milliseconds.*
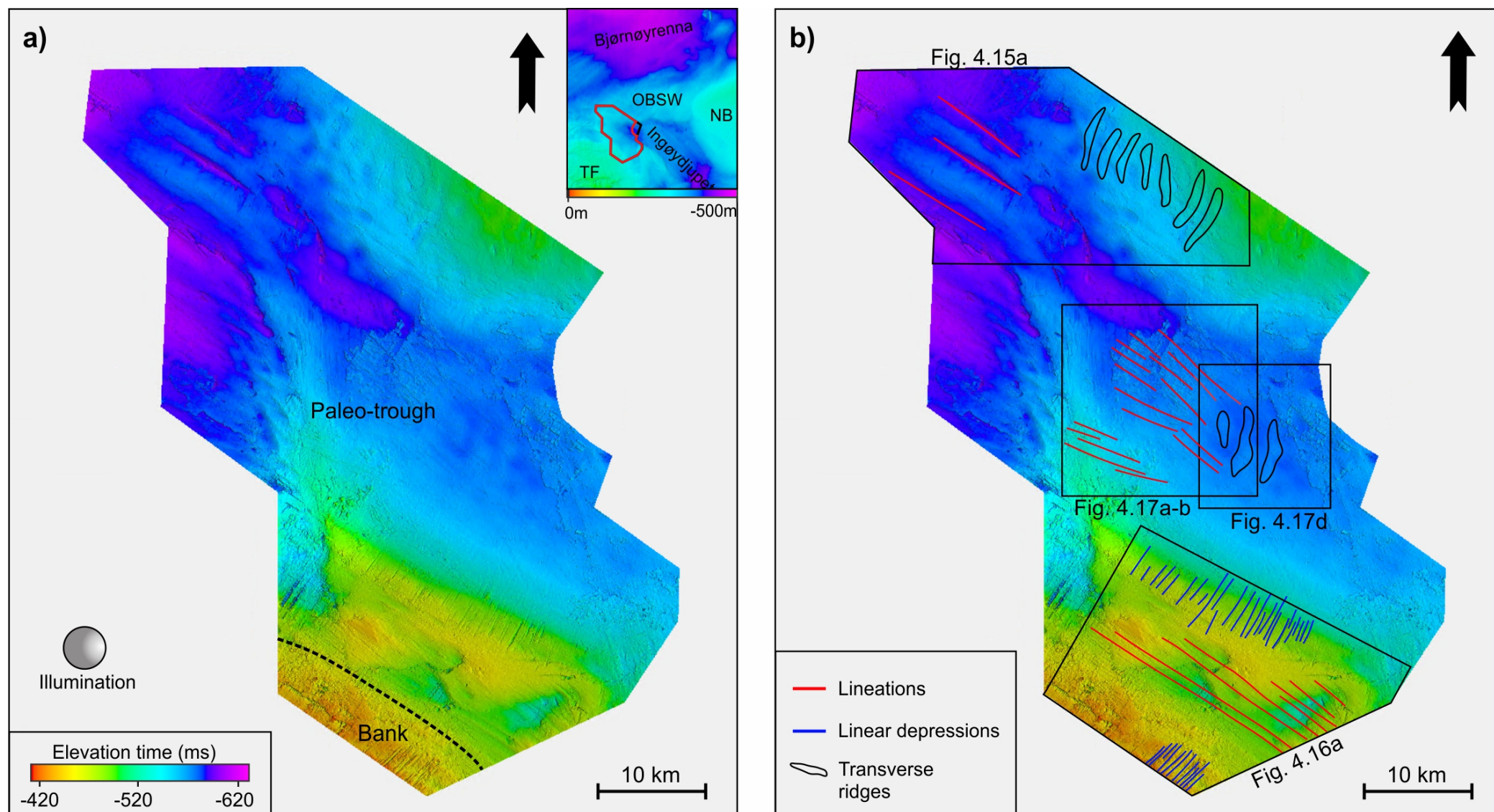
Figure 4.14 *– **a**) Overview of the URU surface of the LN17001 (TopSeis) dataset with a paleo-trough and surrounding bank area outlined by the black stippled lines. The location of the URU surface is indicated with a red polygon on the inset map. **b**) URU surface with interpreted morphological features. Black frames outline figure 4.15a, 4.16a and 4.17a, b and d.*
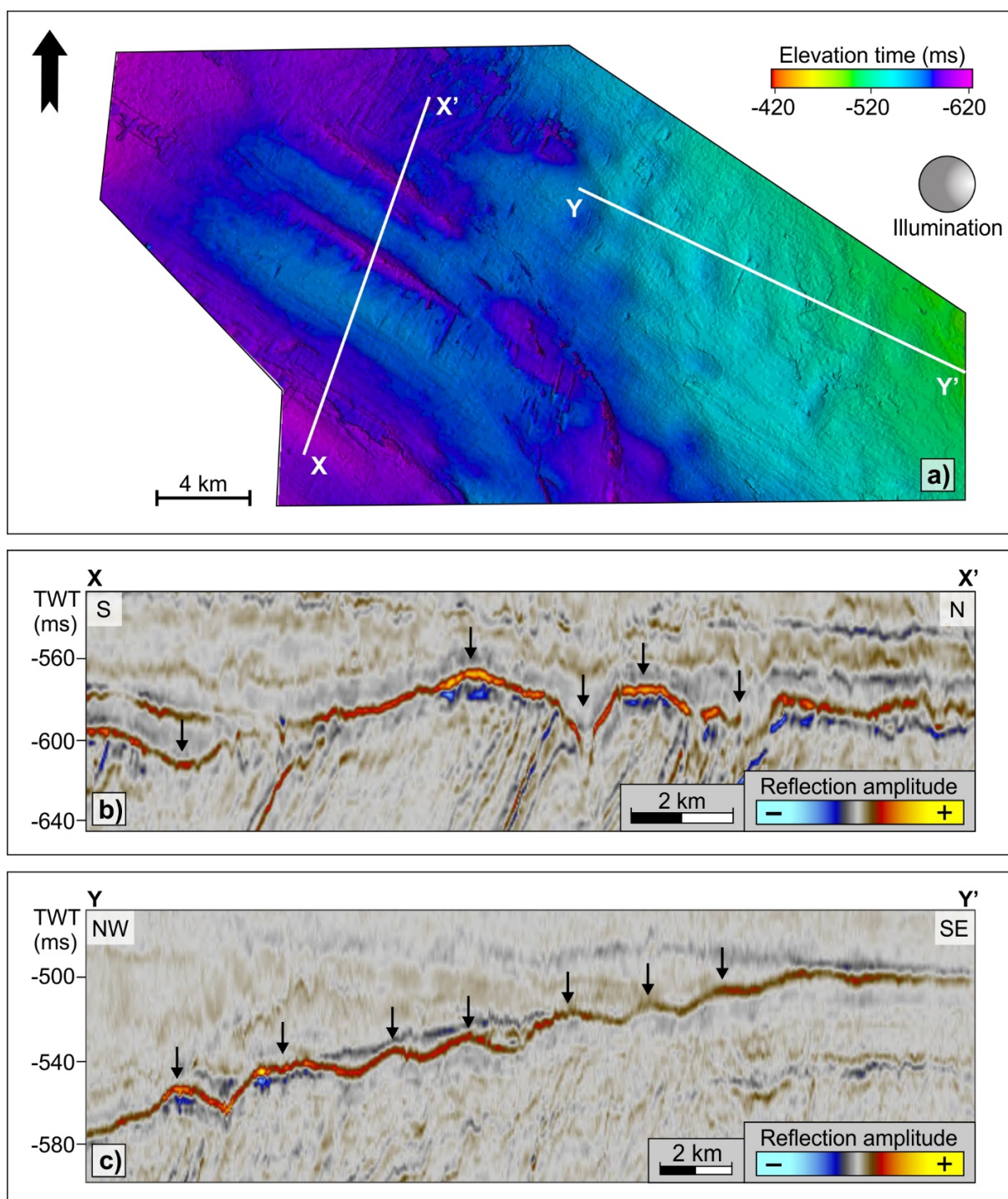
Figure 4.15 *– **a**) NW part of the URU surface featuring elongated heights, depressions and transverse ridges. White lines indicates the locations of the seismic profiles in b (X-X') and c (Y-Y'). **b**) Seismic profile across the elongated heights and depressions. **c**) Seismic profile across the transverse ridges.*
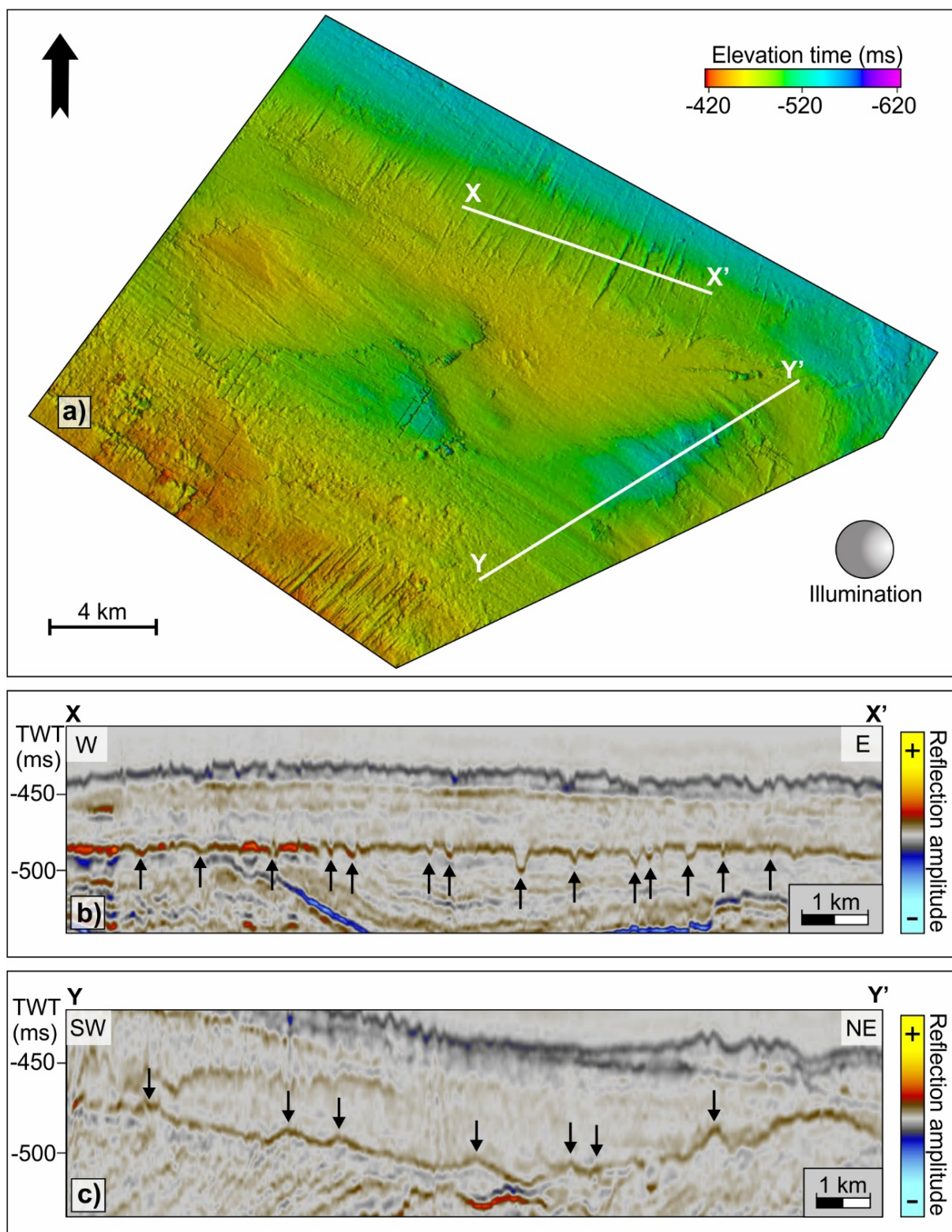
Figure 4.16 – *a*) *Southern part of the URU surface with streamlined landforms. White lines indicates the location of the seismic profiles in e (X-X') and f (Y-Y').* *b*) *Seismic profile across the parallel, elongated ridges.* *c*) *Seismic profile across the interpreted plough marks.*
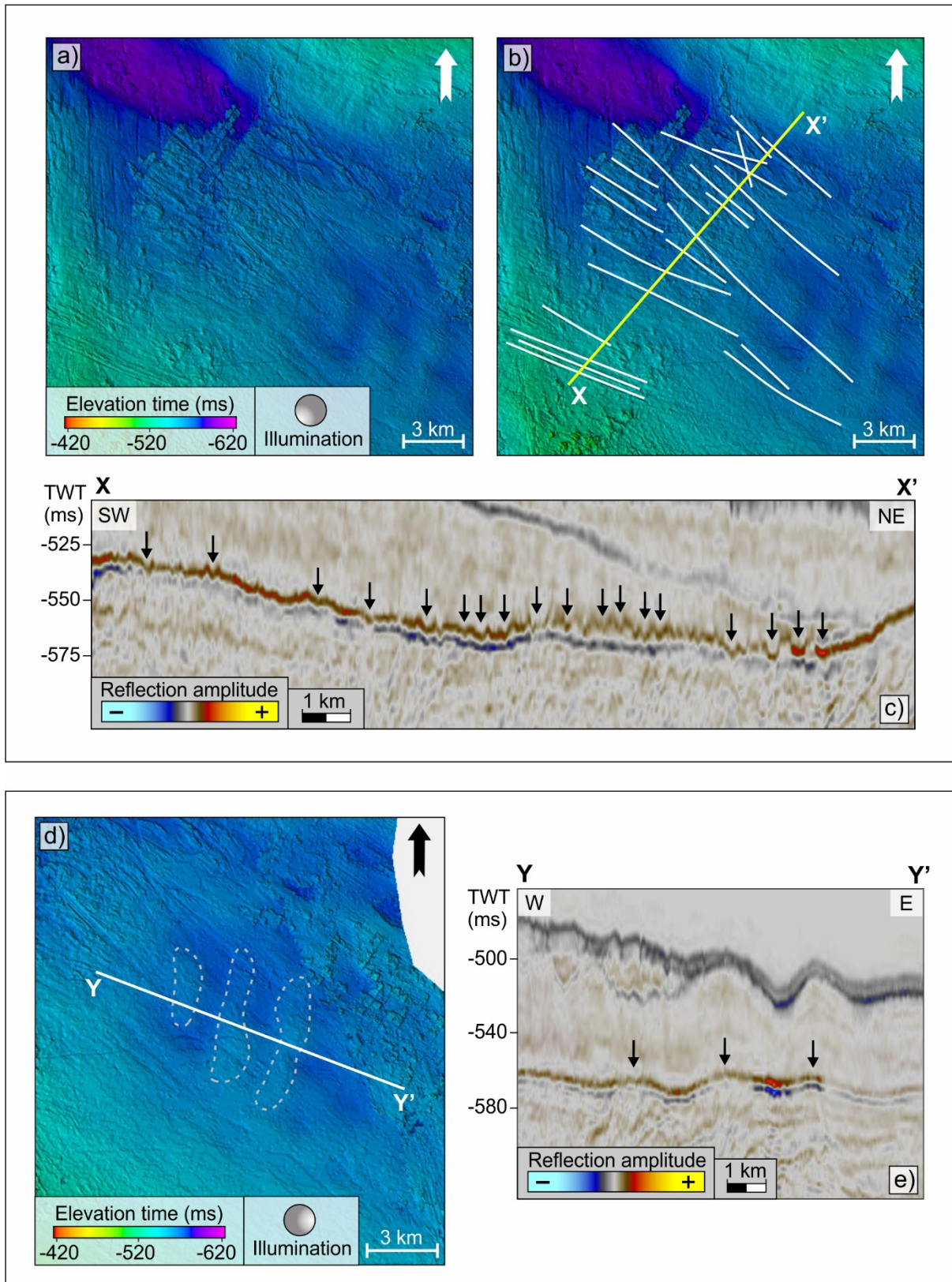
Figure 4.17 *– **a**) Central part of the paleo-trough displaying MSGL. **b**) Interpretation of the MSGL. Yellow line indicates the location of the seismic profile in c (X-X'). **c**) Seismic profile across the MSGL. **d**) URU surface with transverse ridges interpreted as moraines. White line indicates the location of the seismic profile in e (Y-Y'). **e**) Seismic profile across the transverse moraines.*

4.2.2 Seismic unit A_1

Seismic unit A_1 is confined by the base Quaternary (URU) and the intra Q1 horizons (Figure 4.4 & 4.6). In general, the unit is thin in the northern part (between 5 and 20 ms), and thicker in the southern part (25 to 40 ms), where four depocenters are situated (Figure 4.18). Generally, the sediment distribution can be correlated with the topography of the underlying horizon, with exception of the thinner accumulations in the north (Figure 4.13). The internal seismic signature of unit A_1 varies between semi-continuous, sub-parallel reflections of medium- to low amplitudes to transparent reflections (Figure 4.4 & 4.6).
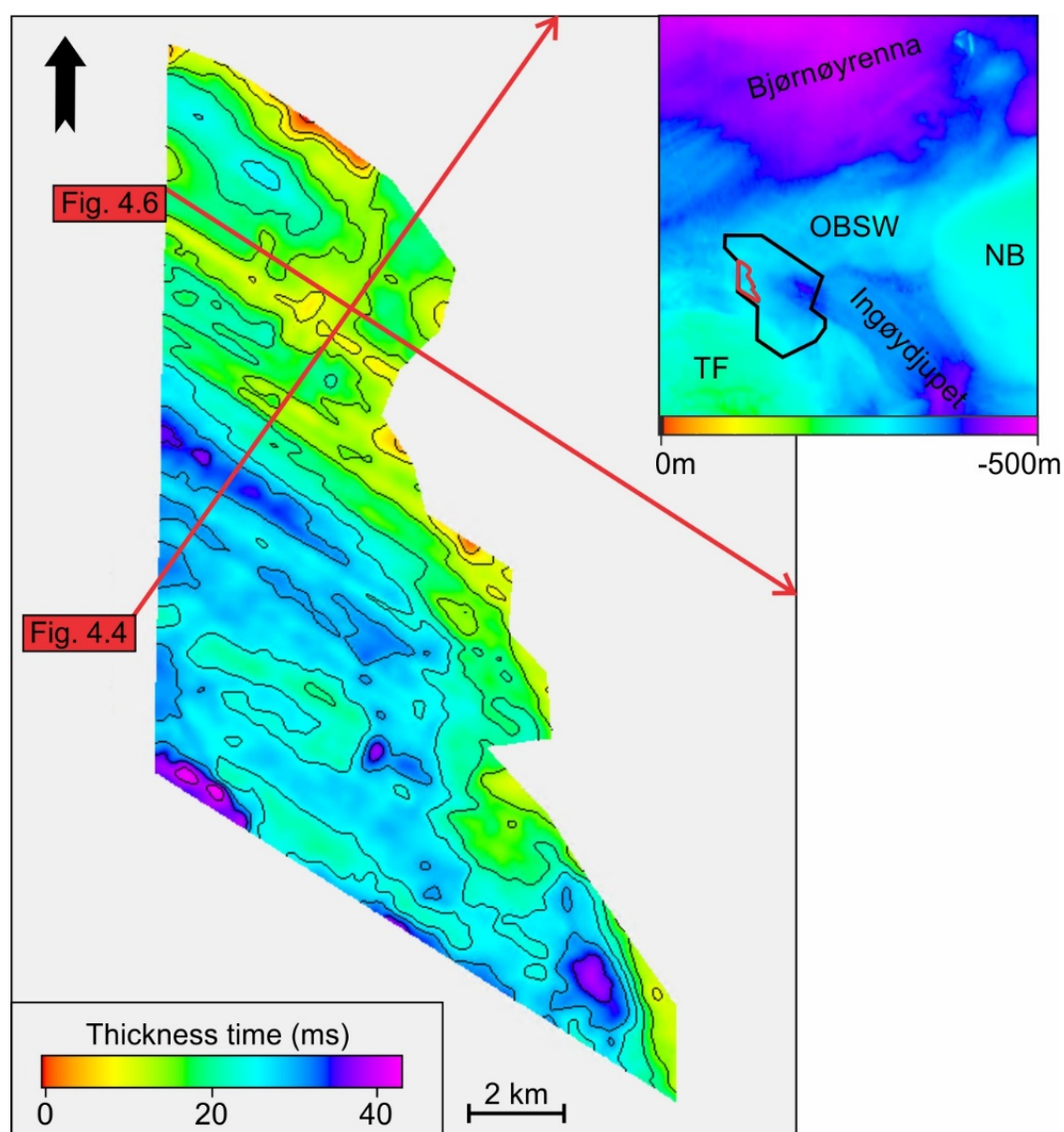
Figure 4.18 *– Isochore map of seismic unit A_1, defined by the URU and intra Q1 horizons. The red polygon on the inset map indicates the location of the unit. Sediment thickness is given in milliseconds two-way travel time. Contour intervals are 5 milliseconds. Red arrows indicate that the seismic lines continue outside the map.*

4.2.3 Intra Quaternary1 horizon

The intra Quaternary1 (intra Q1) horizon represents the top of seismic unit A_1 (Figure 4.4, 4.6 & 4.11). It is characterized by a continuous to semi-continuous peak reflection with high- to medium-amplitudes. In most areas, the intra Q1 horizon downlaps onto the URU horizon (Figure 4.4), with exceptions in some areas where it onlaps onto the URU horizon (Figure 4.6). The horizon represents a gentle northwest dipping paleosurface (Figure 4.19), where the deepest parts occur in the northwestern part, at a depth of 590 ms, while the shallowest area is found in the southeastern part, at a depth of about 530 ms.

Lineations

Lineations consisting of ridges and furrows trending in an NW-SE direction characterize the morphology of the intra Q1 surface (Figure 4.20 & 4.21a-b). The linear features are best developed in the deepest areas of the surface, i.e. in the central and northern part. The lineations generally have a U-or V-shape in cross section (Figure 4.21b), and the elevation difference is up to 12 m. They have lengths varying between 5 and 9 km, and they most likely continue outside the surface. The width of the furrows are between 100 and 300 m, while the width of the ridges have a larger variability, i.e. from 100 to 800 m.

Interpretation

The morphology of the elongated ridge-furrow features are similar to the streamlined features described and interpreted earlier. These features are therefore interpreted to be MSGL, which implies an ice-flow direction towards NW.

Curvilinear furrows

Elongated and curvilinear furrows with a general NW-SE orientation can be observed overprinting some of the ridges (Figure 4.20 & 4.21a). The furrows are U- or V-shaped in cross sections, with levees at their sides (4.21c), and have a negative relief of 10 m. They can be followed up to 4 km and have maximum widths of 150 m.

Interpretation

The curvilinear furrows overprinting the MSGL are interpreted to represent iceberg plough-marks. This is based on their more or less random appearance, as well as their geomorphology and extent. The plough-marks are generally found on the elongated ridges and in the shallower

63

areas of intra Q1. This is probably because the water was too deep in the northern part for the iceberg-keels to reach the seafloor at that time. The iceberg plough-marks overprints the MSGL, indicating that they are the youngest feature, and they likely originate from calving glaciers during a withdrawal of the glacier from the continental shelf. Rafaelsen et al. (2002) have described similar features on a buried glacigenic horizon in the surrounding area.
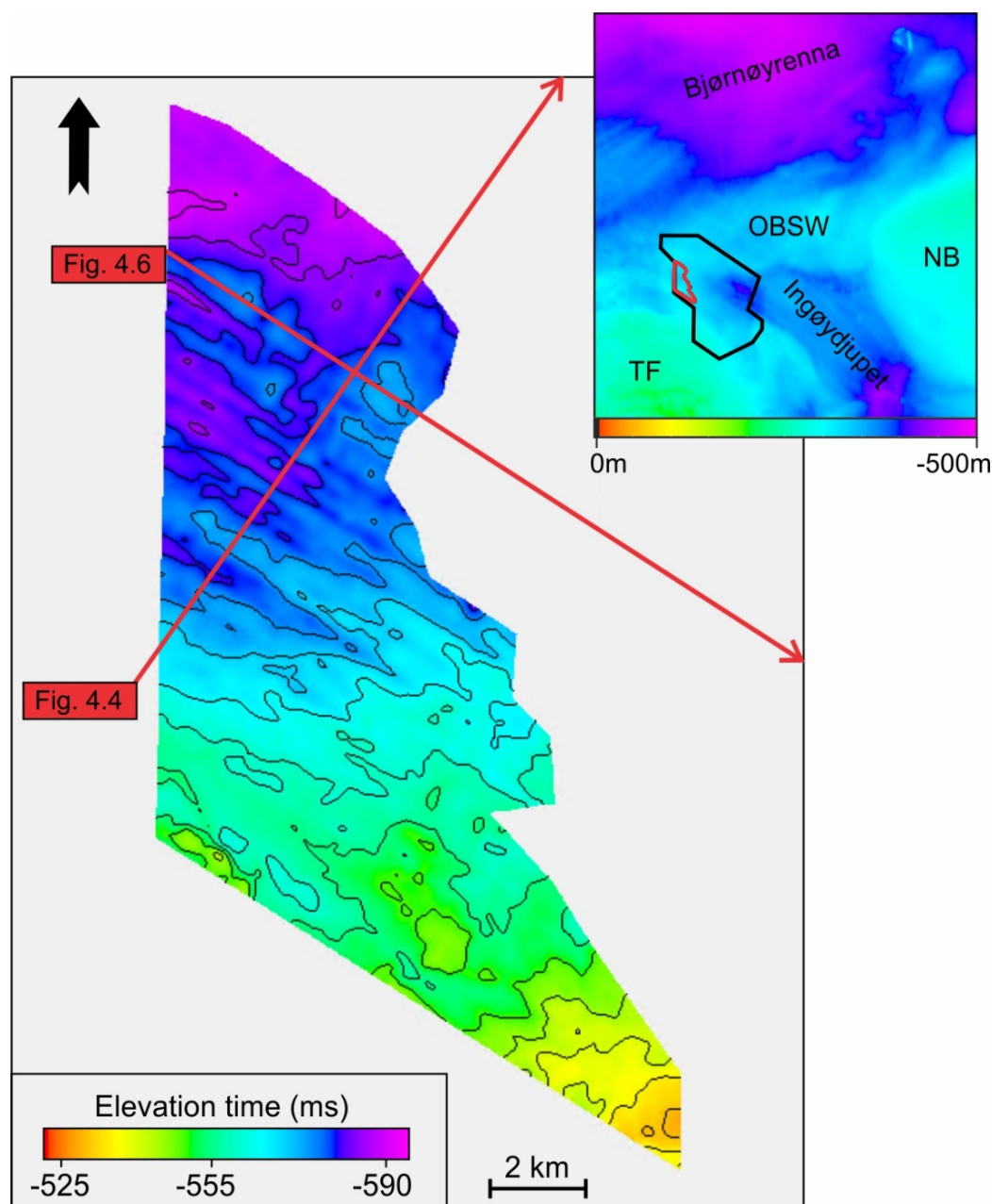
Figure 4.19 *– Intra Q1 horizon with depths in milliseconds two-way travel time. The red polygon on the inset maps indicates the location of the horizon. Contour intervals are 5 milliseconds. Red arrows indicate that the seismic lines continue outside the map.*
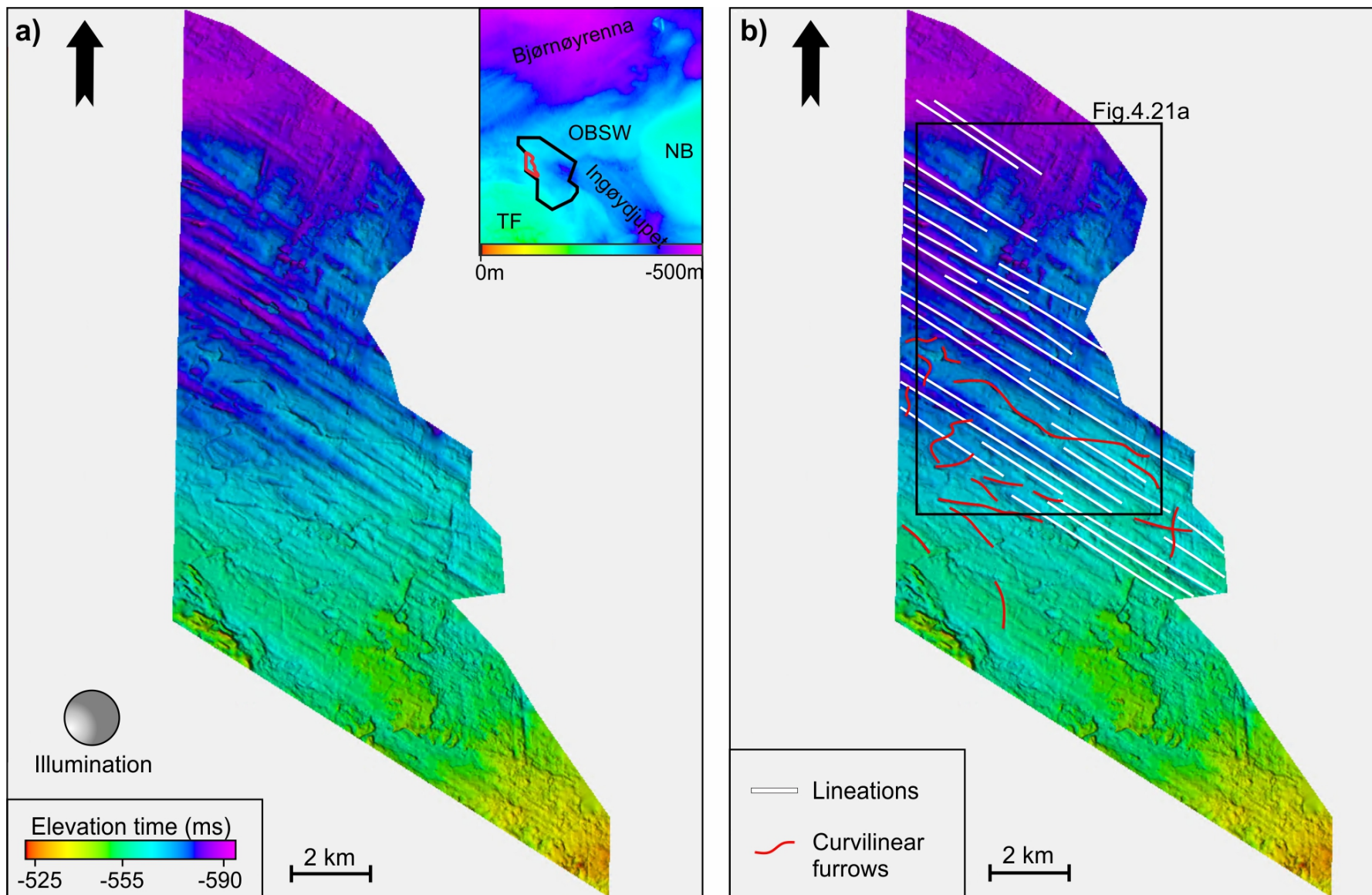
Figure 4.20 – **a)** *Overview of the intra Q1 surface with streamlined landforms. The location of the intra Q1 surface is indicated with a red polygon on the inset map.* **b)** *Intra Q1 surface with interpreted morphological features. Black frame outline figure 4.21a.*
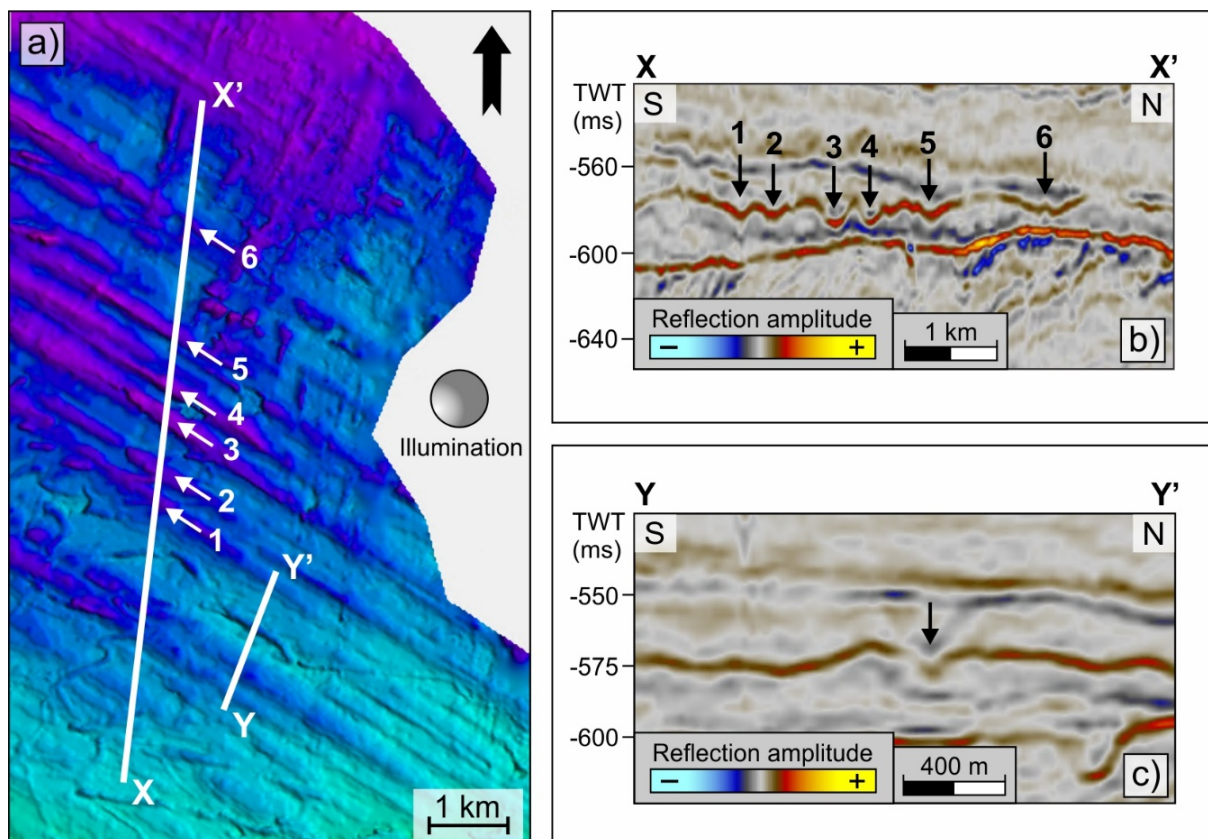
Figure 4.21 *–* ***a)*** *Intra Q1 with elongated ridge-groove features interpreted as MSGL (1-6) and iceberg plough marks. White lines indicates the location of the seismic profiles in b (A-A') and c (B-B').* ***b)*** *Seismic profile across the MSGLs (1-6).* ***c)*** *Seismic profile across the iceberg plough mark.*

4.2.4 Seismic unit A$_2$

Seismic unit A$_2$ is bounded by the intra Q1 and the intra Q2 horizons (Figure 4.4 & 4.6). Generally, the unit is thin in the northern part and along the southeastern margins (10 ms), and gradually thicker towards southwest, where one depocenter is situated (50 ms) (Figure 4.22). The morphology of the underlying intra Q1 horizon appears to have been of minor importance for the sediment distribution, as the depocenter is located in the shallower parts of the horizon (Figure 4.19). Semi-continuous, sub-parallel reflections of medium- to low-amplitudes characterize the internal seismic signature of unit A$_2$ (Figure 4.4 & 4.6).
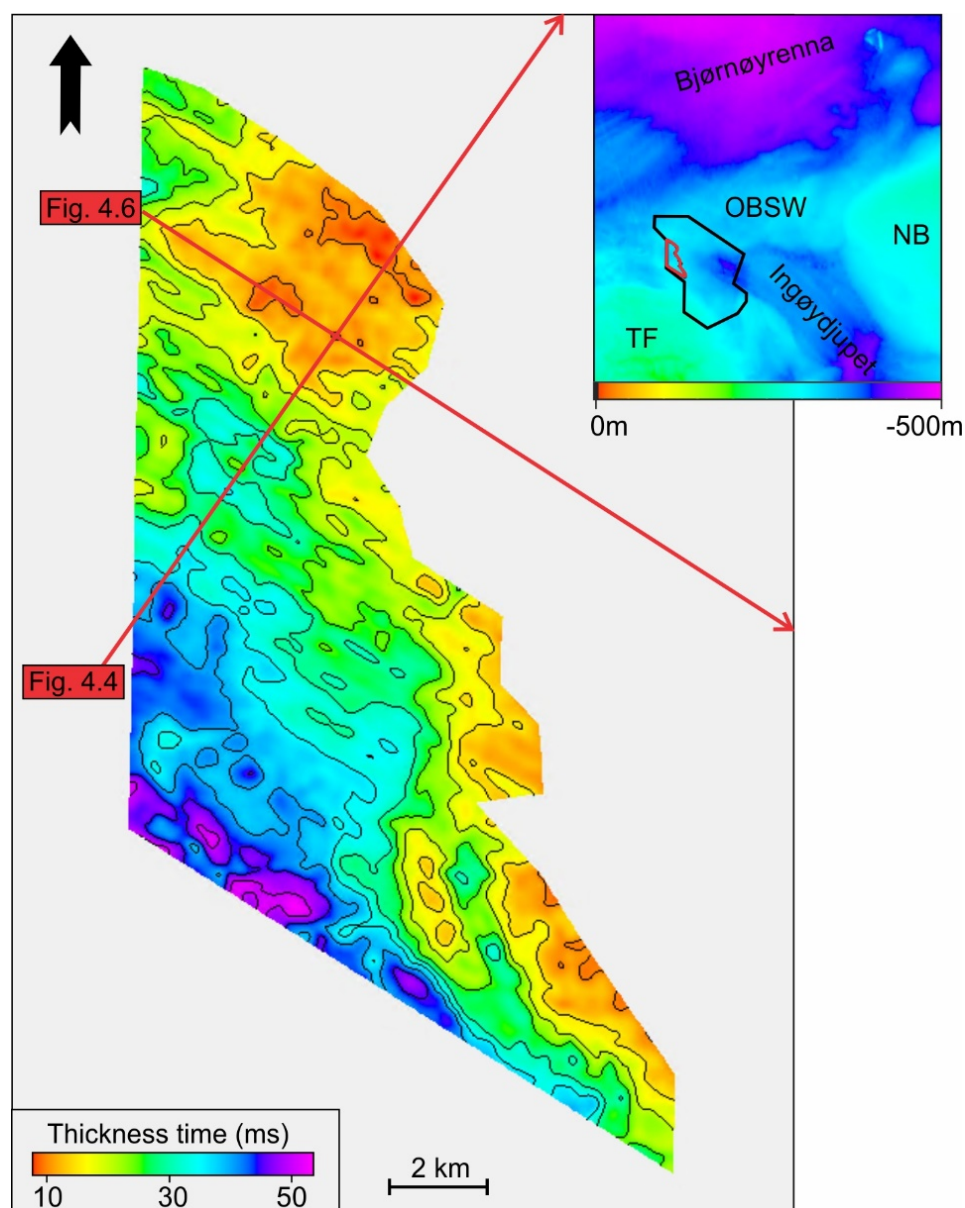
Figure 4.22 *– Isochore map of seismic unit A$_2$, defined by the intra Q1 and intra Q2 horizons. The red polygon on the inset map indicates the location of the unit. Sediment thickness is given in milliseconds two-way travel time. Contour intervals are 5 milliseconds. Red arrows indicate that the seismic lines continue outside the map.*

4.2.5 Intra Quaternary2 horizon

The intra Quaternary2 (intra Q2) horizon represents the top of seismic unit A_2 (Figure 4.4, 4.6, 4.7 & 4.11). The horizon is mostly characterized by a continuous peak reflection, with medium- to low-amplitudes. Generally, the intra Q2 downlap onto the underlying URU horizon (Figure 4.4 & 4.7). The horizon is an irregular paleosurface (Figure 4.23). The deepest part of the horizon is found in the northwestern part and at some locations in the central part (approximately 590 ms), while the shallowest part occurs in the southernmost area (500 ms) (Figure 4.23).

Lineations

The morphology of intra Q2 is generally dominated by lineations consisting of ridges and furrows (Figure 4.24 & 4.25). The majority of the lineations are trending in an NW-SE direction, but the ones located in the northern part are trending in an NE-SW direction (Figure 4.24), where the latter is overprinted by the NW-SE oriented lineations. The lineations can typically be followed 3-4 km, and the longest ones up to 10 km. Their width is up to 200 m and the elevation difference is 5 m.

Interpretation

The lineations display similar characteristics as the lineations described earlier on the URU and intra Q1 horizons, and are therefore interpreted as MSGL. The different orientation of the MSGL are interpreted to represent lineations formed by different ice-streams, i.e. paleo-ice streams in the Bjørnøyrenna and Ingøydjupet Troughs. A further discussion will be done in chapter 5.
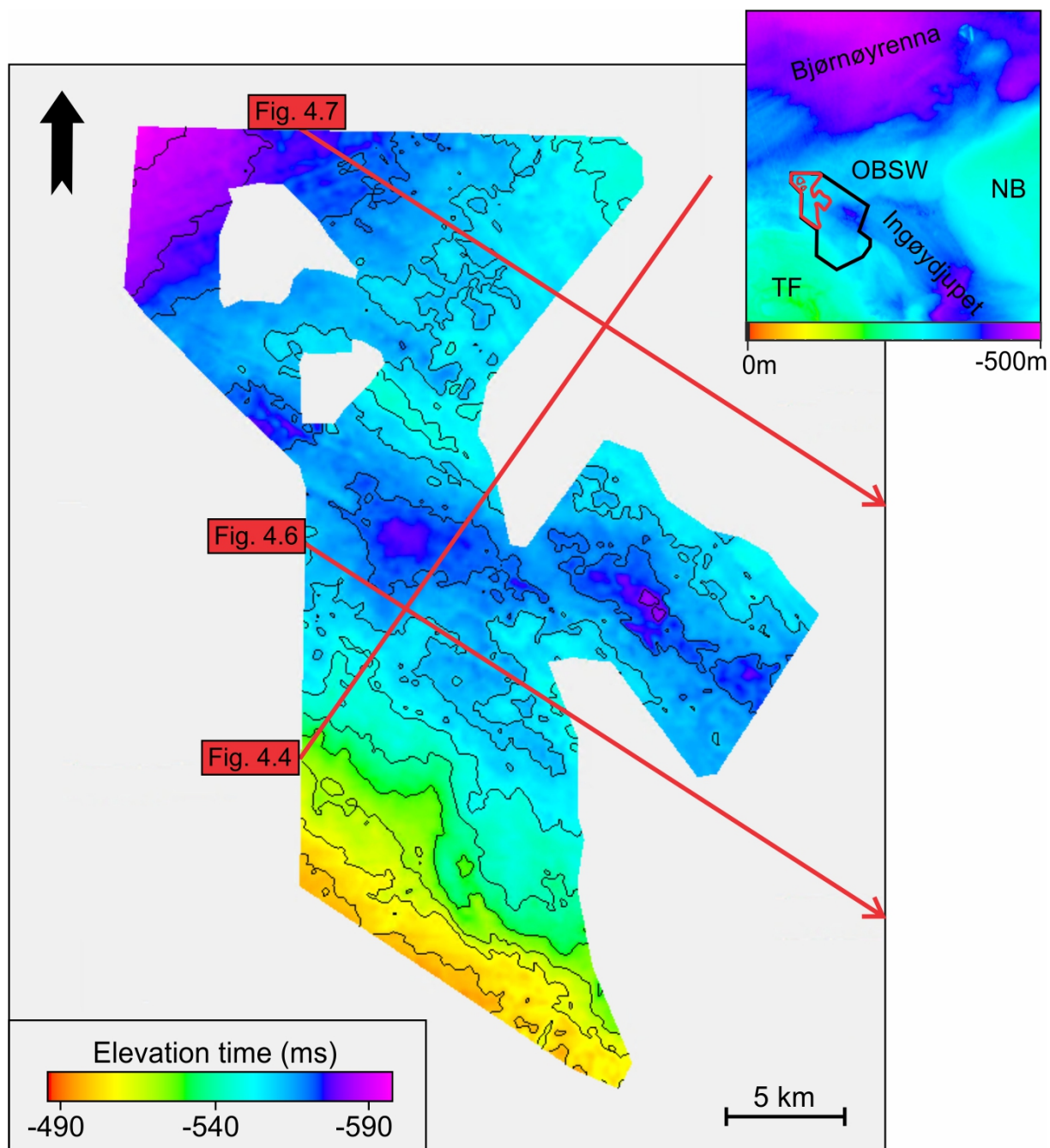
Figure 4.23 *– Intra Q2 horizon with depths in milliseconds two-way travel time. The red polygon on the inset maps indicates the location of the horizon. Contour intervals are 10 milliseconds. Red arrows indicate that the seismic lines continue outside the map.*
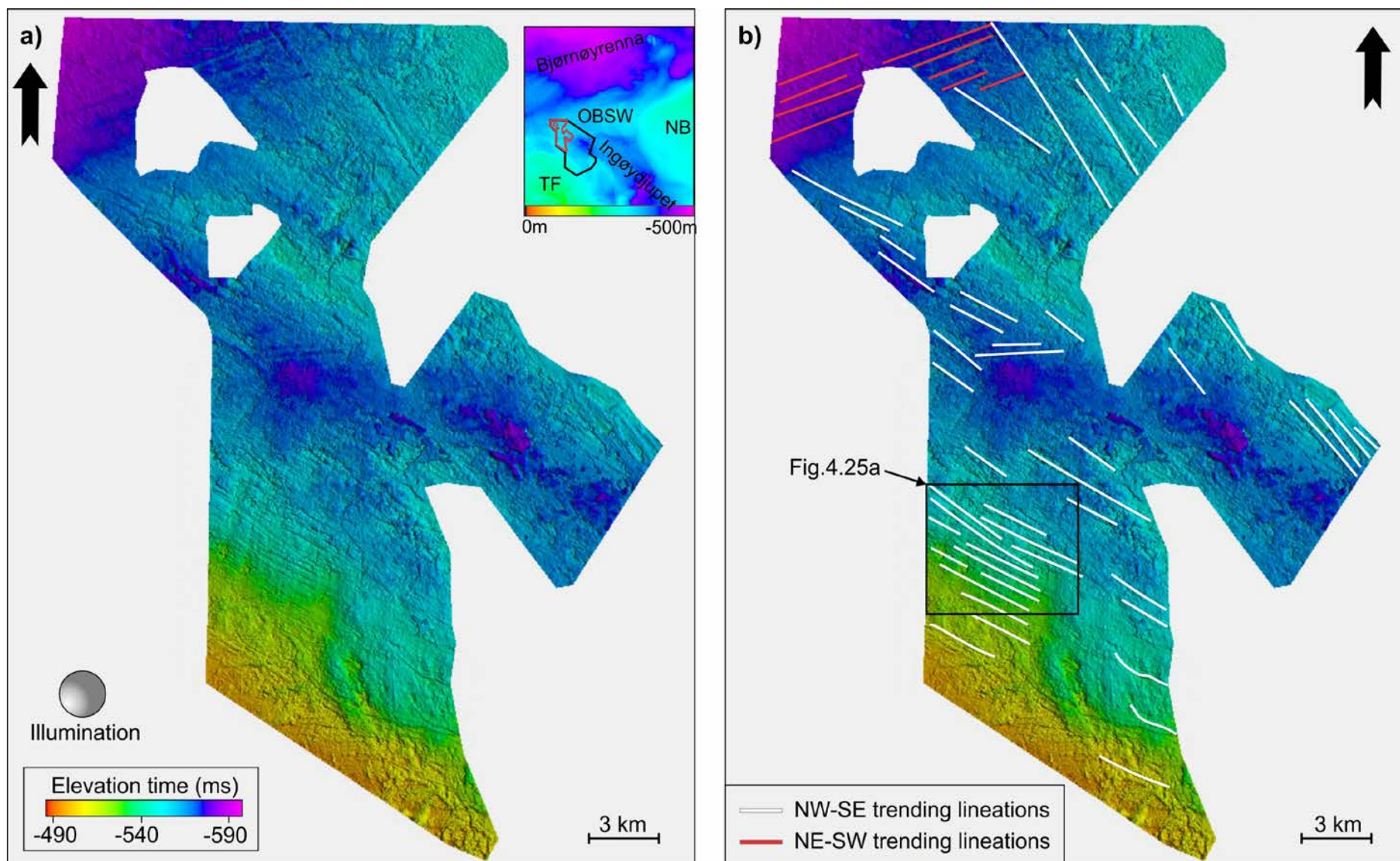
Figure 4.24 – **a**) *Overview of the intra Q2 surface with streamlined landforms. The location of the intra Q2 surface is indicated with a red polygon on the inset map.*
b) *Intra Q2 surface with interpreted lineations. Black frame outline figure 4.25a.*
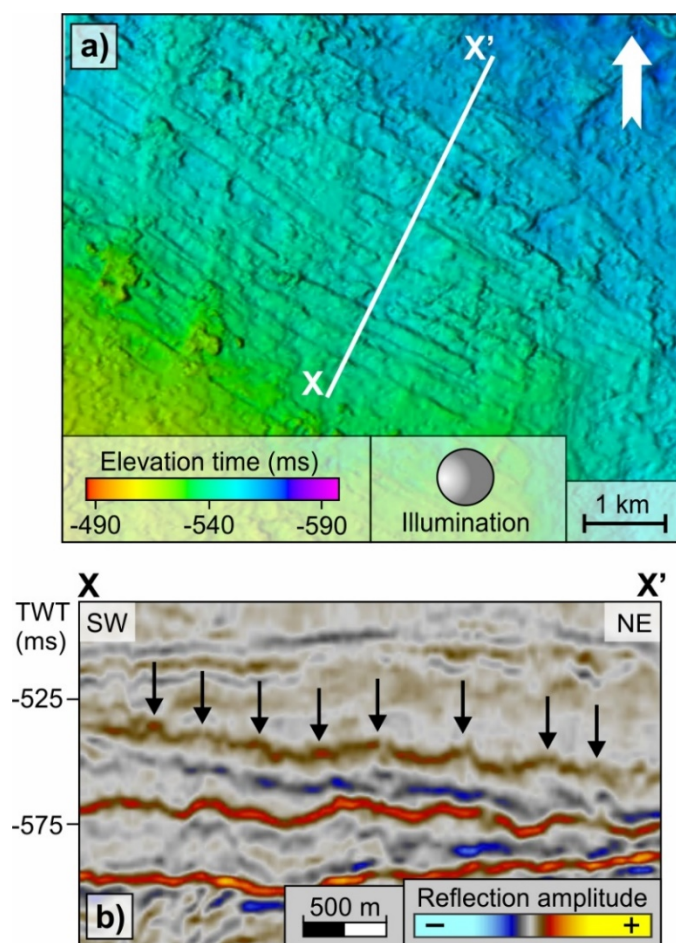
Figure 4.25 – ***a)*** *Southern part of the intra Q2 displaying MSGLs. White line indicates the location of the seismic profile in c (X-X'). **b)** Seismic profile across the MSGLs.*

4.2.6 Seismic unit A$_3$

Unit A$_3$ is defined by the intra Q2 and the intra Q3 horizons (Figure 4.4, 4.6 & 4.7). Generally, the unit is thin in the northeastern part (between 5-15 ms) and thicker in the southern part, where two prominent depocenters are situated, reaching a thickness of 65 ms (Figure 4.26). The sediment distribution can mostly be correlated with the underlying horizon i.e. the depocenters are situated in the deeper parts of intra Q2 (Figure 4.23).

The internal seismic signature of unit A$_3$ consists of semi-transparent reflections of medium- to low-amplitudes (Figure 4.4, 4.6 & 4.7). However, segments of a higher amplitude reflection are observed within the unit (Figure 4.28b and d). These segments appear as darks areas on the timeslice (Figure 4.27) and brighter areas in the RMS amplitude map (Figure 4.28a) generated over a specific volume indicated in Figure 4.28c and e. The sediment blocks have an areal extent

up to 1 km^2. Based on the description, the segments may represent sediment blocks of a different lithology compared to the surrounding sediments i.e. higher product of density and velocity.
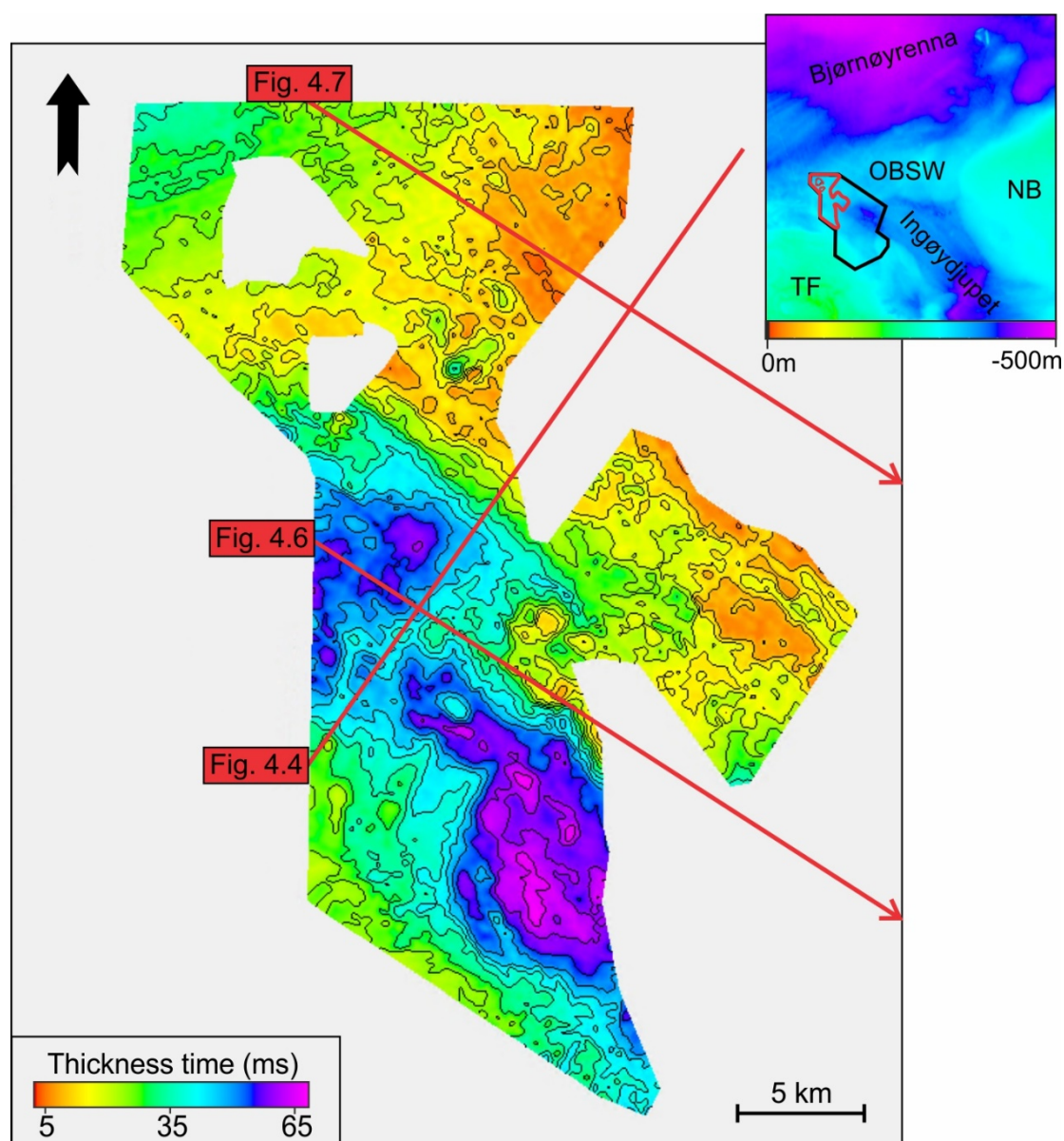
Figure 4.26 *– Isochore map of seismic unit A$_3$, defined by the intra Q2 and intra Q3 horizons. The red polygon on the inset map indicates the location of the unit. Sediment thickness is given in milliseconds two-way travel time. Contour intervals are 5 milliseconds. Red arrows indicate that the seismic lines continue outside the map.*
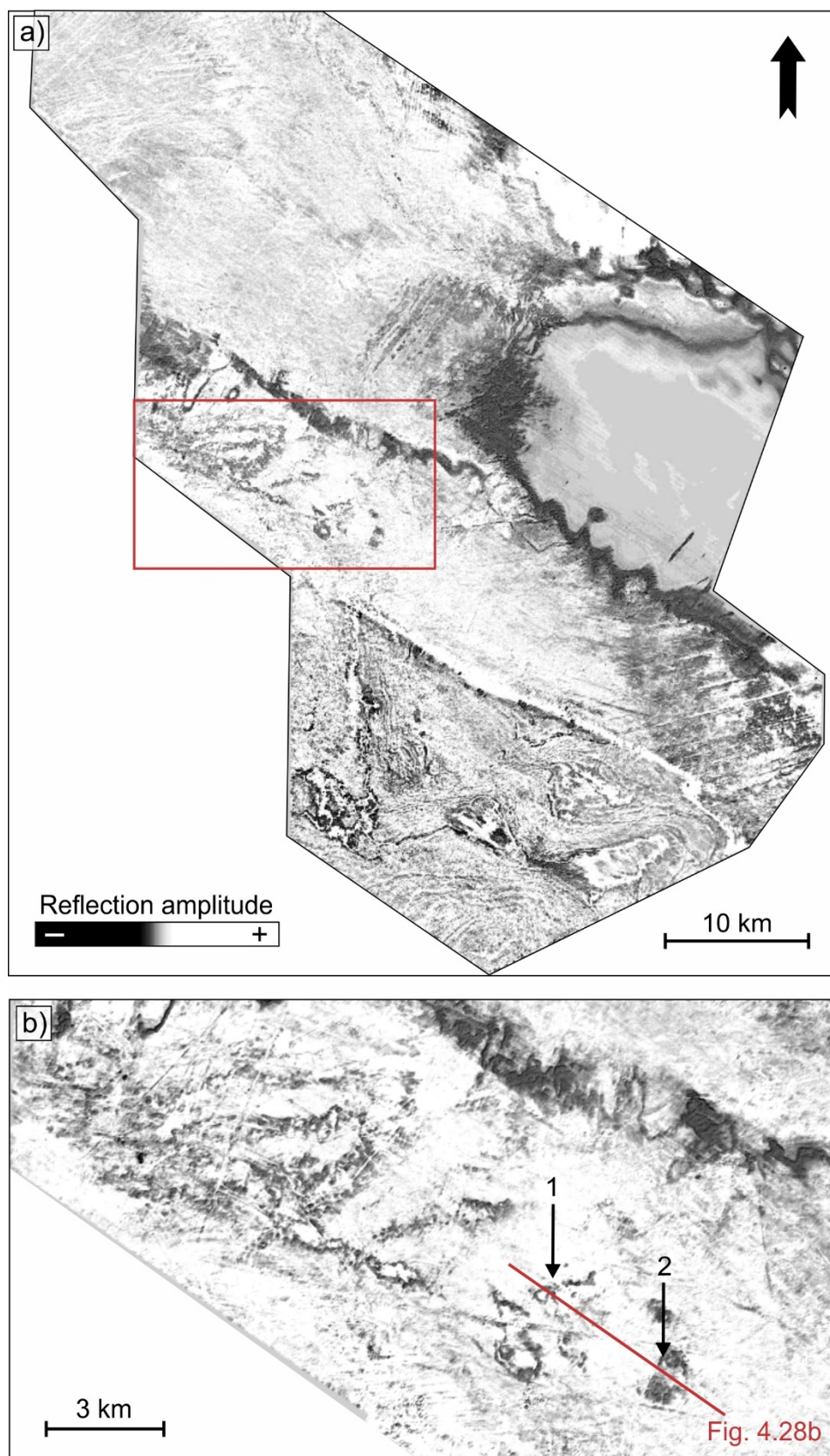
Figure 4.27 – **a)** *Regional timeslice trough unit A₃. Its position is marked with a black stippled line in figure 4.28c. Red frame outlines figure b.* **b)** *Zoomed in area displaying segments of higher amplitude reflection. Red line indicates the location of the seismic profile in figure 4.28b.*
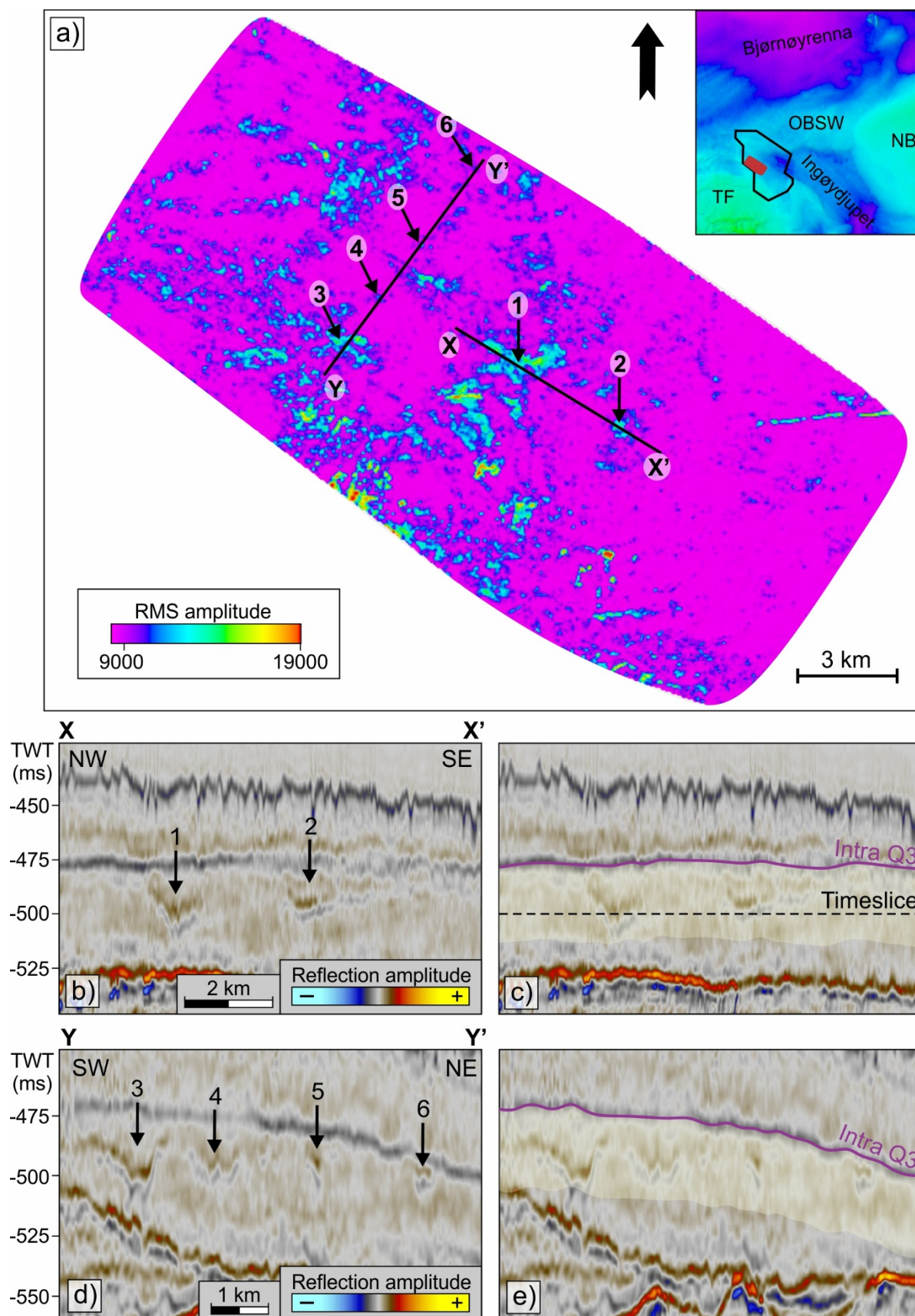
Figure 4.28 – a) RMS seismic amplitude map for the volume with yellow shading in c and d, showing segments in unit A₃ with higher RMS amplitude than surrounding sediments. Lines indicates seismic profiles of b, c, d and e. b) Seismic profile showing high amplitude reflection segments within unit A₃. c) Seismic profile displaying the zone (shaded yellow color) of the RMS volume and the position of the timeslice in figure 4.27. d) Seismic profile showing high amplitude reflection segments within unit A₃. e) Seismic profile displaying the zone of the RMS volume.

4.2.7 Intra Quaternary3 horizon

The intra Quaternary3 (intra Q3) horizon represents the top of seismic unit A_3 (Figure 4.4-4.7 & 4.11) and is characterized by a continuous to semi-continuous trough reflection, with high- to low-amplitudes. The horizon downlap onto the URU horizon in the northern part (Figure 4.4 & 4.7), and is truncated by the seafloor in the southern part (Figure 4.5), while in the central part of the dataset, the intra Q3 horizon is parallel to sub-parallel with the over- and underlying horizons (Figure 4.6).

The horizon displays a north dipping paleosurface (Figure 4.29). The deepest parts are situated in the northern part of the surface (between 530 and 560 ms), and shallower in the southern area (around 400 ms). The most prominent morphological features on the intra Q3 surface are the NW-SE trending paleo-trough and the surrounding bank in the southwestern part of the surface (Figure 4.30a).

Large- and small-scale lineations

Large-scale, elongated grooves trending in an NW-SE direction are observed in the central and southern part of the paleo-trough (Figure 2.30 & 4.31a.). They have lengths varying between 7 and 25 km, and some seem to continue outside the data coverage. The grooves have widths of 1 km, and a negative relief up to 20 m, respectively. The grooves are U-shaped in cross section (Figure 4.31c), and the spacing between them is approximately 800 m.

Further north in the trough, smaller-scale parallel lineations trending in an N-NE to S-SW direction are situated (Figure 4.30 & 4.31a). They have lengths between 6 and 12 km, and seems to continue outside the study area. The lineations have widths of 250 m and a negative relief up to 5 m. In cross section, the lineations are U- or V-shaped (Figure 4.31b).

Interpretation

The large-scale grooves observed in the central and southern part of the trough are similar to the streamlined features described and interpreted earlier. These features are therefore interpreted to be MSGL, indicating an ice-flow direction towards NW-SE. The smaller-scale parallel lineations observed in northern part of the paleo-trough are orientated more or less perpendicular to the trough and the MSGL (Figure 4.30). They are also interpreted to be a result of subglacial erosion based on their morphology, i.e. glacial lineations. Their orientation

perpendicular to the implied paleo-ice flow may indicate that they are formed by a different paleo-ice stream. A discussion of their origin will be done in chapter 5.

Semi-circular depressions

Within the paleo-trough, several semi-circular to elongated depressions appear (Figure 4.30 & 4.31a). The depressions have a slight NE-SW trending elongation. They have a length of approximately 1.5-4 km, measured along their longest axis, a width up to 1 km, and a negative relief of 15 m, respectively. The depressions are U- or V-shaped in cross section (Figure 4.31d).

Interpretation

The semi-circular to elongated depressions are interpreted to be a result of subglacial plucking, where basal freezing of the glaciers and later movement led to removal of sediments. Later, the depressions may have been modified by meltwater, smoothening the edges. Similar features are described and interpreted on buried horizons in the SW Barents Sea by Rafaelsen et al. (2002).
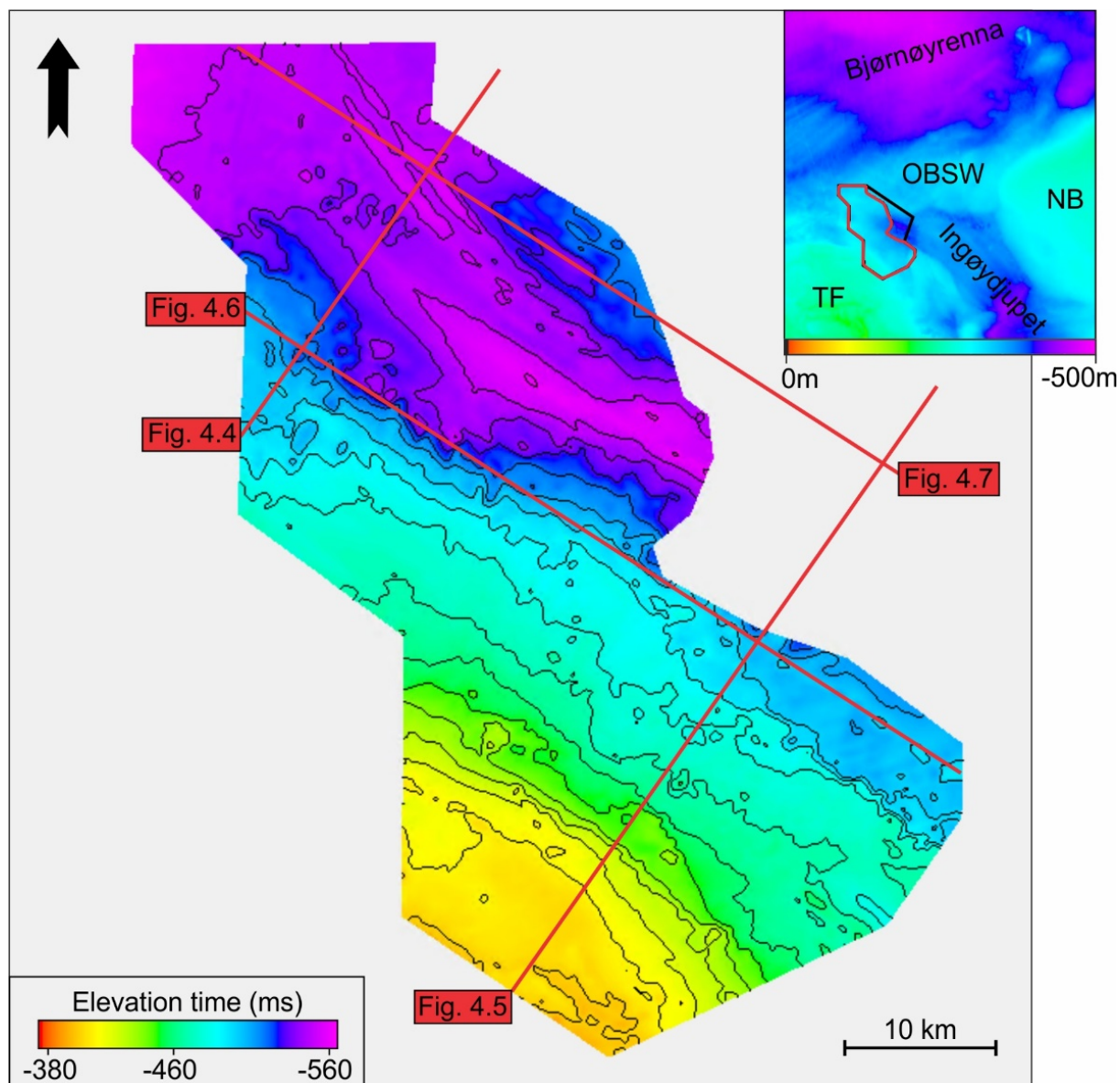
Figure 4.29 *– Intra Q3 horizon with depths in milliseconds two-way travel time. The red polygon on the inset maps indicates the location of the horizon. Contour intervals are 10 milliseconds.*
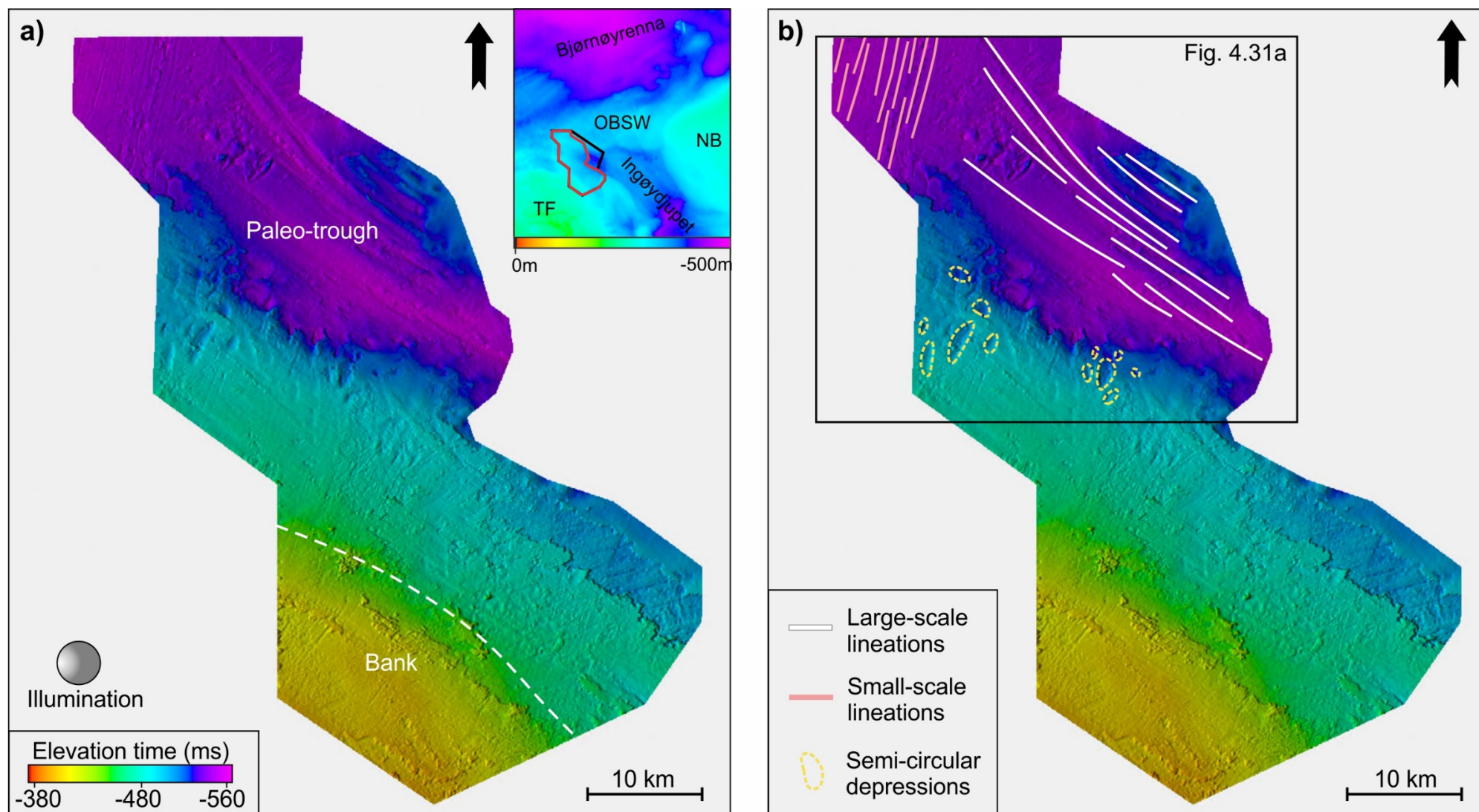
Figure 4.30 – a) Overview of the intra Q3 surface with a paleo-trough and surrounding bank outlined by the white stippled lines. The location of the intra Q3 surface is indicated with a red polygon on the inset map. b) Intra Q3 surface with interpreted morphological features. Black frame outline figure 4.31a.
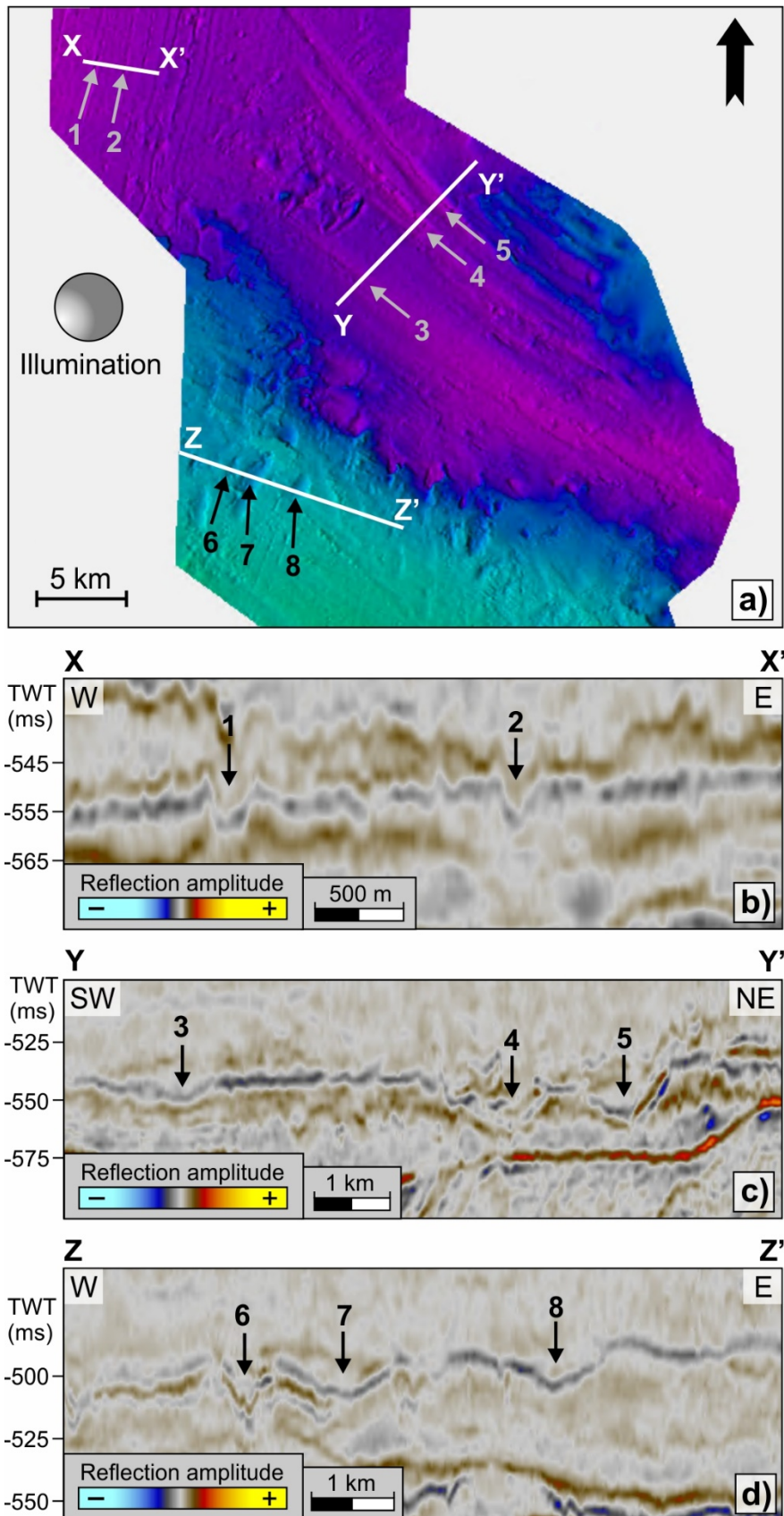
Figure 4.31 – **a)** *Northern part of the Intra Q3 surface displaying large-scale (1-2) and smaller-scale (3-5) linear grooves, and semi-circular depressions (6-8). White lines indicate the locations of the seismic profiles in b (X-X'), c (Y-Y') and d (Z-Z'). **b)** Seismic profile across the large-scale linear grooves. **c)** Seismic profile across the smaller-scale linear grooves. **d)** Seismic profile across the semi-circular depressions.*

79

4.2.8 Seismic unit A_4

Seismic unit A_4 is bounded by the intra Q3 and the intra Q4 horizons (Figure 4.4, 4.6 & 4.7). Overall, the sediment distribution gradually increases from the southeast towards the northwest (Figure 4.32). A prominent depocenter is situated at the outer Bjørnøyrenna sediment wedge, where the thickness reaches approximately 85 to 110 ms, while the thinnest sediment cover is observed at the margins of the Ingøydjupet Trough (20 to 30 ms) (Figure 4.32). In general, the sediment distribution can be correlated with the morphology of the underlying intra Q3 horizon (Figure 4.29). With exceptions of the thinner accumulations in the southeastern part of the unit.

The internal seismic signature of unit A_4 is mostly semi-transparent to transparent (Figure 4.4, 4.6 & 4.7). However, a local undulating horizon of higher amplitude reflections are observed within the unit (Figure 4.34b). The undulating horizon appear as darker areas on the timeslice (Figure 4.33) and brighter areas in the RMS amplitude map (Figure 4.34a) generated over a specific volume indicated in Figure 4.34c.
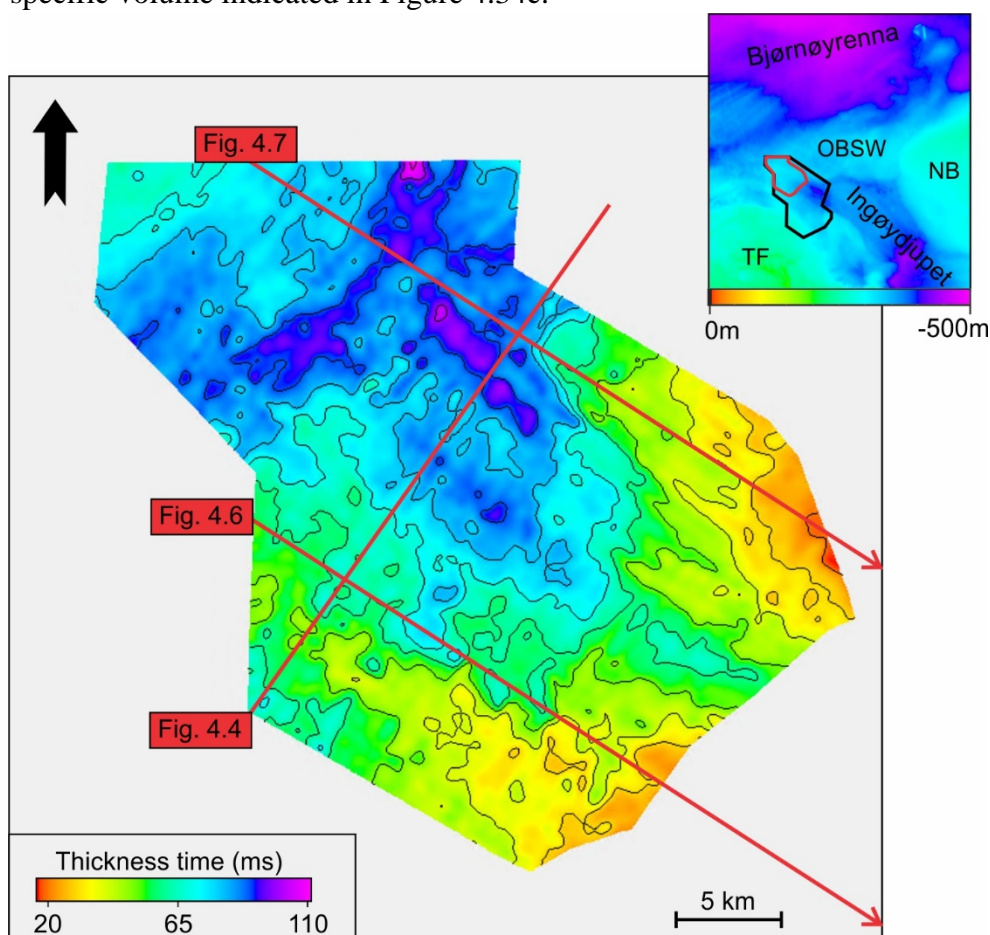
Figure 4.32 *– Isochore map of seismic unit A_4, defined by the intra Q3 and intra Q4 horizons. The red polygon on the inset map indicates the location of the unit. Sediment thickness is given in milliseconds two-way travel time. Contour intervals are 10 milliseconds. Red arrows indicate that the seismic lines continue outside the map.*
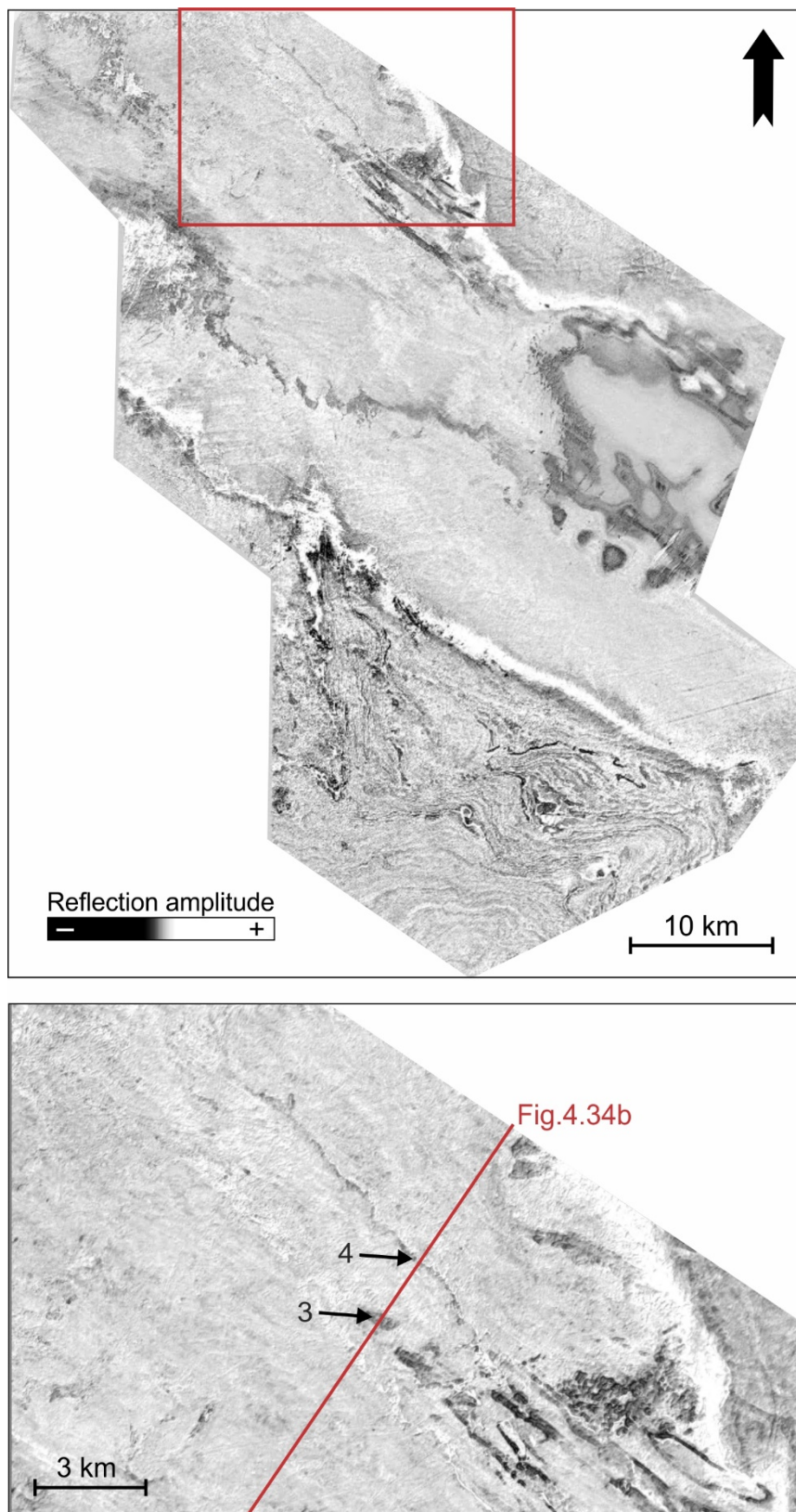
Figure 4.33 *– **a**) Regional timeslice trough unit A₄. Its position is marked with a black stippled line in figure 4.34c. Red frame outlines figure b. **b**) Zoomed in area displaying an area of higher amplitudes (3-4). Red line indicates the location of the seismic profile in figure 4.34b.*

81
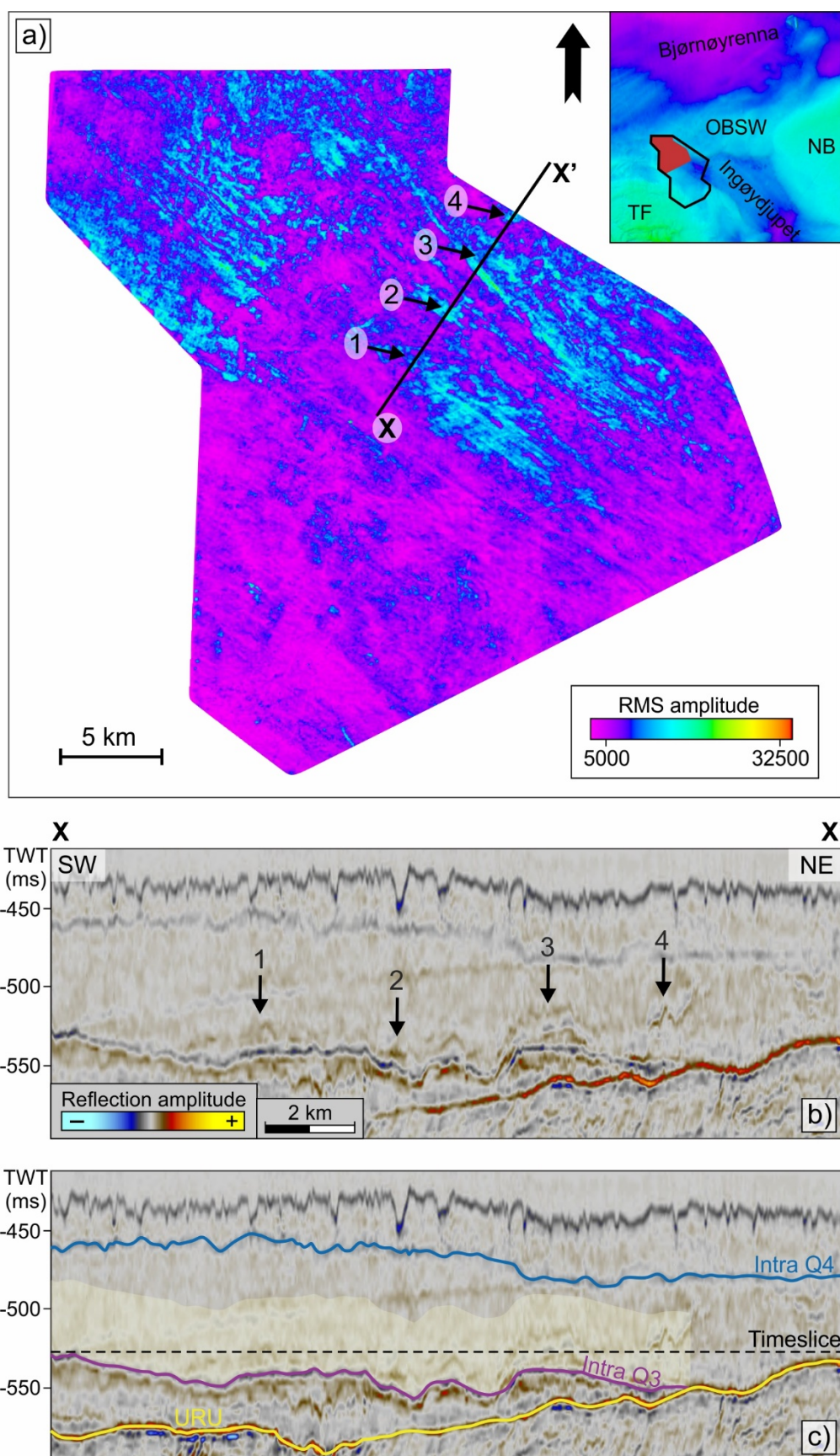
Figure 4.34 – **a)** *RMS seismic amplitude map for the volume with yellow shading in c, showing segments in unit A₄*
with higher RMS amplitude than surrounding sediments. Lines indicates seismic profiles of b and c. **b)** *Seismic profile*
showing high amplitude reflection segments within unit A₄. **c)** *Seismic profile displaying the zone (shaded yellow color)*
of the RMS volume and the position of the timeslice in figure 4.33.

4.2.9 Intra Quaternary4 horizon

The intra Quaternary4 (intra Q4) horizon represents the top of seismic unit A_4 (Figure 4.4, 4.6, 4.7 & 4.11). It is defined by a continuous to semi-continuous trough reflection with medium- to low-amplitude. Overall, the intra Q4 horizon has a parallel relationship with the overlying seafloor horizon (Figure 4.4), with exceptions in the Ingøydjupet Trough where the horizon is truncated by the seafloor (Figure 4.6 & 4.7). The horizon is deepest in the southeast (between 530 and 540 ms), and shallower in the southwest (approximately 430 ms) (Figure 4.35). The surrounding area generally has a depth between 470 and 500 ms.

Lineations

The morphology of intra Q4 is characterized by several sets of lineations trending in an NE-SW direction (Figure 4.36). The lineations consist of linear ridges and furrows (Figure 4.37a-b). They have lengths up to 25 km and some seem to continue outside the study area. The furrows have widths of approximately 300 m, while the widths of the ridges vary from 300 m to 1 km, respectively. In cross section, the ridges are U-shaped, while the furrows are V- to U-shaped (Figure 4.37b), and the elevation difference is up to 12 m.

Interpretation

The sets of lineations are similar to the features described and interpreted earlier, and are therefore interpreted to be MSGL.

Curvilinear furrows

At some locations in the shallowest part of the intra Q4 surface, curvilinear furrows are overprinting the linear features (Figure 4.36 & 4.37c). They are V-shaped in cross section, with levees on their sides (Figure 4.37d), and have a negative relief of approximately 10 m. The curvilinear furrows have lengths varying between 3 km and 10 km, and a width of 400 m.

Interpretation

The curvilinear furrows are interpreted to be iceberg plough-marks, as they resemble features described and interpreted earlier.

Teardrop-shaped ridges

Several teardrop-shaped ridges trending in an NW-SE direction are situated in the eastern part of the surface (Figure 4.36 & 4.37e). In cross section, the ridges are asymmetrical, with a generally steeper proximal side (Figure 4.37f). The ridges can be followed up to 3 km. Their width is between 500-800 m, and they have a positive relief of 20 m (measured from the proximal side).

Interpretation

The teardrop-shaped ridges observed in the eastern part of the surface are, based on their geomorphology, interpreted to be drumlins. They indicate an ice-flow direction towards NW, which are perpendicular to the implied ice-flow direction from the MSGLs (Figure 4.36).
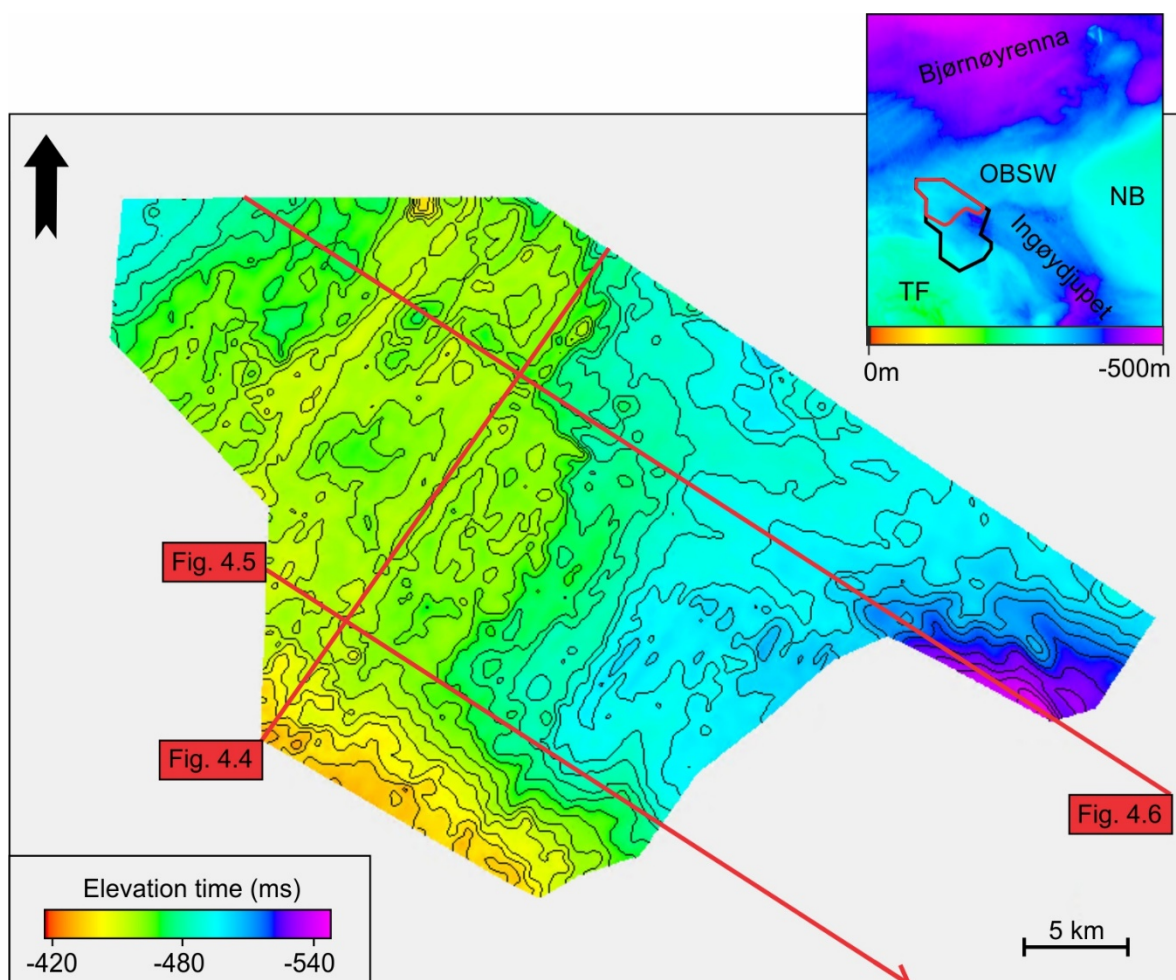
Figure 4.35 *– Intra Q4 horizon with depths in milliseconds two-way travel time. The red polygon on the inset maps indicates the location of the horizon. Contour intervals are 5 milliseconds. Red arrows indicate that the seismic lines continue outside the map.*

84
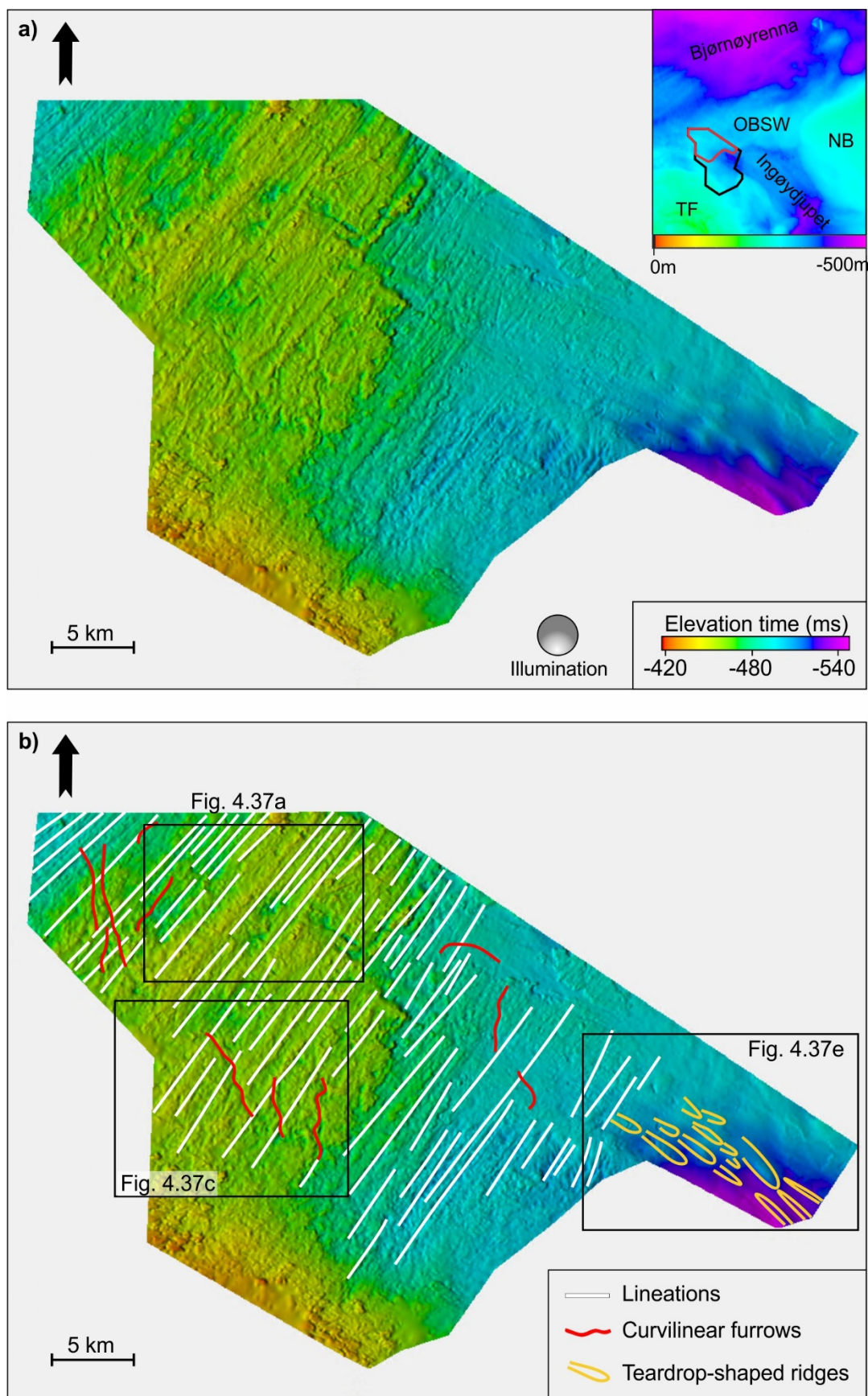
Figure 4.36 – *a) Overview of the intra Q4 surface with streamlined features. The location of the intra Q4 surface is indicated with a red polygon on the inset map. b) Intra Q4 surface with interpreted morphological features. Black frames outline figure 4.37 a, c and e.*

85
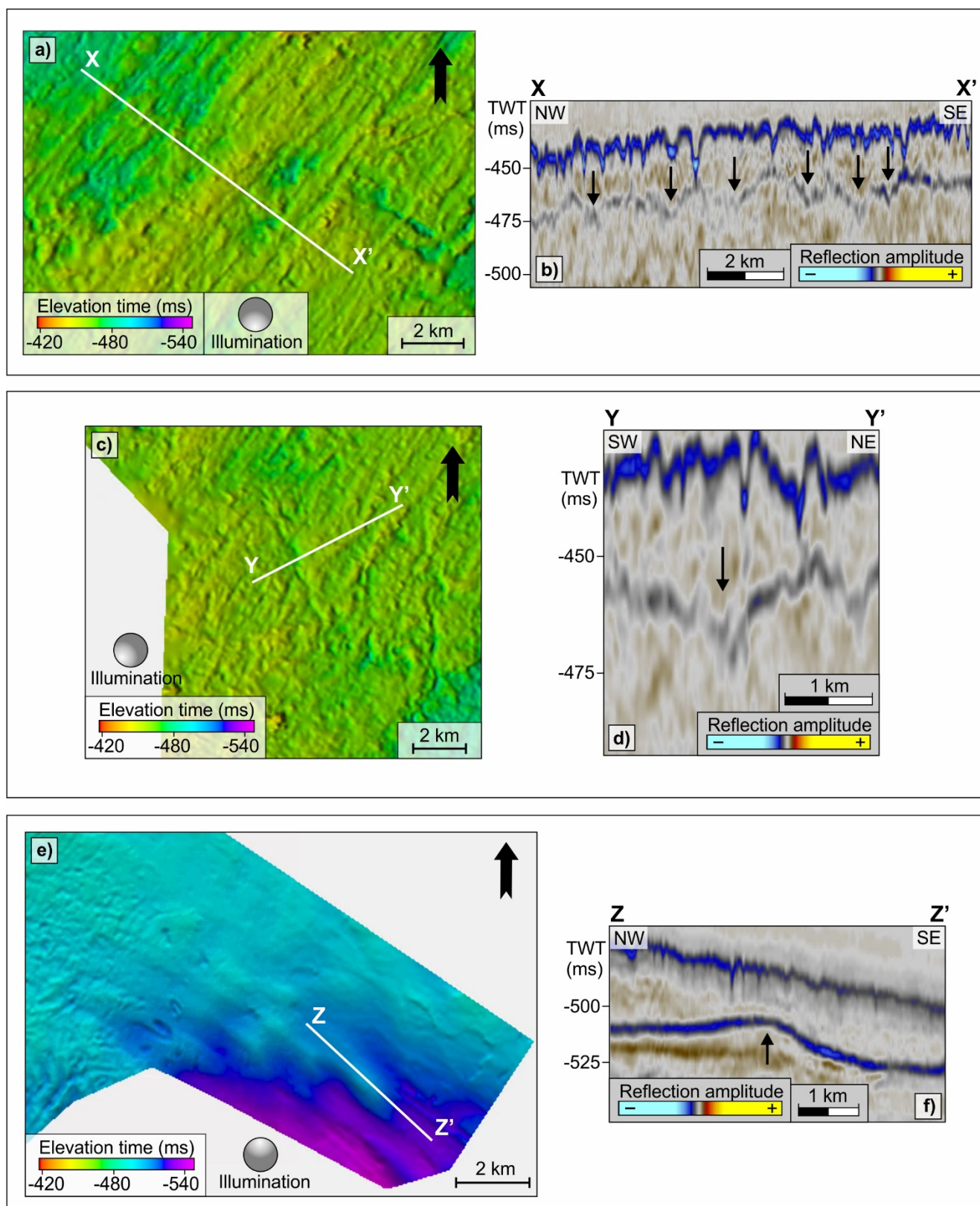
Figure 4.37 – ***a****) Northwestern part of intra Q4 displaying MSGL. White line indicates the location of the seismic profile in b (X-X'). **b***) Seismic profile across the MSGL. **c***) Curvilinear furrows interpreted as iceberg plough-marks. White line indicates the location of the seismic profile in d (Y-Y'). **d***) Seismic profile across one iceberg plough-mark. **e***) Eastern part of the intra Q4 surface displaying teardrop-shaped ridges interpreted as drumlins. White line indicates the location of the seismic profile in f (Z-Z'). **f***) Seismic profile across one drumlin.*

4.2.10 Seismic unit A_5

Seismic unit A_5 is defined by the intra Q4 and the seafloor horizons (Figure 4.4, 4.6 & 4.7). The isochore map displays two prominent depocenters situated in the northeastern part of the unit, at the outer Bjørnøyrenna sediment wedge, reaching 60 ms in sediment thickness (Figure 4.38). The thinnest sediment cover is found at the margins in the southern part of the unit (0-5 ms). In general, the sediment distribution can be correlated with the topography of the underlying horizon (Figure 4.35), with exception of the largest depocenter in the northeastern part of the surface. Transparent reflections characterize the internal seismic signature of unit A_5 (Figure 4.4, 4.6 & 4.7).
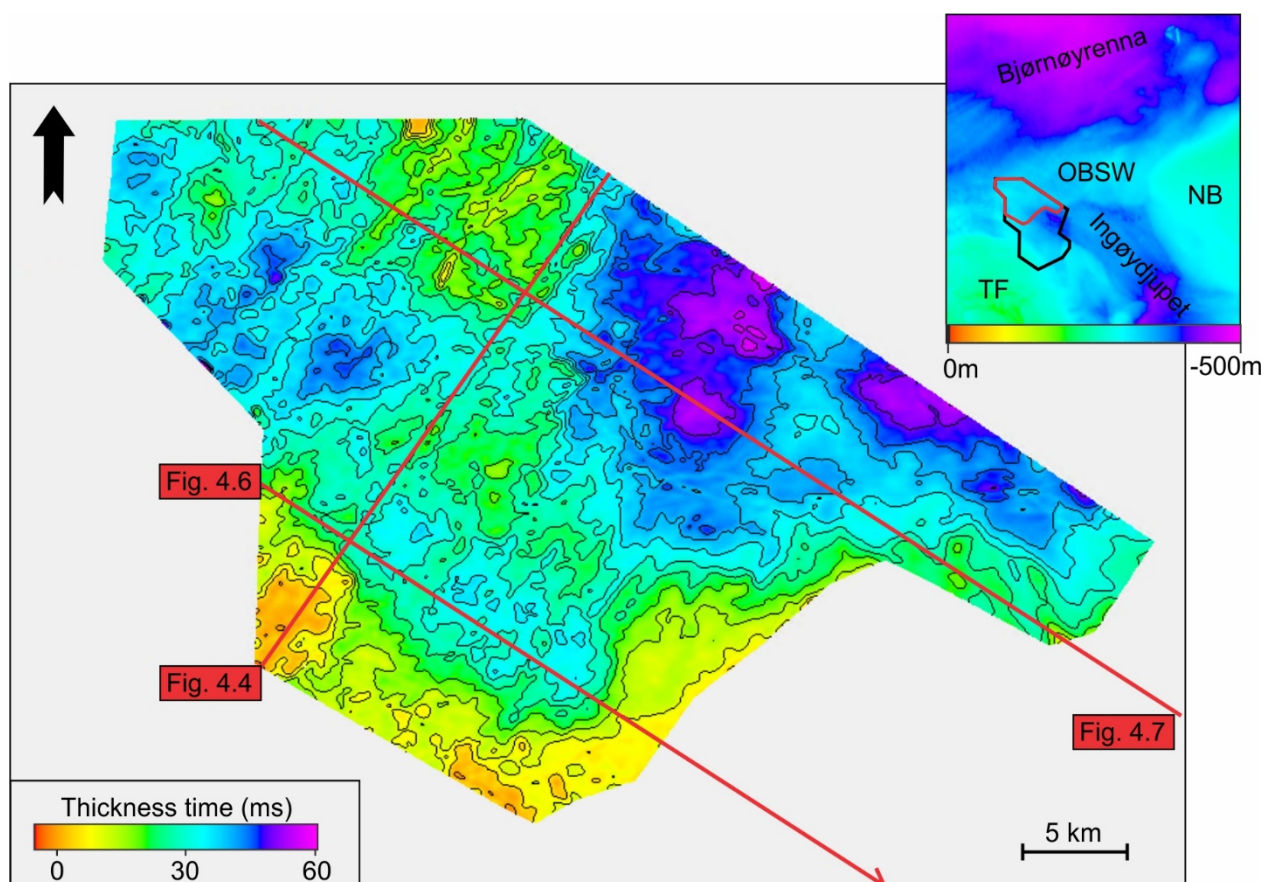
Figure 4.38 *– Isochore map of seismic unit A_5, defined by the intra Q4 and seafloor horizons. The red polygon on the inset map indicates the location of the unit. Sediment thickness is given in milliseconds two-way travel time. Contour intervals are 5 milliseconds. Red arrows indicate that the seismic lines continue outside the map.*

4.2.11 Seafloor horizon

The seafloor horizon is defined by a continuous trough reflection with high- to medium-amplitude (Figure 4.4-4.7). The horizon displays the present-day seafloor morphology, i.e. deeper parts located in the Ingøydjupet Trough (between 520 and 560 ms), and shallower parts are situated on the surrounding bank area, i.e. Tromsøflaket, and the outer Bjørnøyrenna sediment wedge (between 380 and 430 ms) (Figure 4.39).

Elongated sinuous ridges and narrow ridges

In the deepest parts of Ingøydjupet, i.e. in the northwestern part, four NNE-SSW trending elongated sinuous ridges are observed (Figure 4.40 & 4.41a and d). The ridges have a length of 5 km, widths between 500 and 900 m, and a positive relief of 20 m.

In the north central parts of the Ingøydjupet Trough, there are observed large-scale elongated sinuous ridges with an N-NE and S-SW orientation (Figure 4.40 & 4.41a). The ridges are up to 11 km long, 1.8 km wide, and 25 m high, and have a spacing of approximately 300-800 m. In the seismic profile, the ridges are more or less symmetrical (Figure 4.41b). The ridges are terminated by the depression in the southwest, the sediment accumulation in southeast and the outer Bjørnøyrenna sediment wedge in the north. However, the ridges seem to continue underneath the sediment wedge (Figure 4.41.c).

Further east of the elongated ridges, a swarm of closely spaced, narrow ridges with an NE-SW orientation occurs (Figure 4.40 & 4.41a and e). The ridges vary in size, from approximately 1 to 5 km in length, 30 to 600 m in width and 12 to 20 m in height, and they have a spacing between 100 and 300 m, respectively.

Interpretation

The ridges observed in the deepest parts of the Ingøydjupet Trough (Figure 4.40) display similar characteristics as the transverse ridges described earlier on the URU horizon, and are therefore interpreted as moraines deposited in front of the ice, possibly during several small re-advances and/or stillstands during the deglaciation. The elongated sinuous ridges situated in the north central parts of the Ingøydjupet Trough have the same orientation as the latter, i.e. more or less perpendicular to the implied ice-flow (4.40). One interpretation can be that they represent larger recessional moraines deposited during temporary glacial standstills during the deglaciation.

The ridge swarm appearing in the northeastern parts of the Ingøydjupet Trough have an orientation perpendicular to the implied ice-flow direction (Figure 4.40), indicating that the ridges are deposited at the glacier front. They are interpreted to be ice-flow transverse De Geer moraines formed during brief stillstands or minor re-advances where sediments are deposited or pushed up in front of the glacier. Similar features are found in the SW Barents Sea by Winsborrow et al. (2012).

Depressions

In the western part of the Ingøydjupet Trough, a prominent large-scale depression occurs (Figure 4.40 & 4.42a-b). The depression have a slight NW-SE trending elongation. It has a length of 30 km, a width of 17 km, at its widest, and a negative relief of 112 m compared to the surrounding seafloor.

In the northeastern part of the trough, a meandering depression is observed (Figure 4.40 & 4.42c-d). This has a length of approximately 14 km, a width of 400 m to 2 km, and a depth between 15 to 60 m, measured from the surrounding seafloor. Several protruding highs can be observed in the western part of the meandering depression (Figure 4.42c). They have a semi-circular shape, and are up to 30 m higher than the surrounding seafloor. Additionally, several semi-circular depressions occur in the surrounding area of the meandering feature (Figure 4.40 & 4.42c).

In the southern part of the Ingøydjupet Trough, three oblong depressions trending in an NW-SE direction appear (Figure 4.40 & 4.42e). The depressions have a length of 3-6 km, and the largest of them seems to continue outside the study area. Their width vary from 600 m up to 1.4 km, and they have a negative relief of 40-60 m. In cross sections, the depressions are U-shaped with levees on their sides (Figure 4.41f).

Interpretation

The large-scale depression observed in the northwestern part of the Ingøydjupet Trough (Figure 4.40) are interpreted to be a result of subglacial erosion.

The meandering depression situated in the northeastern part of the trough is interpreted to be a subglacial tunnel valley formed by a meltwater channel (Figure 4.40). This is based on its

morphology and order of size. The tunnel valley seems to be a part of an older channel feature that is overlain by the Nordkappbanken wedge (Figure 4.42c-d). In the seismic profile, the channel continues underneath the interpreted URU horizon, implying that the channel has an older origin than the other geomorphic features observed on the seafloor. The channel is preserved on the seafloor, indicating that the sedimentation in this area has probably been limited after the ice sheet retreated. The semi-circular depressions occurring northwest of the tunnel valley may be eroded by the same meltwater that formed the valley, and the protruding highs are interpreted to be eroded material.

Furthermore, the three oblong depressions appearing in the southern part of the Ingøydjupet Trough (Figure 4.40 & 4.42e-f) are interpreted to be a result of erosion by meltwater. This is based on their morphology as well as their abrupt occurrence.

Curvilinear furrows

Elongated curvilinear furrows dominates the shallower areas surrounding Ingøydjupet (Figure 4.40 & 4.42g). The furrows have a more or less chaotic cross-cutting pattern. They can be followed up to 50 km, have a width between 100 and 300 m, and a negative relief of approximately 10-20 m. In cross section, the furrows are U- or V-shaped with some displaying levees on their sides (Figure 4.42h).

Interpretation

The elongated curvilinear furrows are similar to the features described and interpreted earlier on the intra Q1 and intra Q4 surfaces. These features are thus interpreted to be iceberg plough-marks.
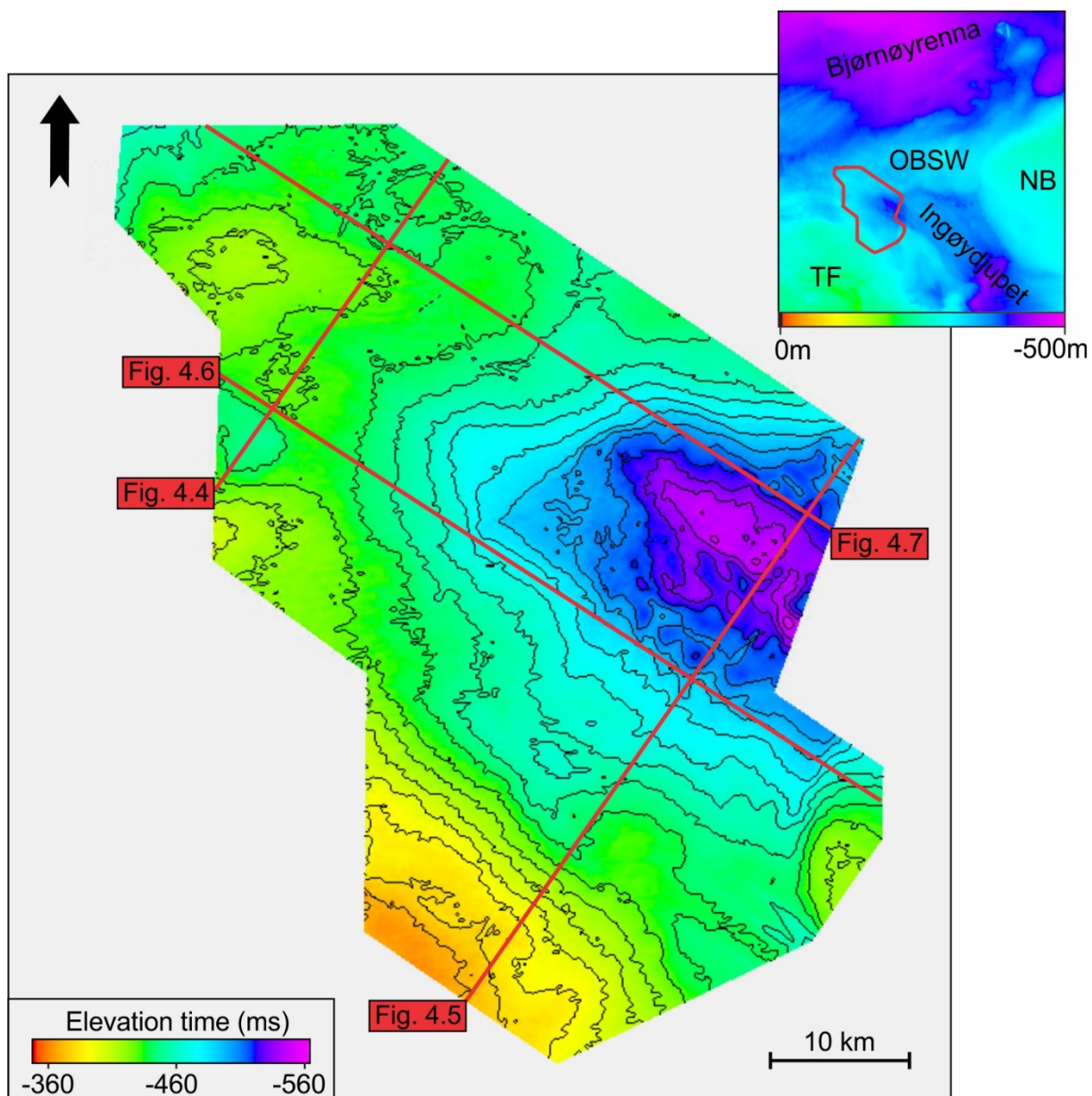
Figure 4.39 – *Seafloor horizon with depths in milliseconds two-way travel time. The red polygon on the inset maps indicates the location of the horizon. Contour intervals are 10 milliseconds.*
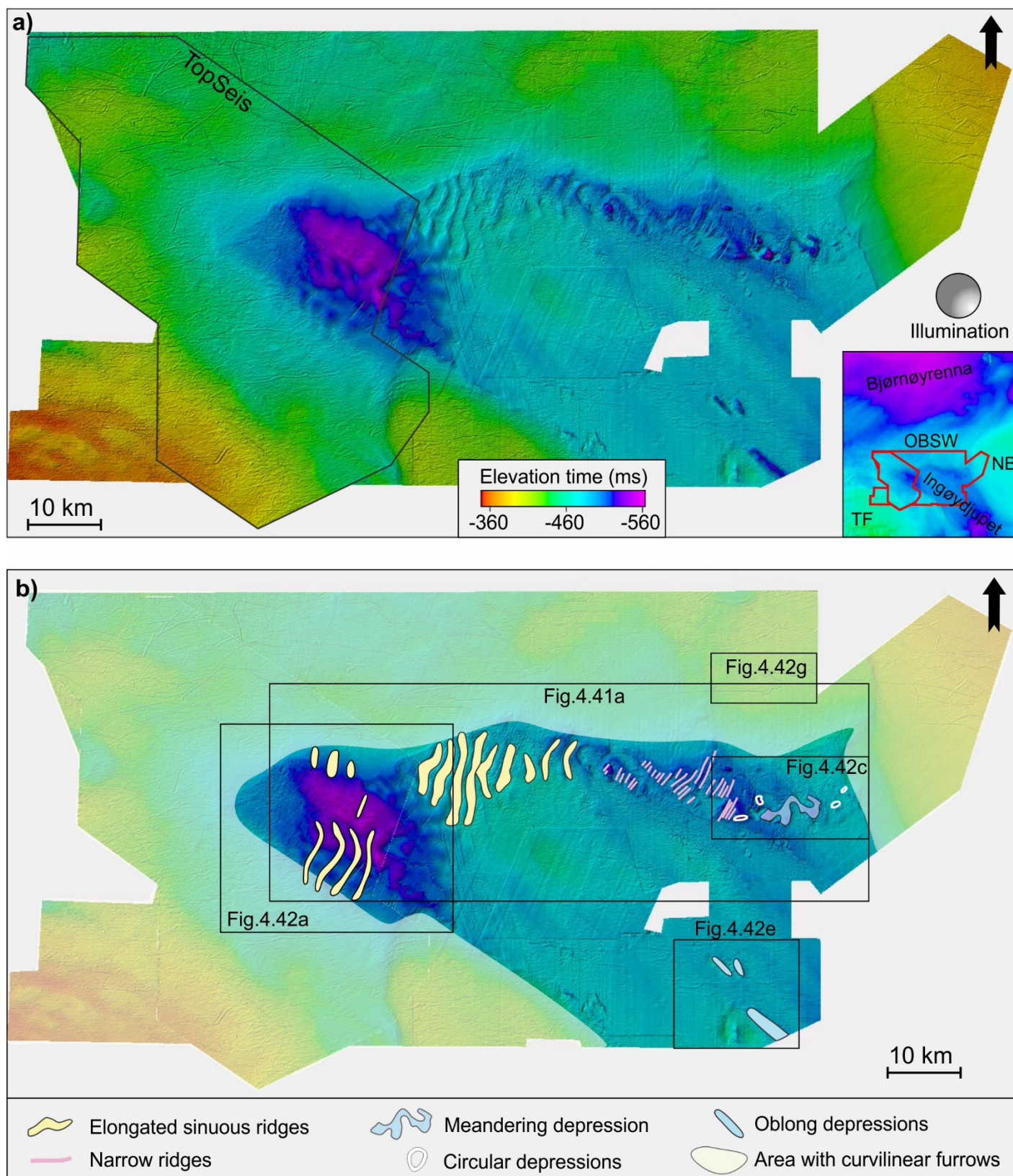
Figure 4.40 – a) Overview of the seafloor in the Ingøydjupet area. The black polygon outlines the seafloor surface of the LN17001 (TopSeis) dataset, while the surrounding seafloor is from the 3D-merge. The location of the seafloor surface is indicated with a red polygon on the inset map. b) The seafloor surface with interpreted morphological features. Black frames outline figure 4.41a and 4.42a, c, e and g.
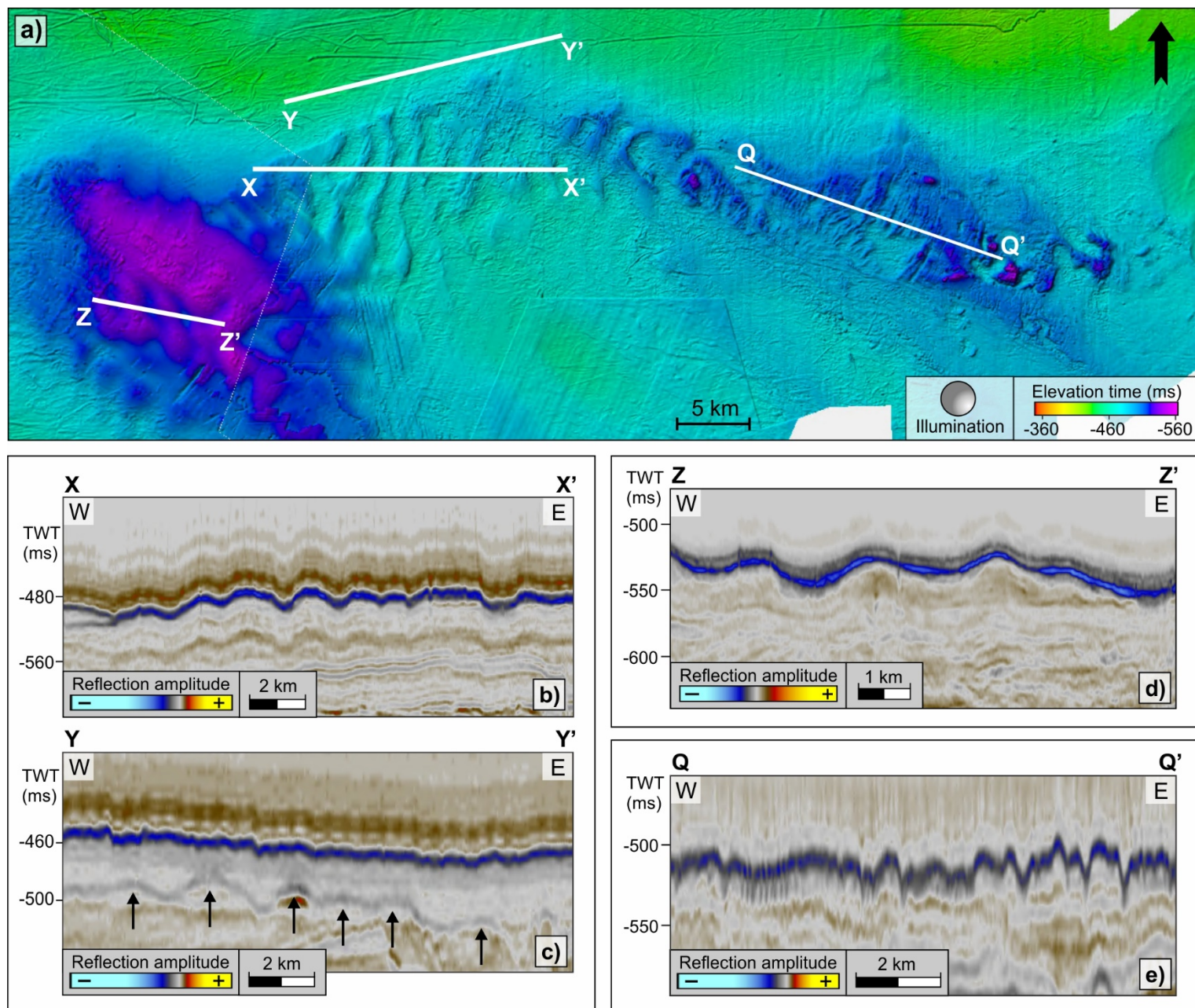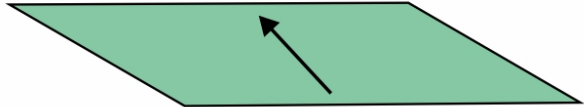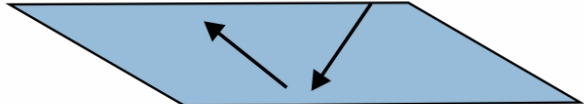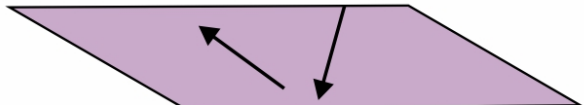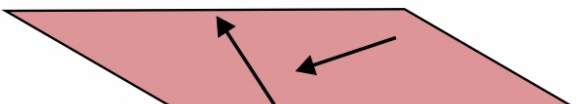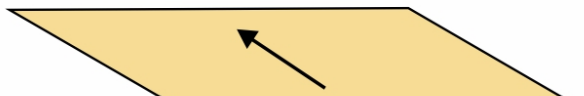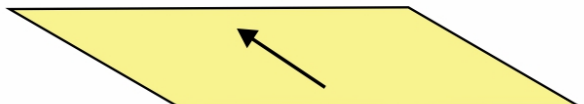
Figure 4.41 – *a) Northern part of Ingøydjupet. White lines indicate the locations of the seismic profiles in b (X-X'), c (Y-Y') and d (Z-Z') and e (Q-Q'). b) Seismic profile across the elongated sinuous ridges. c) Seismic profile across the OBSW. Notice the ridges continues underneath the OBSW. d) Seismic profile across the elongated sinuous ridges. e) Seismic profile across the closely spaced, narrow ridges.*
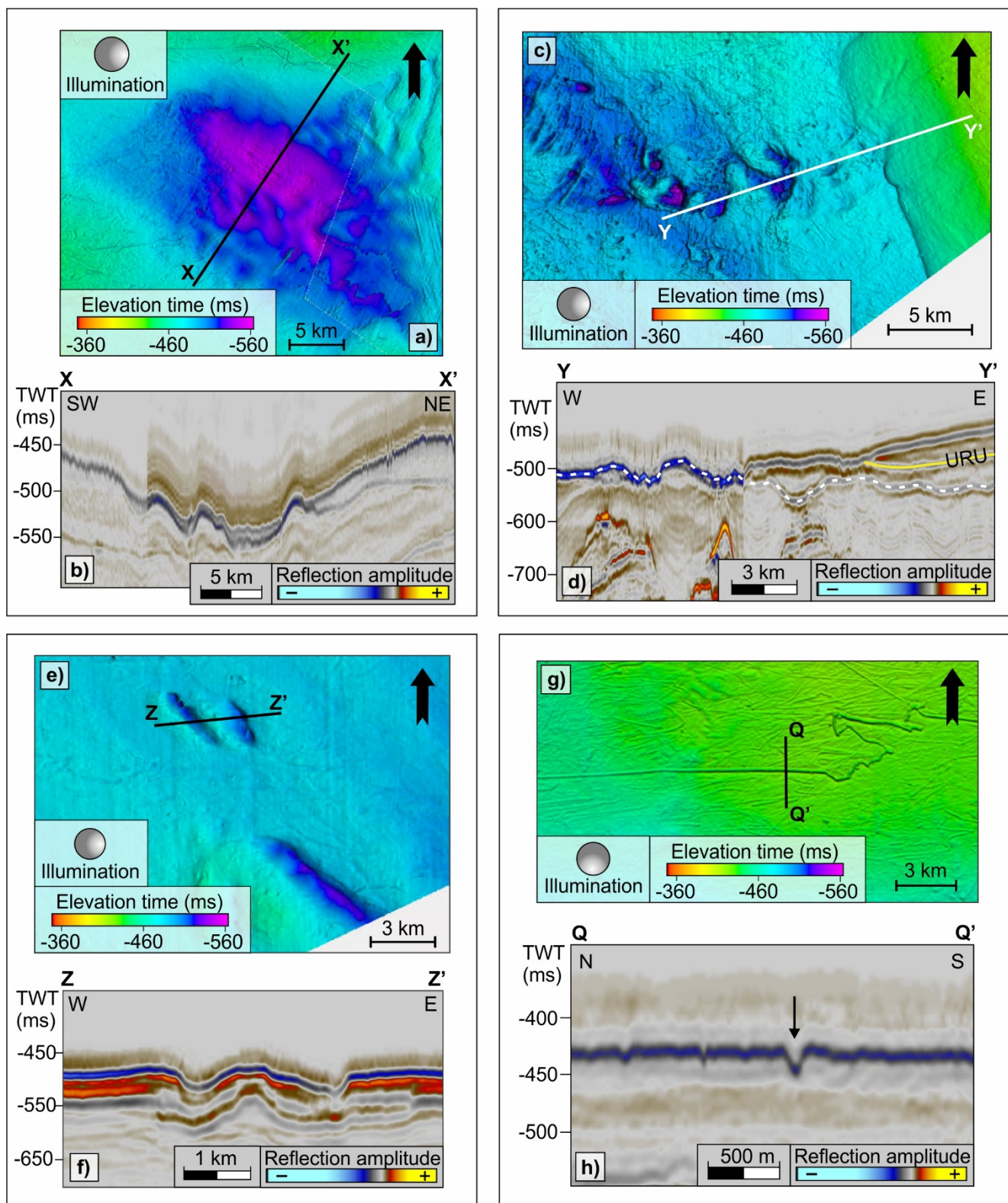
Figure 4.42 *– **a**) Large-scale depression in the western part of Ingøydjupet. Black line indicates the location of the seismic profile in b (X-X'). **b**) Seismic profile across the large-scale depression. **c**) Meandering depression situated in the northeastern part of Ingøydjupet. White line indicates the location of the seismic profile in d (Y-Y'). **d**) Seismic profile across the meandering depression. **e**) Three oblong depressions located in the southern part of Ingøydjupet. Black line indicates the location of the seismic profile in f (Z-Z'). **f**) Seismic profile across two of the depressions. **g**) Example of one curvilinear furrow on the grounding-zone wedge. Black line indicates the location of the seismic profile in b (Q-Q'). **b**) Seismic profile across the curvilinear furrow.*

4.2.12 Summary

The buried surfaces and the seafloor display several geomorphological features that can be used for a reconstruction of paleo-ice sheets in the study area (Table 4.1). Indications of fast-flowing ice, e.g. paleo-troughs and MSGLs have been identified on all the buried surfaces and the seafloor. Figure 4.43 display a sketch of the surfaces with arrows indicating the flow-directions of paleo-ice streams.

Figure 4.43 – *Sketch of the buried surfaces with arrows indicating the flow directions of paleo-ice streams in the study area.*

Table 4.1 – *Summary of the geomorphological features interpreted on all the horizons. The dimensions are based on the largest and most distinct features of their kind. MSGL: mega-scale glacial lineations.*

Features	URU			Intra Q1			Intra Q2			Intra Q3			Intra Q4			Seafloor		
	Size (m) l: length, w: width, h: heigth																	
	l	w	h	l	w	h	l	w	h	l	w	h	l	w	h	l	w	h
MSGL	15 000	500	18	9000	300	12	10 000	200	5	25 000	1000	-20	25 000	300	12			
Iceberg plough-marks	6000	200	-17	4000	150	-10							10 000	400	-10	50 000	300	-20
Transverse moraines	5000	1500	10													11 000	1800	25
Semi-circular depressions	1500		-15							4000	1500	-15				1500		-15
Drumlins													3000	800	20			
De Geer moraines																5000	600	20
Meltwater channels																14 000	2000	60

5 Discussion

The discussion chapter consists of two parts. In the first part, the chronological framework for the seismostratigraphic units A_1-A_5 will be correlated to previous work in the area. In the second part, the morphology of the interpreted surfaces and the stratigraphy of the units will be discussed in relations to paleo-ice sheet dynamics and the late Quaternary deposition environment of the southwestern Barents Sea shelf.

5.1 Correlation of seismic stratigraphy to previous work

The seismic stratigraphic framework in this study has been correlated with previous studies of the glacigenic succession in the surrounding area on the southwestern Barents Sea continental shelf, i.e. Vorren et al. (1990), Sættem et al. (1992), Rafaelsen et al. (2002) and Laberg et al. (2012) (Figure 5.1). The correlations are based on similarities found in the internal seismic signature and on the buried paleo-surfaces.

Figure 5.2 show the correlation between the five units interpreted in this study (A_1-A_5) and the units identified in the previous studies. The age estimate of the unit boundary of the main seismic unit GIII by Faleide et al. (1996) has been adjusted to a more recent study of Laberg et al. (2012). Vorren et al. (1990) divided the GIII stratigraphy on the outer Barents Sea shelf into four units (1W-4W) based on regional interpretation of 2D-seismic data (Figure 5.1 & 5.2), whereas Sættem et al. (1992) divided it into seven seismic units (B, C, D_1, D_2, E, F and G) in the outer Bjørnøyrenna. Their study was also based on 2D-seismic data, in addition to shallow boreholes (Figure 5.1 & 5.2). One of the boreholes used for their investigations are the 7317/10-U-01 site which is located slightly west from the study area of this thesis (Figure 5.1). Based on analysis from magneto-, amino- and bio-stratigraphy of the glacigenic sediments from this borehole, their seismostratigraphic units were age estimated. This makes it possible to say something about the ages of the interpreted horizons and units of this study. However, the reliability of the presented dates can be discussed as glacigenic sediments are typically difficult to date. This is because many of the methods only are useful for a limited period of time. Additionally, subglacial tills mostly consist of reworked sediments, which can give misleading dating as they may comprise organic matter that has been incorporated into the sediment from external sources, and therefore the age may be an over-estimation of the true sedimentation age (Fuchs & Owen, 2008).

Seismostratigraphic correlation has also been done between the units interpreted by Rafaelsen et al. (2002) (Figure 5.2). They were the first to study the glacigenic sequence of the southwestern Barents Sea shelf by using 3D-seismic data. They identified five glacigenic units (A-E) and mapped several generations of subglacial lineations on buried horizons. Some of the buried horizons are correlated with the horizons interpreted in this study, i.e. bA and bB, representing URU in the 3D-areas SG9810 and SG9804, respectively (Figure 5.1), bD and bE (Figure 5.3).
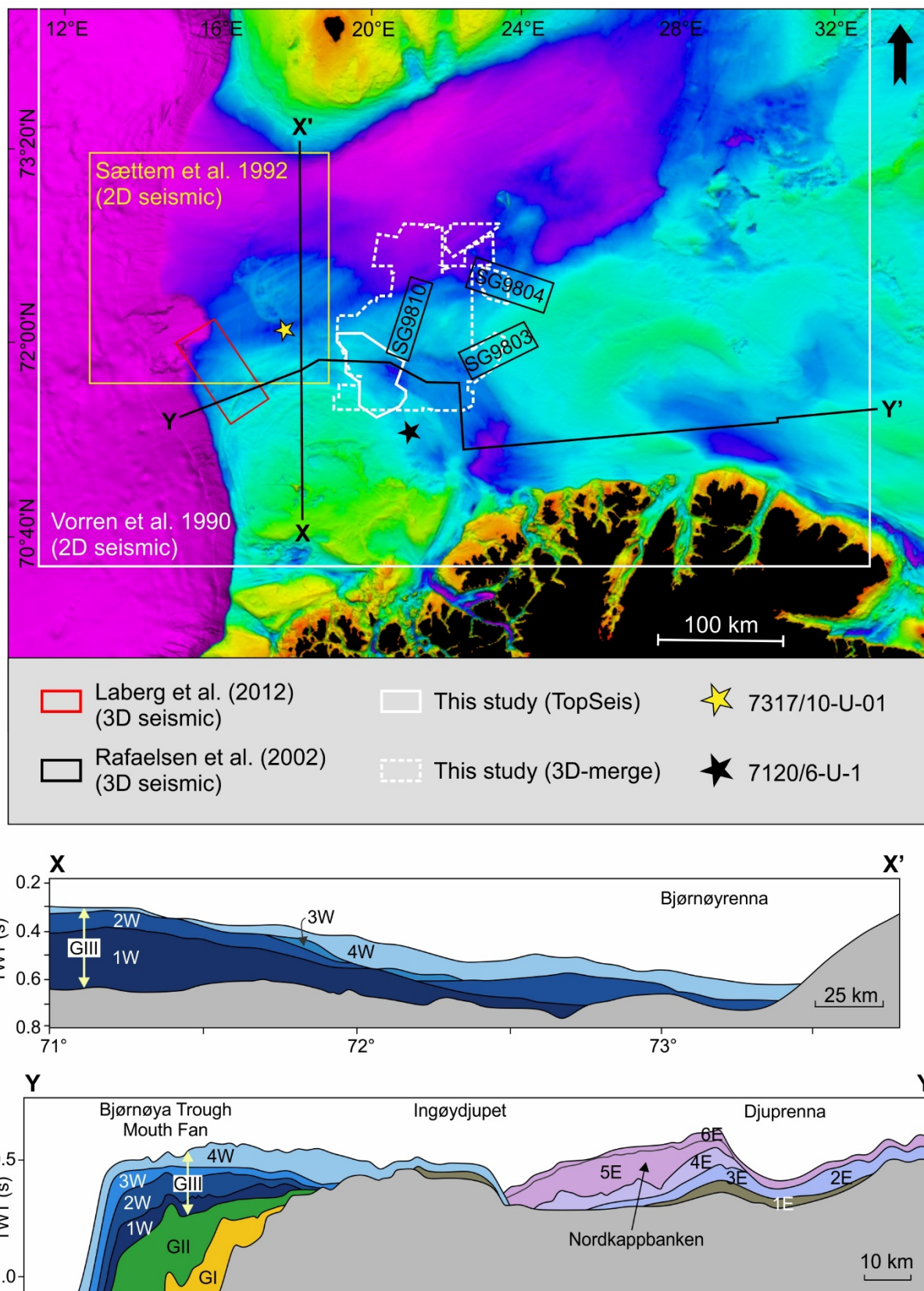
Figure 5.1 – *Regional geomorphology of the SW Barents Sea and a compilation of previous work, in addition to stratigraphic relationship of the late Pliocene to Pleistocene succession in the SW Barents Sea, whereas the geoseismic line X-X' is modified from Larsen et al. (2003) and Y-Y' is modified from Andreassen et al. (2008).*

W ⟶ **E**
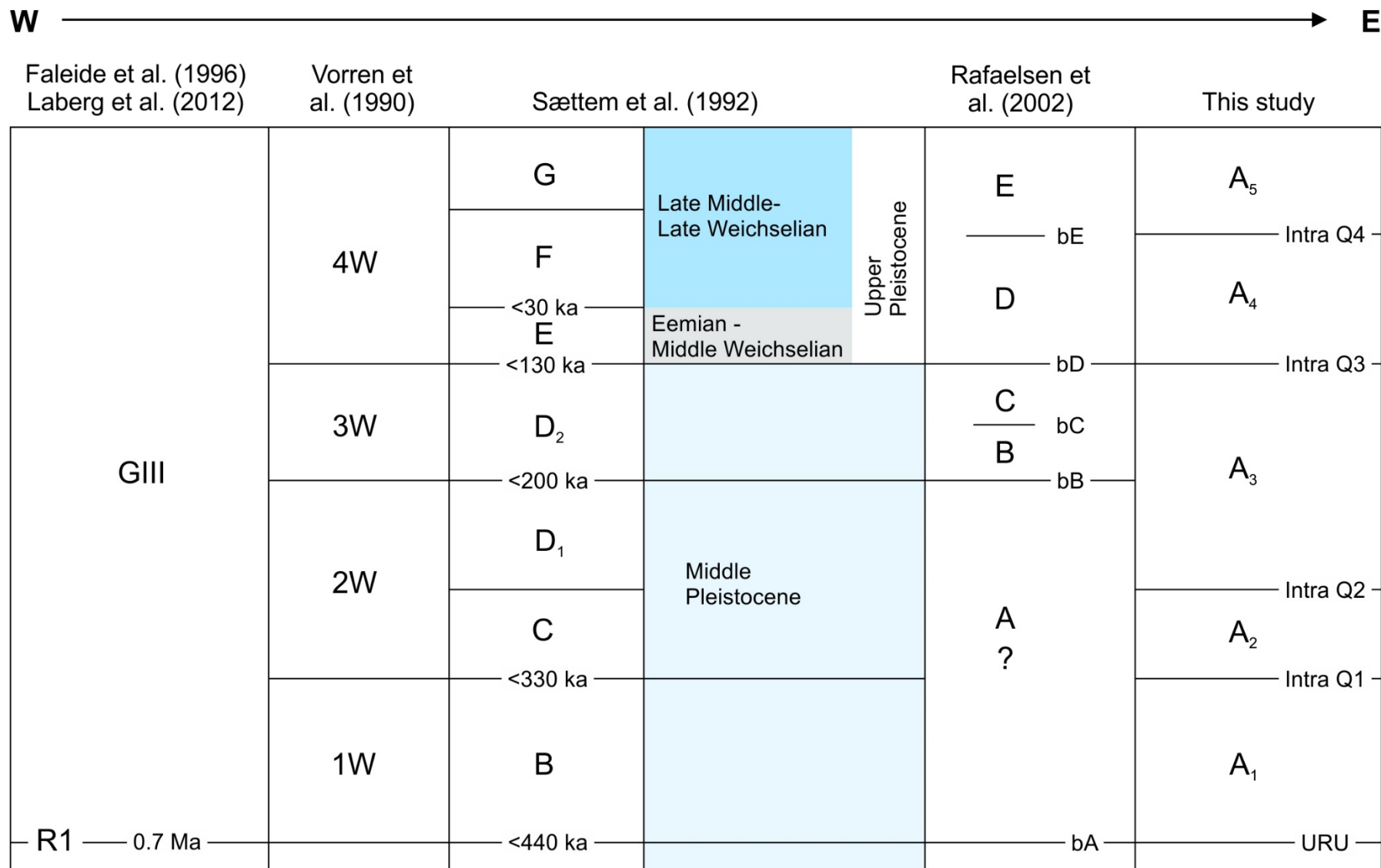
Figure 5.2 – Correlation of seismic units and horizons from studies done on the SW Barents Sea shelf. The stratigraphy extends from west towards east.
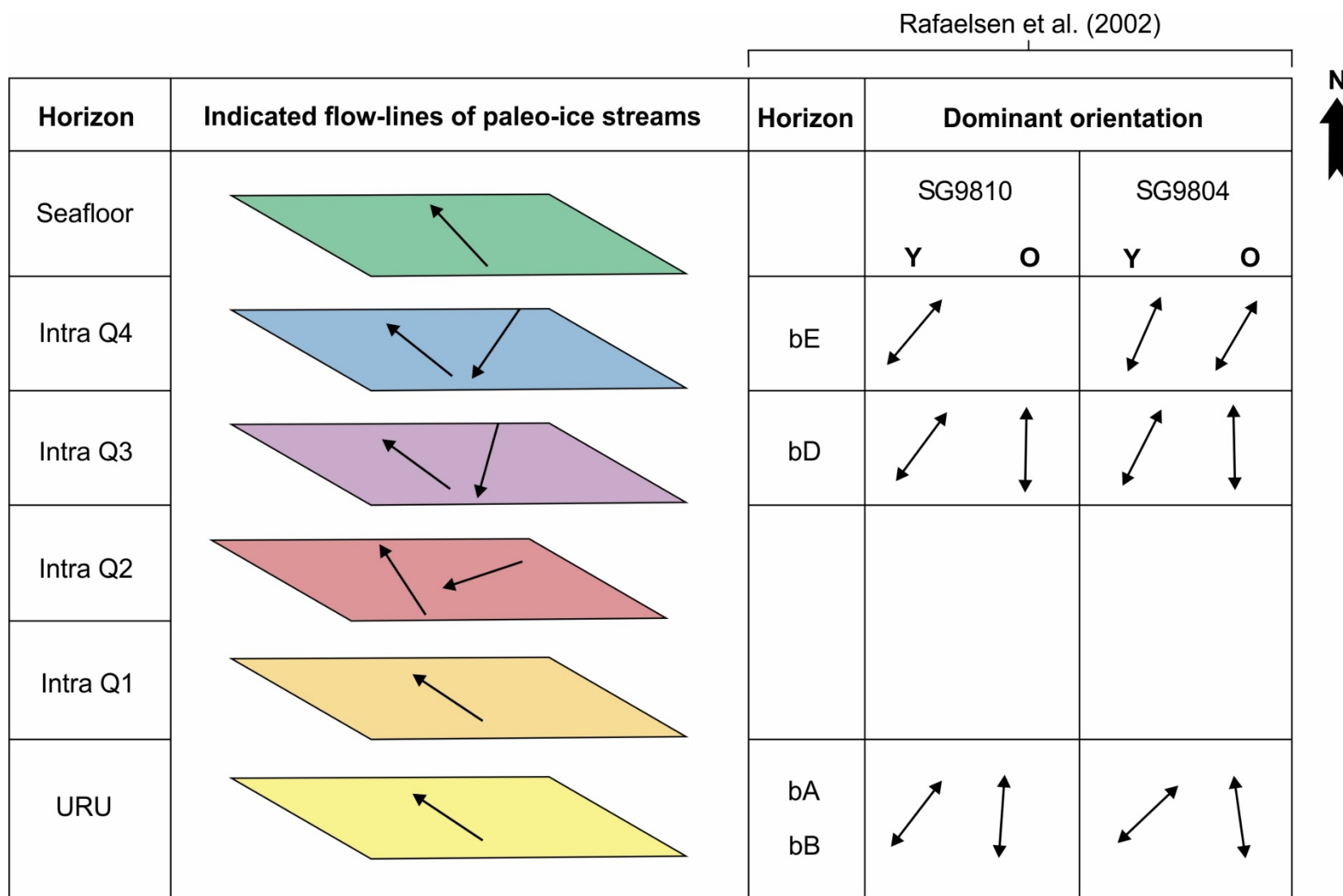
Figure 5.3 *– Indicated flow-lines of paleo-ice streams interpreted from the orientation of subglacial lineations from the surfaces in this study (to the left) and from the study of Rafaelsen et al. (2002), including the subsurfaces in 3D-surveys SG9810 and SG9804 (see figure 5.1 for location). Y = youngest generation lineations, O = oldest generation lineations.*

5.2 Reconstruction of ice-sheet dynamics and deposition environment in the outer Ingøydjupet area

The well-preserved subglacial landforms on the buried surfaces and on the seafloor, and the internal reflection terminations observed in the seismic stratigraphy show that both extensive glacial erosion and deposition has taken place in the outer Ingøydjupet area. Some of the geomorphological features superimpose other, which makes it possible to reconstruct the relative age of their formation. A reconstruction of the ice-sheet configuration and flow-direction on the interpreted surfaces is outlined in the next sub-chapters.

5.2.1 Base Quaternary: URU

The URU landform assemblage in the outer Ingøydjupet area shows a complex and dynamic paleo-ice stream (Figure 5.5). The topography of the paleo-surface and the MSGLs indicate that the ice stream followed the Ingøydjupet Trough. The MSGLs indicate one main ice-flow direction towards NW, suggesting a source area from the Scandinavian mainland, i.e. from the Fennoscandian Ice Sheet (Figure 5.5a).

Ice contact landforms formed at the margin of the retreating ice sheets provide information about the retreat rate and dynamic during the deglaciation (Figure 5.4). The recessional moraines observed within the paleo-trough implies that the paleo-ice stream occupying Ingøydjupet underwent several small re-advances or stillstands during an overall retreat of the ice sheet, i.e. following full-glacial conditions (Figure 5.5b). Some of the MSGLs are cutting the recessional moraines, e.g. in the central part of the paleo-trough, which indicate that the glacier front re-advanced following the formation of these moraines (Figure 5.5c). However, the advance may have been limited to the southern area of the trough, as the recessional moraines in the northeastern part of the trough are not overprinted by MSGLs (Figure 5.5c).
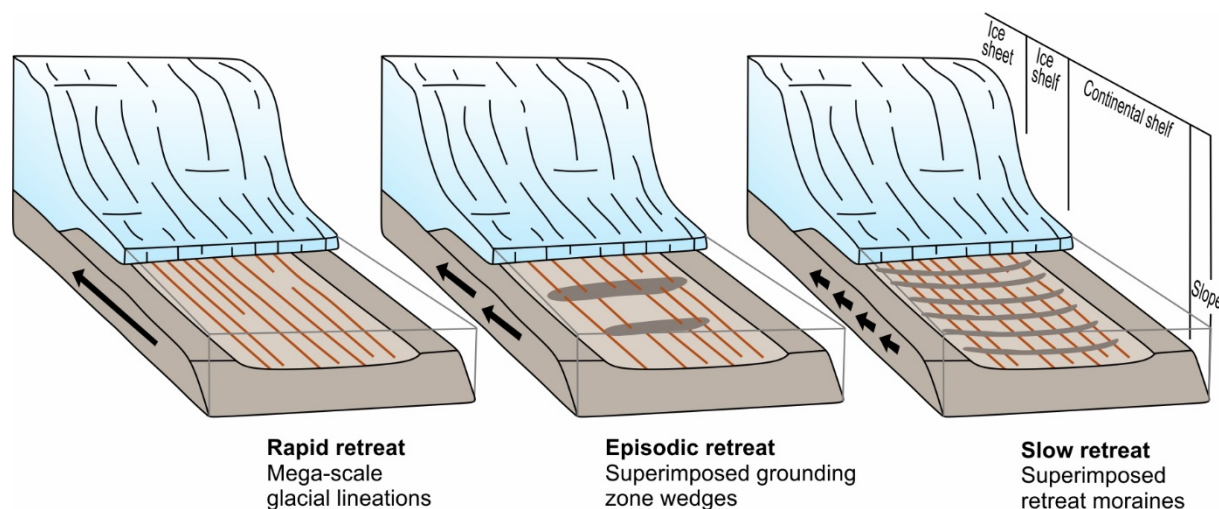
Figure 5.4 – *Schematic diagram of submarine landform assemblage indicating rapid, episodic and slower retreat of ice streams. Modified from Dowdeswell et al. (2008).*

The linear depressions interpreted to be a result of iceberg ploughing indicates a glaciomarine environment, where icebergs were drifting in the SW Barents Sea (Figure 5.5d). The linear and parallel shape of the plough-marks suggest that they were formed by larger icebergs or by a set of icebergs trapped in a sea-ice floe, having a uniform drifting towards NE, i.e. following the present-day ocean currents (see chapter 2.3.4, Figure 2.4).

Rafaelsen et al. (2002) found MSGLs on two URU surfaces, i.e. on bA and bB (Figure 5.3). The oldest lineations are here trending in an NNE-SSW and NNW-SSE direction, and the youngest in an NE-SW direction (Figure 5.3). Based on their orientation, they suggest an ice-flow direction towards north, while the observations in this study suggest an ice-flow towards northwest. As both the study areas of this thesis and the study of Rafaelsen et al. (2002) are located in the outer part of the Ingøydjupet Trough, it is reasonable to suggest that the ice-flow of the Ingøydjupet Ice Stream diverged in the outer part of the trough when entering the Bjørnøyrenna, and that their oldest lineations may be a result of this. The youngest lineations on the other hand, based on their different orientation (Figure 5.3), may be a result of an active ice stream draining through Bjørnøyrenna (Figure 5.5a). Hence, the observations from this thesis and the study by Rafaelsen et al. (2002) suggest that ice streams were active in both the Ingøydjupet- and the Bjørnøyrenna Troughs during the formation of the URU surface.
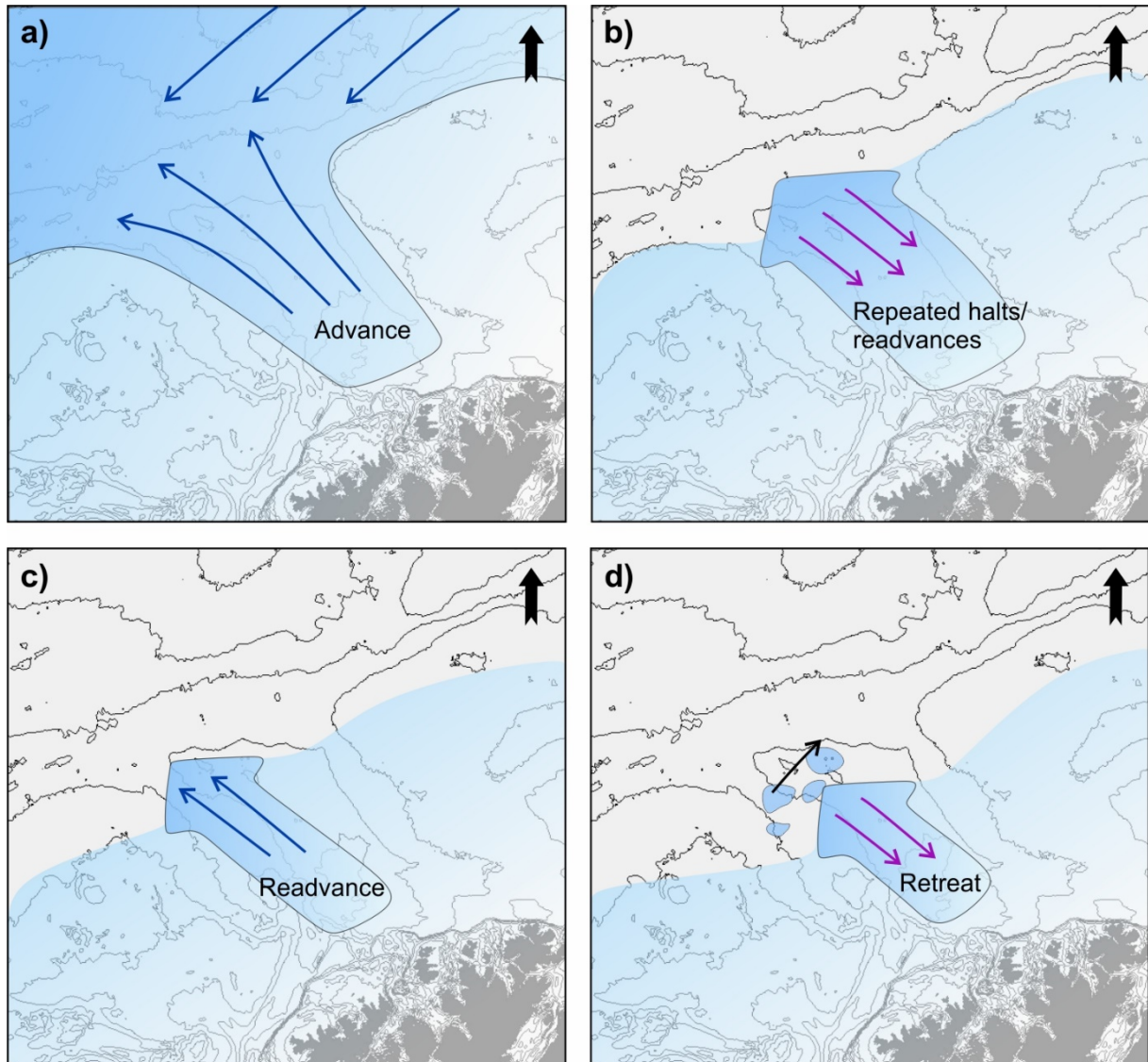
Figure 5.5 – *Reconstruction of the ice dynamics in the Ingøydjupet and Bjørnøyrenna Troughs during the development of the URU surface. Blue lines represent the ice-flow direction and the black arrow in figure d represent the uniform drifting of icebergs. Bathymetric contour map in the background where the contour intervals are 50 milliseconds.*

5.2.2 Deposition of unit A_1-A_2 and formation of the intra Quaternary1 surface

Unit A_1 and A_2 is only represented in a limited part of the study area (Figure 4.12) and comprises a relatively thin sediment distribution. This may be due to severe erosion by later glacier advances in the area, or because the units were only deposited in a limited area. The sediment thickness pattern shows that the relief of the underlying URU horizon generally controlled the deposition of unit A_1, while the relief of the base of unit A_2 have been of minor importance when the unit deposited. This may be because there were less erosion during subsequent advances in the southern part of the unit as it is located close to the Tromsøflaket, i.e. a shallower area, where the ice likely was more stagnant.

The glacigenic sediments were presumably transported to the area by an ice stream flowing through the Ingøydjupet Trough as the under- and overlying erosional surfaces shows indications of an ice-flow directed towards northwest. The glacigenic sediments of unit A_1 and A_2 are therefore interpreted to represent subglacial till. The top of unit A_2 also shows indications of an ice-flow directed towards southwest, suggesting that the Bjørnøyrenna Ice Stream also may have influenced the deposition of unit A_2. This indicates that the unit A_2 is preserved from a glacial maximum.

Correlation with studies done by Vorren et al. (1990) shows that unit A_1 correspond to their unit 1W, and unit A_2 to their unit 2W (Figure 5.2 & 5.6). Unit 1W and 2W can be identified on the continental slope (profile Y-Y' in Figure 5.1), implying that they were deposited during glacial maximums. Of their interpreted units on the slope, 1W and 2W shows the most pronounced progradation which they suggest indicate that the glacier margin had a position near the shelf break for longer periods. From investigations done in the outer Bjørnøyrenna by Sættem et al. (1992), their unit B may relate to unit A_1, and C to unit A_2 (Figure 5.2). Based on the results from borehole 7317/10-U-01, which is located slightly west from the study area of this thesis (Figure 5.1), their unit B and C comprises of till deposited by grounded ice during Middle Pleistocene (<440-330).
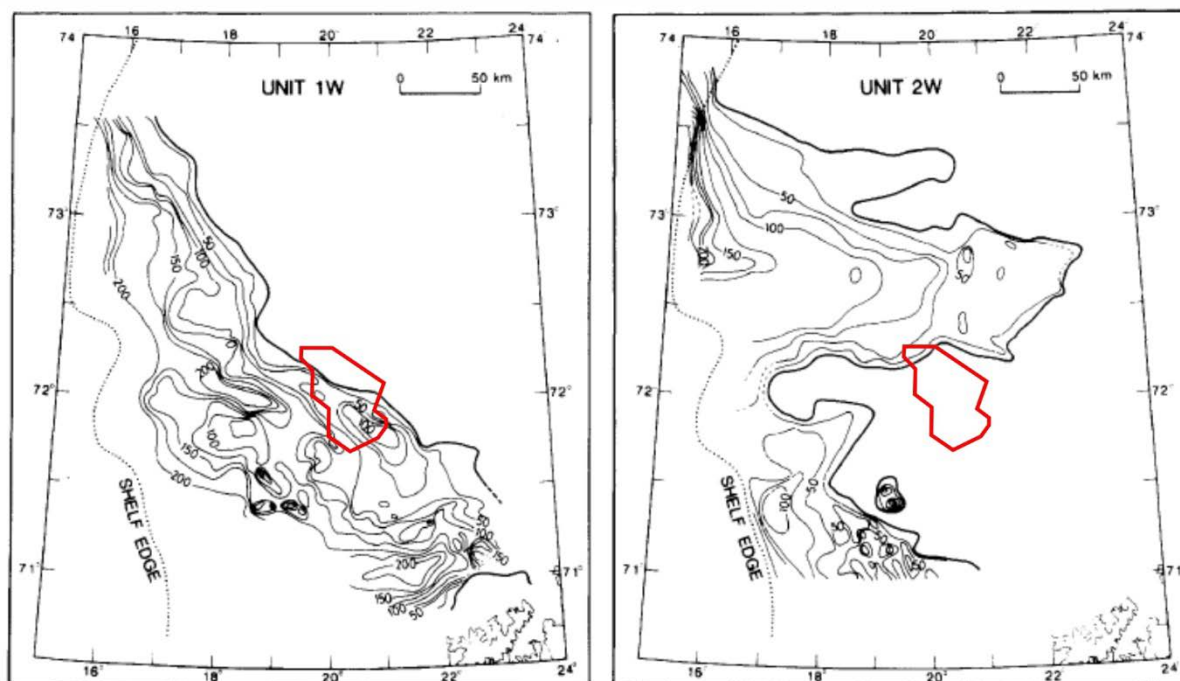
Figure 5.6 *– Isopach map of the units 1W and 2W from Vorren et al. (1990) with the position of the TopSeis-dataset used in this study (red polygon).*

Between the deposition of unit A_1 and A_2, a glacier advance probably formed the intra Q1 surface (Figure 5.7a). The well-developed MSGLs observed on this surface indicate that fast-flowing, warm-based ice was active at this time. The orientation of the MSGLs suggest a drainage pattern towards northwest, probably from the Scandinavian mainland and out the Ingøydjupet Trough (Figure 5.7a). Based on the observations of the intra Q1 surface, the glacial lineations most likely continue outside the study area, suggesting that the Ingøydjupet Ice Stream extended out in the Bjørnøyrenna, and likely coalesced with the Bjørnøyrenna Ice Stream during the development of this paleo-surface (Figure 5.7a).

Iceberg plough-marks have been identified on the intra Q1 surface, indicative of a glacimarine environment, where icebergs were drifting in Ingøydjupet (Figure 5.7b). The icebergs are likely to have originated from calving glaciers, meaning that the ice front must have reached sea level during this time. The plough-marks have a general orientation from SE to NW, which is the same direction as the indicated ice-flow. This may be due to alternating currents, driven by meltwater and katabatic winds transporting the calving icebergs away from the glacial front (Vorren et al., 1990) (Figure 5.7b). The iceberg plough-marks generally overprint the MSGLs on the surface, indicating that they were the last features to form.

The landform assemblage of the intra Q1 imply an overall rapid retreat of the Ingøydjupet Ice Stream where MSGLs are preserved (Figure 5.4), and that the ice margin reached the sea level causing the ice front to calve (Figure 5.7b).
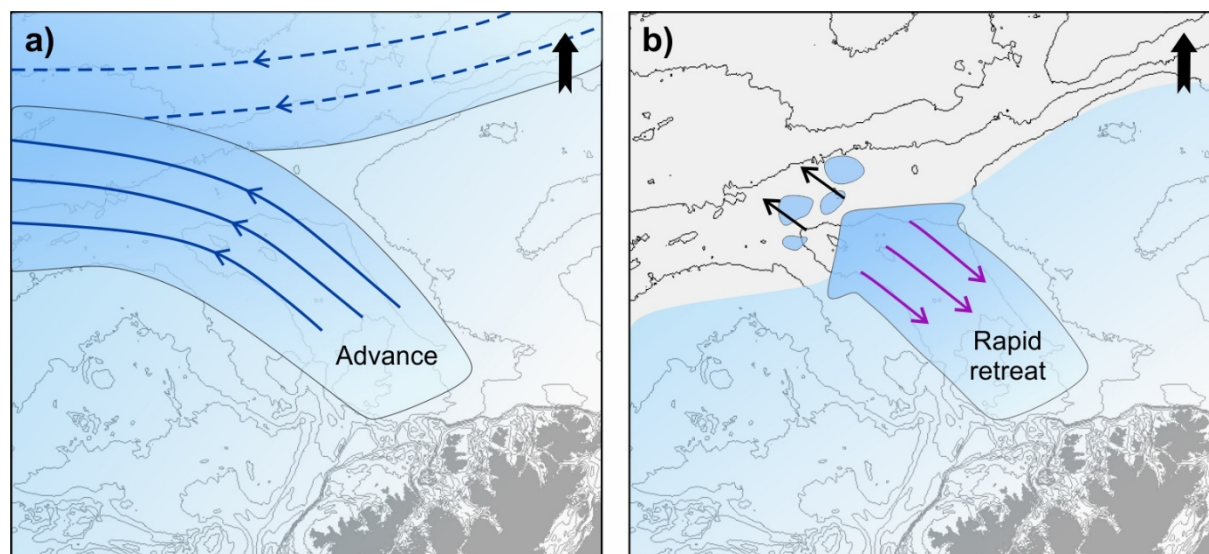

Figure 5.7 – Reconstruction of the ice dynamics in the Ingøydjupet and Bjørnøyrenna Troughs during the development of the intra Q1 surface. Blue lines represent the ice-flow direction, whereas the blue stippled lines represent assumed ice-flow directions, and the black arrows in figure b represent the general orientation of the drifting icebergs. Bathymetric contour map in the background where the contour intervals are 50 milliseconds.

5.2.3 Intra Quaternary2 and 3

Both the intra Q2 and intra Q3 surfaces show, unlike the older buried surfaces, evidence of two ice streams with different flow-directions operating in the area (Figure 5.3). On both the surfaces, the dominant flow-set has an NW-SE orientation, suggesting that the ice stream followed the Ingøydjupet Trough (Figure 5.8a). The NW-SE trending flow-set is the youngest on the intra Q2 surface, as these lineations seems to be cutting some of the perpendicular-oriented lineations. As such, this indicate that the oldest flow-set is a result of an ice stream operating from a northern ice dome, likely flowing through the Bjørnøyrenna Trough (Figure 5.8a). As the NW-SE oriented lineations are cutting the oldest flow-set, it is likely that the Ingøydjupet Ice Stream re-advanced following the formation of these lineations (Figure 5.8b).

It is difficult to determine the relative age of the different flow-sets on the intra Q3 surface, as none of the lineations superimposes others. Some of the dominating MSGLs on the intra Q3 surface tends to have a curvation towards north (Figure 4.30). This is suggested to be a result of a minor shift in the flow-pattern of the Ingøydjupet Ice Stream (Figure 5.8e). According to the correlation, intra Q3 corresponds to the bD surface from Rafaelsen et al. (2002). The

interpreted lineations on their bD surface are trending in an NNE-SSW and NE-SW direction, respectively (Figure 5.3), which Rafaelsen et al. (2002) suggest indicate a glacial advance where the paleo-ice flow was directed towards north. This supports the indications of the Ingøydjupet Ice Stream flowing in a more northern direction at the time intra Q3 was developed (Figure 5.8e).

According to Rafaelsen et al. (2002), the different orientations of the sets of lineations found on buried surfaces may reflect different ice-flow patterns. However, the lineations found in their study only had minor orientation differences, while the lineations found in this study have orientations more or less perpendicular to each other. Thus, they are interpreted to be a result of different ice streams, i.e. the Ingøydjupet and Bjørnøyrenna Ice Streams, which have been active at different times in the study area.

The retreat of the ice sheet is, based on the occurrence of MSGLs on the intra Q2 and Q3 surfaces, suggested to be rapid (Figure 5.8c & f). The MSGLs are also evident of a warm-based, grounded glacier. However, the semi-circular depressions on the intra Q3 surface suggests a shift of the basal conditions, where the glacier underwent periods of basal freezing resulting in plucking and removal of glacigenic sediments (Figure 5.8e).
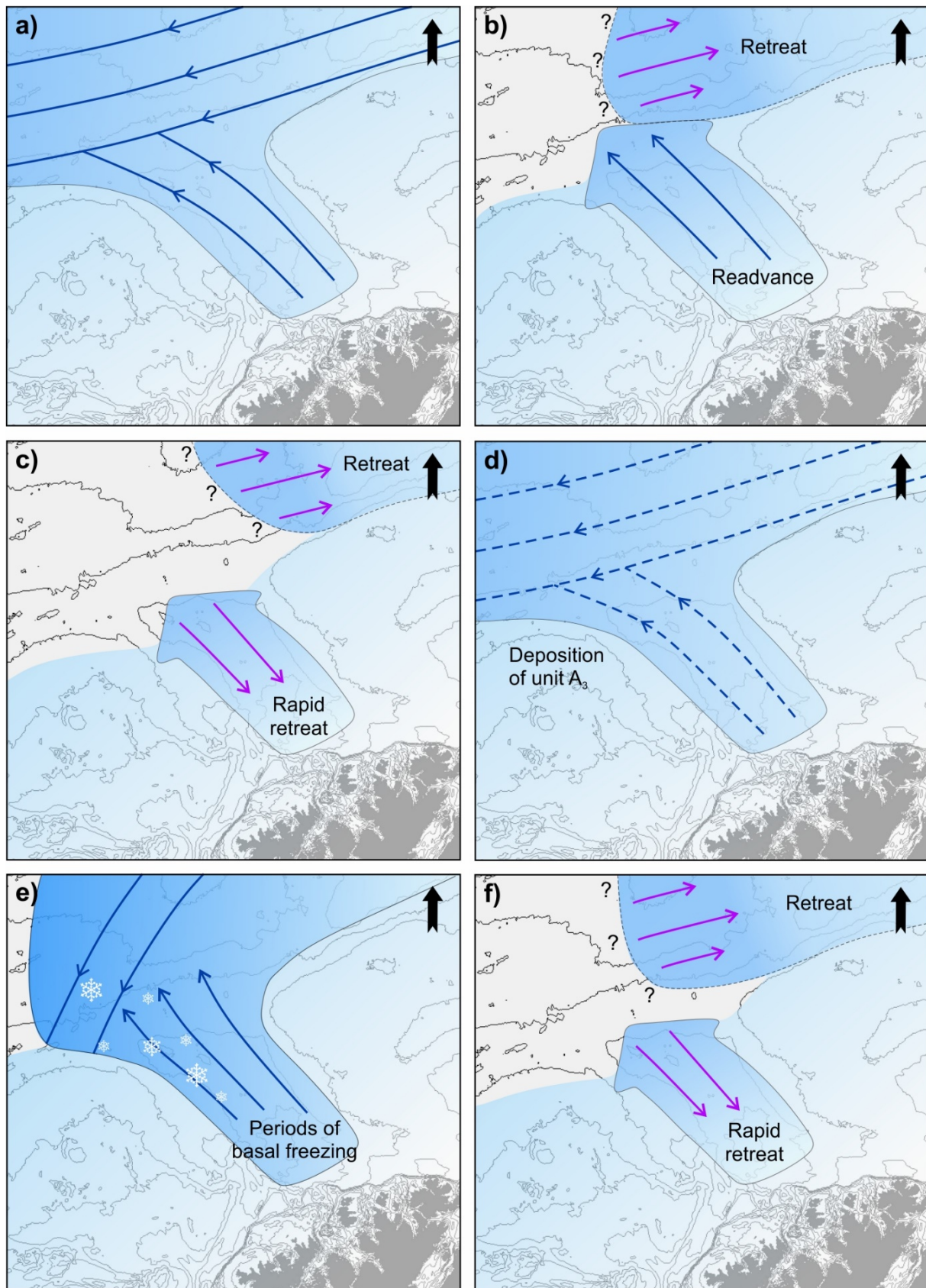
Figure 5.8 *– Reconstruction of the ice dynamics in the Ingøydjupet- and Bjørnøyrenna Troughs during the development of the intra Q2 and Q3 surfaces. Blue lines represent the ice-flow directions, whereas the blue stippled lines represent assumed ice-flow directions. Bathymetric contour map in the background where the contour intervals are 50 milliseconds.*

5.2.4 Deposition of unit A₃

Compared to the lowermost units, A$_1$ and A$_2$, unit A$_3$ is represented in a larger part of the study area (Figure 4.12) and consists of a relatively thicker succession. Most of the unit has a rather transparent acoustic signature, indicating that the unit mainly comprise of glacial till deposited by grounded ice. This is supported by the landforms identified at the top and base of the unit, i.e. paleo-trough, MSGLs and semi-circular depressions.

The occurrence of high amplitude reflections within seismic unit A$_3$ have been interpreted as sediment blocks of a different lithology compared to the surrounding sediments (Figure 4.27 & 4.28). The sediment blocks are interpreted to be transported and deposited subglacially by paleo-ice streams that have undergone periods of basal freezing. Basal freezing may cause pore-water extraction and consolidation of subglacial fine-grained sediments (Figure 5.9a-b). This process results in accretion of subglacial water and debris onto the ice base (Figure 5.9c), and the debris are transported within the ice and later re-deposited (Figure 5.9d). Buried sediment blocks have only been observed in the southern part of unit A$_3$, i.e. close to the Tromsøflaket, a shallower area where the ice was likely more stagnant. This suggests that the basal freezing may have been limited to the ice stream margin, i.e. in the transition-zone between the more stagnant ice on Tromsøflaket and the fast-flowing Ingøydjupet Ice Stream.

The observed amplitude anomalies have similar characteristics with megablocks and rafts described from several stratigraphic levels in the outer parts of Bjørnøyrenna (Andreassen et al., 2004, 2007). However, they are not as closely distributed as the ones found in their study, nor aligned in separate chains. Andreassen et al. (2004) hypothesize that paleo-ice streams draining through the Bjørnøyrenna Trough underwent periods of basal freezing near their margins, caused by fast downward advection of cold surface ice and that frozen sediment blocks were entrained by the glacier and transported along thrust planes to a higher position in the ice. Moreover, they interpreted that the internal structure of the sediment blocks suggested that shearing or thrusting was involved in the process. They explains that the freezing and dewatering process produces a contrast between the sediments close to the ice base and the sediments at depth, i.e. overconsolidated and less consolidated sediments, which may lead to thrust deformation at this transition. Their suggested explanation for the alignment of the sediment blocks and rafts in separate chains are that the block material was entrained from a

local source, i.e. point or line source, causing the material to be distributed in limited locations within the ice stream and subsequently deposited as single block trains.
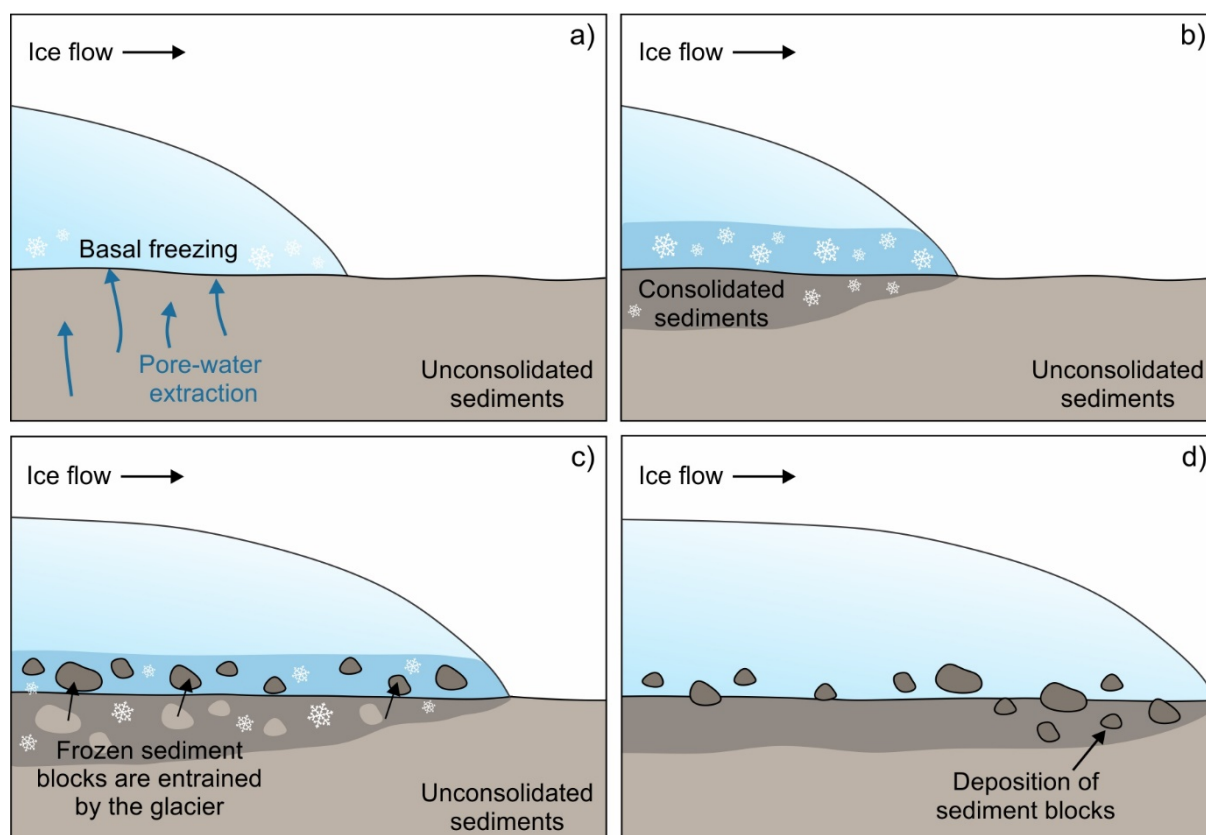
Figure 5.9 – *Schematic model for the process of basal freezing and transportation and deposition of sediment blocks. **a**) Basal freezing may cause pore-water extraction at the base of the glacier, **b**) the pore-water accretes onto the ice base as a layer of segregation ice, **c**) frozen sediment blocks (not to scale) are entrained by the glacier and transported within the ice before **d**) being re-deposited.*

The thickness and reflection configuration of unit A_3 is suggested to reflect a depositional environment linked to a glacial maximum in the Barents Sea. Unit A_3 correspond to unit D1 and D2 (Figure 5.2) by Sættem et al. (1992), whereas unit D1 and D2 consist of a thick succession in the outer shelf and comprise both glaciomarine and till deposits. Following the age estimates by Sættem et al. (1992), unit D1 and D2 were deposited between <330 and <130 ka. Thus, it is possible that unit A_3 was deposited during the Saalian glaciation. Little is known about variations during this glaciation, however, it is evident that the maximum Saalian glaciation was larger than any of the subsequent Weichselian glaciations, and that its age correlate with the younger part of oxygen isotope stage 6 which ended around 130 ka (Mangerud et al., 1996; Larsen et al., 2003).

5.2.5 Deposition of unit A_4 and A_5

Unit A_4 and A_5 are likely from the two last glaciations of the southwestern Barents Sea shelf. They are represented in a larger part of the study area compared to the other units of this study (Figure 4.12), and consist of a relatively thick sediment distribution. The generally transparent internal seismic signature, indicating till deposits, and the relatively thick sediment distribution of these units may reflect a depositional environment linked to maximum glaciations on the shelf. The base of unit A_4 shows indications of a dominant ice-flow towards northwest, while the top surface indicate a dominant ice-flow directed towards southwest (Figure 5.3). This suggests that the area was likely fed with ice masses and sediments from both the Ingøydjupet- and the Bjørnøyrenna Ice Streams. Unit A_5 show similar characteristic, although, the base indicate a dominating ice-flow towards southwest, while the top towards northwest (Figure 5.3).

Within unit A_4, the appearance of a local undulating horizon of higher amplitude reflections suggest that sediments of another characteristic than the surrounding sediments were deposited (Figure 4.34). Based on the morphology of the horizon and the local appearance within the unit, it may represent a buried moraine, however, it has not been mapped in detail and it is thus difficult to determine the origin of the feature. Sættem et al. (1992) interpreted an undulating, chaotic subunit within their unit G as buried glaciotectonic cupola-hills with possible occurrence of local, isolated glaciotectonic rafts. Considering this, the possibility of the undulating horizons observed within unit A_4 also representing glaciotectonic sediments cannot be excluded. Sættem et al. (1992) emphasize that the cupola-hills strongly suggests that the basal part of unit G was deposited in contact with grounded ice.

Unit A_4 and A_5 can be correlated with unit 4W from the study by Vorren et al. (1990) (Figure 5.2 & 5.10). 4W is their youngest seismic unit and its seismic signature is characterized by several discontinuous reflectors. Samples recovered from this unit consist of overconsolidated diamictons. They suggest that much of the glacigenic sediments deposited on the outer shelf was originally of glaciomarine origin, and that frequent glacial advances have compacted and disturbed these sediments and probably also deposited basal till in some areas. However, Sættem et al. (1992) interpreted that the diamictons are mostly tills and that they are associated with acoustically chaotic or transparent seismic units. Their youngest seismic units, F and G, comprise of massive muddy diamictons, which they therefore interpreted to represent tills mainly deposited subglacially during late Middle/Late Weichselian. This supports the

interpretation of unit A_4 and A_5 to be linked to the last maximum glaciations on the Barents Sea continental shelf.
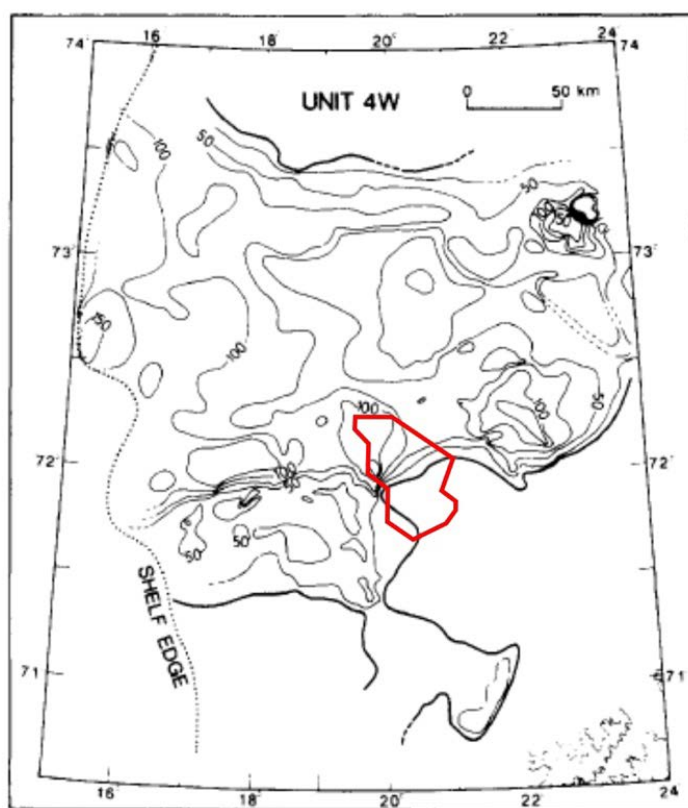
Figure 5.10 – Isopach map of the unit 4W from Vorren et al. (1990) with the position of the TopSeis-dataset used in this study (red polygon).

5.2.6 Intra Quaternary4 and the seafloor

The intra Q4 surface separates the A_4 and A_5 units and probably represent an unconformity formed during a glacial advance. The NE-SW oriented MSGLs that dominate the surface indicate that the general drainage pattern of the fast-flowing ice streams have changed direction from the underlying surfaces. Thus, it is likely that the Bjørnøyrenna Ice Stream dominated in this area during intra Q4 times (Figure 5.11a). However, the interpreted drumlins found in the eastern part of the surface have an orientation perpendicular to the implied ice-flow direction from these MSGLs, suggesting that the Ingøydjupet Ice Stream was still active at this time, but in a limited area within the Ingøydjupet Trough (Figure 5.11a).

Horizon bE in Rafaelsen et al. (2002) likely corresponds to intra Q4. Their results shows that horizon bE have lineations trending in more or less the same direction as the dominant flow-direction on the intra Q4 surface (Figure 5.3), which implies that the Bjørnøyrenna Ice Stream

dominated at that time. However, Rafaelsen et al. (2002) interpreted the ice-flow to have derived from a southern source, i.e. the Ingøydjupet Trough, and that the Bjørnøyrenna may have acted as a calving bay during a glacial retreat. The findings in this study suggest that the lineations are a result of the ice-flow draining through the Bjørnøyrenna Trough, and that the overall retreat was rapid as the landform assemblage represent indications of fast-flowing ice (Figure 5.11b). The iceberg plough-marks observed on the surface truncates the MSGLs, suggesting that they are the youngest features. They implies an overall retreat of the ice-stream margin, resulting in a glaciomarine environment where icebergs were scouring the paleo-seafloor (Figure 5.11b). Iceberg plough-marks were also found on the correlated surface bE in 3D-survey SG9810 (Figure 5.1) from Rafaelsen et al.'s (2002) study, which may suggest that the plough-marks are a result of the same retreat-event.

Most of the geomorphological features on the seafloor represent the last glaciation, i.e. the Weichselian, on the southwestern Barents Sea shelf. There are no MSGLs observed on the seafloor in the study area, however, the direction of the Ingøydjupet Trough indicates an ice flow direction towards northwest. Additionally, several studies done in the same area have observed and interpreted NW-SE oriented MSGLs in the Ingøydjupet (e.g. Andreassen et al., 2008; Winsborrow et al., 2010). During the Late Weichselian maximum, the Barents Sea- and Scandinavian- ice sheets were confluent, and the entire Barents Sea continental shelf was glaciated.

In the study area, two types of moraines have been identified on the seafloor; larger recessional moraines and smaller De Geer-type moraines. The larger recessional moraines in the north central part of Ingøydjupet seems to continue underneath the outer Bjørnøyrenna sediment wedge (OBSW), suggesting that the moraines were deposited prior to this. As the moraines are preserved on the seafloor, they are likely linked to the deglaciation of the Ingøydjupet Trough. Ice contact landforms formed at the margin of the retreating ice sheets provide information about the retreat rate and dynamics during the deglaciation. The landform assemblage within the Ingøydjupet Trough indicates a complex deglaciation, including slow retreat as well as rapid retreat of a grounded ice margin (Figure 5.4). In the northern part of the Ingøydjupet Trough, the closely spaced recessional moraines indicate a slow retreat of grounded ice towards southeast, which formed the moraines during minor stillstands and/or small re-advances during the retreat phase (Figure 5.11d). The smaller width of the De Geer-type moraines indicate that the stillstands and/or re-advances were shorter.

According to Rüther et al. (2011), the OBSW was deposited during a rapid re-advance of the Bjørnøyrenna Ice Stream. Cores taken downstream of the sediment wedge are dated to be around 17.1 and 16.6 ka. These dates are suggested to represent an age for the OBSW deposition and a minimum deglaciation age for the outer Bjørnøyrenna. This suggests that the recessional moraines in the Ingøydjupet were deposited before 17.1 ka. Rüther et al. (2011) also suggests that the OBSW was deposited as one body of sediment. However, the findings in this study indicate that the Bjørnøyrenna Ice Stream underwent at least one glacial advance resulting in the formation of the intra Q4 surface (Figure 5.11a-b).

The deglaciation of the central parts of Ingøydjupet is suggested to have been more rapid (Figure 5.11e), as recessional moraines or grounding zone wedges are absent, and several MSGLs have been identified within the central parts of the Ingøydjupet Trough (e.g. Andreassen et al., 2008, Winsborrow et al., 2010). Studies of benthic foraminiferal assemblage indicates that the northern most parts of Ingøydjupet had been deglaciated in 18.7 ka (Junttila et al., 2010). During the rapid retreat, episodes of meltwater erosion probably occurred, resulting in the oblong depressions appearing in the southern part of the Ingøydjupet Trough (Figure 4.40).

The shallower areas surrounding Ingøydjupet, i.e. the OBSW, Tromsøflaket and Nordkappbanken, are clearly affected by iceberg plough-marks. As they truncates other geomorphological features on the seafloor, it is evident that they were the last features to form. The calving of icebergs are likely caused by the retreat of the ice margin during the deglaciation (Figure 5.11e-f). According to Siegert & Dowdeswell (2002), there were two periods of pronounced iceberg ploughing during the deglaciation, one 16 ka which correlates with the minimum deglaciation age of the outer Bjørnøyrenna (Figure 5.11e), and a smaller one around 13.5 ka (Figure 5.11f).
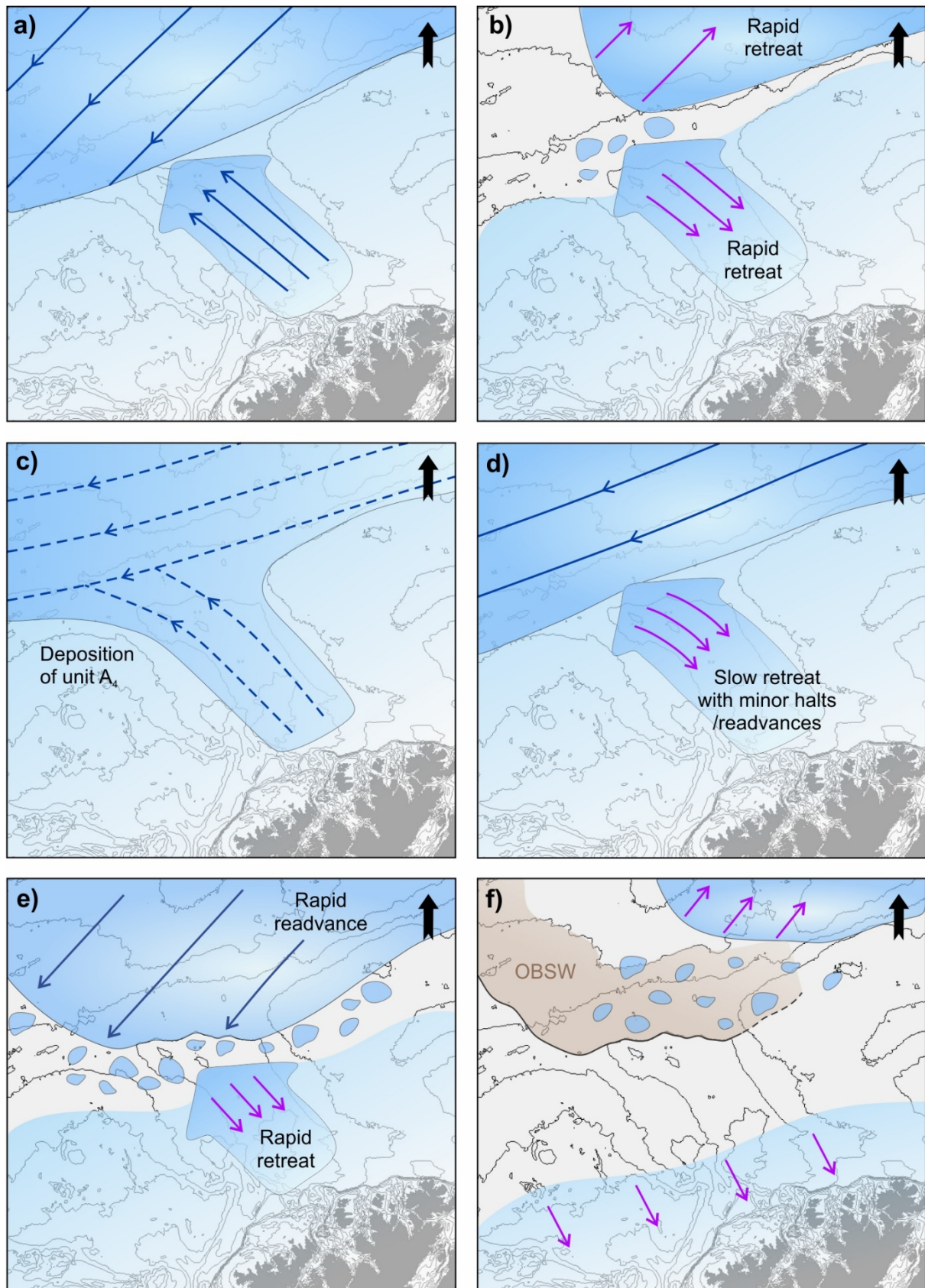
Figure 5.11 – *Reconstruction of the ice dynamics in the Ingøydjupet and Bjørnøyrenna Troughs during the development of the intra Q4 and the present-day seafloor. Blue lines represent the ice-flow direction. Bathymetric contour map in the background where the contour intervals are 50 milliseconds.*

6 Conclusions

The late Quaternary evolution in the outer Ingøydjupet area have been studied using both high-resolution and merged 3D-seismic data. The focus has been on the stratigraphy between the URU and the seafloor. The main findings of this study can be summarized in the following points:

- The glacigenic succession in the study area has been divided into five seismic units (A_1-A_5) separated by six glacial unconformities (URU, intra Q1-Q4 and the seafloor). The units are interpreted to mainly comprise glacial till deposited by grounded ice. This is based on the transparent acoustic signature of the seismic units, and the presence of MSGLs identified at the top and base of the units, i.e. landforms which are evident of grounded and fast-flowing ice.

- The seismic stratigraphic framework has been correlated with previous studies of the glacigenic succession in the surrounding area on the southwestern Barents Sea continental shelf. The correlation suggests that the units A_1-A_3 are deposited during middle Pleistocene, where the thicker A_3 unit are suggested to represent sediments from the Saalian glaciation (200-130 ka), and A_4-A_5 during Upper Pleistocene, i.e. late Middle-Late Weichselian.

- The geomorphology of the buried paleo-shelf surfaces and the seafloor, together with the glacigenic units, show several episodes of extensive glacial erosion and deposition. MSGLs and buried troughs show that fast-flowing ice streams occupied the outer Ingøydjupet at least five times since the development of the URU. The geomorphology on some of the buried paleo-surfaces (intra Q2-Q4) suggest an ice-flow directed into the outer Ingøydjupet Trough sourced from the Bjørnøyrenna Trough in the north.

- Within unit A_3, local amplitude anomalies have been identified. They are interpreted to represent sediment blocks that are formed from basal freezing, entrainment and transportation by the paleo-ice streams. This indicates that the ice sheet not only had phases of advance and retreat of fast-flowing ice streams, but also periods of basal freezing and forward movement resulting in re-deposition of the sediment blocks.

117

- The geomorphology of the buried paleo-surfaces and the seafloor indicate differences in the deglaciation dynamics following full-glacial conditions. The landform assemblage on the oldest paleo-surface (URU) and the seafloor, i.e. recessional moraines, suggest that the ice sheet underwent repeated halts and/or re-advances during overall retreat, whereas the intra Q1-Q4 surfaces shows a rather rapid retreat, where MSGLs were preserved on the paleo-surfaces.

7 Research outlook

The results of this study have increased the knowledge regarding the paleo-ice sheet dynamics and the deposition environment in the outer Ingøydjupet area during the late Quaternary. Further research in the area should focus on expanding this knowledge. Some recommendations for further work are therefore:

- Core sampling and dating of the southern part of the outer Bjørnøyrenna sediment wedge (as previous work has been focusing on the frontal and upstream part of the wedge), and the recessional moraines observed in the outer Ingøydjupet area, as they seems to continue underneath this sediment wedge. This could improve our understanding on the deglaciation of the Ingøydjupet Trough.

- Extend the seismic stratigraphic framework in the surrounding area by using the 3D-merge to get a better understanding of the lateral extent of the glacigenic units in this area, and to further investigate the interplay between the ice streams that were active in the Bjørnøyrenna and Ingøydjupet Troughs.

- Further investigation of local amplitude anomalies within the glacigenic sediments to study the interaction between ice streaming and glacitectonics during the glaciations.

- Regional study of ice dome switching in the Barents Sea. The results of this study shows indications of ice-flows directed into the outer Ingøydjupet Trough sourced from the Bjørnøyrenna Trough in the north. This implies that the source area may have, through ice divide migration, affected the ice-flow directions of the outer Bjørnøyrenna Ice Stream.

8 References

Ahlborn, M., & Stemmerik, L. (2015). Depositional evolution of the Upper Carboniferous–Lower Permian Wordiekammen carbonate platform, Nordfjorden High, central Spitsbergen, Arctic Norway. *Norwegian Journal of Geology, 95*, 91-126.

Andreassen, K., Bjarnadóttir, L. R., Rüther, D. C., & Winsborrow, M. C. M. (2016). Retreat patterns and dynamics of the former Bear Island Trough Ice Stream. *Geological Society, London, Memoirs, 46*(1), 445-452.

Andreassen, K., Laberg, J. S., & Vorren, T. O. (2008). Seafloor geomorphology of the SW Barents Sea and its glaci-dynamic implications. *Geomorphology, 97*(1-2), 157-177.

Andreassen, K., Nilssen, L. C., Rafaelsen, B., & Kuilman, L. (2004). Three-dimensional seismic data from the Barents Sea margin reveal evidence of past ice streams and their dynamics. *Geology, 32*(8), 729-732.

Andreassen, K., Ødegaard, C. M., & Rafaelsen, B. (2007). Imprints of former ice streams, imaged and interpreted using industry three-dimensional seismic data from the south-western Barents Sea. *277*(1), 151-169.

Badley, M. E. (1985). *Practical seismic interpretation*. Boston: International Human Resources Development Corporation.

Bellec, V., Wilson, M., Bøe, R., Rise, L., Thorsnes, T., Buhl-Mortensen, L., & Buhl-Mortensen, P. (2008). Bottom currents interpreted from iceberg ploughmarks revealed by multibeam data at Tromsøflaket, Barents Sea. *Marine Geology, 249*(3-4), 257-270.

Bellwald, B., Planke, S., Piasecka, E. D., Matar, M. A., & Andreassen, K. (2018). Ice-stream dynamics of the SW Barents Sea revealed by high-resolution 3D seismic imaging of glacial deposits in the Hoop area. *Marine Geology, 402*, 165-183.

Bennett, M. R. (2003). Ice streams as the arteries of an ice sheet: their mechanics, stability and significance. *Earth-Science Reviews, 61*(3-4), 309-339.

Brown, A. R. (1999). *Interpretation of three-dimensional seismic data* (5th ed.). Tusla, Oklahoma, U.S.A: The American Association of Petroleum Geologists and the Society of Exploration Geophysicists.

Bulat, J. (2005). Some considerations on the interpretation of seabed images based on commercial 3D seismic in the Faroe-Shetland Channel. *Basin Research, 17*(1), 21-42.

Butt, F. A., Elverhøi, A., Solheim, A., & Forsberg, C. F. (2000). Deciphering Late Cenozoic development of the western Svalbard Margin from ODP Site 986 results. *Marine Geology, 169*(3-4), 373-390.

Catuneanu, O., Abreu, V., Bhattacharya, J., Blum, M., Dalrymple, R., Eriksson, P., Fielding, C. R., Fisher, W., Galloway, W., & Gibling, M. J. (2009). Towards the standardization of sequence stratigraphy. *Earth-Science Reviews, 92*(1), 1-33.

Dowdeswell, J. A., & Hogan, K. A. (2016). Huge iceberg ploughmarks and associated corrugation ridges on the northern Svalbard shelf. *Geological Society, London, Memoirs, 46*(1), 269-270.

Dowdeswell, J. A., Ottesen, D., Evans, J., Cofaigh, C. O., & Anderson, J. B. (2008). Submarine glacial landforms and rates of ice-stream collapse. *Geology, 36*(10), 819-822.

Elverhøi, A., & Solheim, A. (1983). The Barents Sea ice sheet-a sedimentological discussion. *Polar Research, 1*(1), 23-42.

Faleide, J. I., Bjørlykke, K., & Gabrielsen, R. H. (2015). Geology of the Norwegian Continental Shelf. In K. Bjørlykke (Ed.), *Petroleum Geoscience: From Sedimentary Environments to Rock Physics* (pp. 603-637). Berlin, Heidelberg: Springer Berlin Heidelberg.

Faleide, J. I., Gudlaugsson, S. T., & Jacquart, G. (1984). Evolution of the western Barents Sea. *Marine Petroleum Geology, 1*(2), 123-150.

Faleide, J. I., Solheim, A., Fiedler, A., Hjelstuen, B. O., Andersen, E. S., & Vanneste, K. (1996). Late Cenozoic evolution of the western Barents Sea-Svalbard continental margin. *Global Planetary Change, 12*(1-4), 53-74.

Faleide, J. I., Tsikalas, F., Breivik, A. J., Mjelde, R., Ritzmann, O., Engen, O., Wilson, J., & Eldholm, O. (2008). Structure and evolution of the continental margin off Norway and the Barents Sea. *Episodes, 31*(1), 82-91.

Faleide, J. I., Vågnes, E., & Gudlaugsson, S. T. (1993). Late Mesozoic-Cenozoic evolution of the south-western Barents Sea in a regional rift-shear tectonic setting. *Marine Petroleum Geology, 10*(3), 186-214.

Fiedler, A., & Faleide, J. I. (1996). Cenozoic sedimentation along the southwestern Barents Sea margin in relation to uplift and erosion of the shelf. *Global and Planetary Change, 12*(1-4), 75-93.

Firth, J., & Vinje, V. (2018). On Top of the Spread: Explore the challenges of imaging the shallow reservoirs of the Barents Sea. *Oilfield Technology*.

Fuchs, M., & Owen, L. A. (2008). Luminescence dating of glacial and associated sediments: review, recommendations and future directions. *Boreas, 37*(4), 636-659.

Halland, E. K., Bjørnestad, A., Magnus, C., Riis, F., Meling, I. M., Gjeldvik, I. T., Tappel, I. M., Mujezinovic, J., Bjørheim, M., & Rød, R. S. (2014). *CO2 Storage Atlas Barents Sea*. Retrieved from http://www.npd.no/global/norsk/2-tema/lagring-og-bruk-av-co2/co2-atlas-barents-sea.pdf

Helmke, J. P., Bauch, H. A., & Erlenkeuser, H. (2003). Development of glacial and interglacial conditions in the Nordic seas between 1.5 and 0.35 Ma. *Quaternary Science Reviews, 22*(15-17), 1717-1728.

Henriksen, S., & Vorren, T. O. (1996). Late Cenozoic sedimentation and uplift history on the mid-Norwegian continental shelf. *Global and Planetary Change, 12*(1-4), 171-199.

Hughes, A. L., Gyllencreutz, R., Lohne, Ø. S., Mangerud, J., & Svendsen, J. I. (2016). The last Eurasian ice sheets–a chronological database and time-slice reconstruction, DATED-1. *Boreas, 45*(1), 1-45.

Jakobsson, M., Mayer, L., Coakley, B., Dowdeswell, J. A., Forbes, S., Fridman, B., Hodnesdal, H., Noormets, R., Pedersen, R., Rebesco, M., Schenke, H. W., Zarayskaya, Y., Accettella, D., Armstrong, A., Anderson, R. M., Bienhoff, P., Camerlenghi, A., Church, I., Edwards, M., Gardner, J. V., Hall, J. K., Hell, B., Hestvik, O., Kristoffersen, Y., Marcussen, C., Mohammad, R., Mosher, D., Nghiem, S. V., Pedrosa, M. T., Travaglini, P. G., & Weatherhall, P. (2012). The international bathymetric chart of the Arctic Ocean (IBCAO) version 3.0. *Geophysical Research Letters, 39*(12).

Junttila, J., Aagaard-Sørensen, S., Husum, K., & Hald, M. (2010). Late Glacial–Holocene clay minerals elucidating glacial history in the SW Barents Sea. *Marine Geology, 276*(1-4), 71-85.

Kearey, P., Brooks, M., & Hill, I. (2002). *An introduction to geophysical exploration* (Third Edition ed.): Blackwell Science Ltd.

Knies, J., Matthiessen, J., Vogt, C., Laberg, J. S., Hjelstuen, B. O., Smelror, M., Larsen, E., Andreassen, K., Eidvin, T., & Vorren, T. O. (2009). The Plio-Pleistocene glaciation of the Barents Sea–Svalbard region: a new model based on revised chronostratigraphy. *Quaternary Science Reviews, 28*(9), 812-829.

Laberg, J. S., Andreassen, K., Knies, J., Vorren, T. O., & Winsborrow, M. C. M. (2010). Late Pliocene–Pleistocene development of the Barents Sea ice sheet. *Geological Society of America, 38*(2), 107-110.

Laberg, J. S., Andreassen, K., & Vorren, T. O. (2012). Late Cenozoic erosion of the high-latitude southwestern Barents Sea shelf revisited. *Geological Society of America Bulletin, 124*(1-2), 77-88.

Larsen, E., Andreassen, K., Nilssen, L., & Raundalen, S. (2003). The prospectivity of the Barents Sea: ice ages, erosion and tilting of traps. *NGU Report, 102*.

Larsen, E., Kjær, K. H., Demidov, I. N., Funder, S., Grøsfjeld, K., Houmark-Nielsen, M., Jensen, M., Linge, H., & Lysa, A. (2006). Late Pleistocene glacial and lake history of northwestern Russia. *Boreas, 35*(3), 394-424.

Lundin. (2016). Ny seismikkteknologi klar for Barentshavet. Retrieved from https://www.lundin-norway.no/2016/08/29/ny-seismikkteknologi-klar-for-barentshavet/?fbclid=IwAR1wu4vu7oxtxsclznws39qm85B-MJLHAB3n49ubd3JRfoGgEK84ybLHAuU

Mangerud, J., Dokken, T., Hebbeln, D., Heggen, B., Ingolfsson, O., Landvik, J. Y., Mejdahl, V., Svendsen, J. I., & Vorren, T. O. (1998). Fluctuations of the Svalbard–Barents Sea Ice Sheet during the last 150 000 years. *Quaternary Science Reviews, 17*(1-3), 11-42.

Mangerud, J., Gyllencreutz, R., Lohne, Ø., & Svendsen, J. I. (2011). Glacial history of Norway. In *Developments in Quaternary Sciences* (Vol. 15, pp. 279-298): Elsevier.

Mangerud, J., Jansen, E., & Landvik, J. Y. (1996). Late Cenozoic history of the Scandinavian and Barents Sea ice sheets. *Global and Planetary Change, 12*(1-4), 11-26.

Marfurt, K. J., Scheet, R. M., Sharp, J. A., & Harper, M. G. (1998). Suppression of the acquisition footprint for seismic sequence attribute mapping. *Geophysics, 63*(3), 1024-1035.

Martinsen, O., & Nøttvedt, A. (2013). Av hav stiger landet. In *Landet blir til* (pp. 440-477). Trondheim: Norwegian Geological Society.

Mitchum, R. M., Vail, P. R., & Sangree, J. B. (1977). Seismic Stratigraphy and Global Changes of Sea Level, Part 6: Stratigraphic Interpretation of Seismic Reflection Patterns in Depositional Sequences. In C. E. Payton (Ed.), *Seismic Stratigraphy--Applications to Hydrocarbon Exploration* (Vol. 26, pp. 117-133). Tulsa, Oklahoma, U.S.A.: The American Association of Petroleum Geologists.

Newton, A. M., & Huuse, M. (2017). Glacial geomorphology of the central Barents Sea: Implications for the dynamic deglaciation of the Barents Sea Ice Sheet. *Marine Geology, 387*, 114-131.

NPD-FactMaps. (2019a). Retrieved from: http://gis.npd.no/factmaps/html_21/.

NPD-Factpages. (2019b). Retrieved from: http://factpages.npd.no/factpages/.

Nyland, B., Jensen, L. N., Skagen, J. L., Skarpnes, O., & Vorren, T. (1992). Tertiary uplift and erosion in the Barents Sea: magnitude, timing and consequences. In *Structural and tectonic modelling and its application to petroleum geology* (pp. 153-162): Elsevier.

Ottesen, D., Dowdeswell, J. A., & Rise, L. (2005). Submarine landforms and the reconstruction of fast-flowing ice streams within a large Quaternary ice sheet: The 2500-km-long Norwegian-Svalbard margin (57–80 N). *Geological Society of America Bulletin, 117*(7-8), 1033-1050.

Rafaelsen, B., Andreassen, K., Kuilman, L. W., Lebesbye, E., Hogstad, K., & Midtbø, M. (2002). Geomorphology of buried glacigenic horizons in the Barents Sea from three-dimensional seismic data. *Geological Society, London, Special Publications, 203*(1), 259-276.

Rydningen, T. A., Vorren, T. O., Laberg, J. S., & Kolstad, V. (2013). The marine-based NW Fennoscandian ice sheet: glacial and deglacial dynamics as reconstructed from submarine landforms. *Quaternary Science Reviews, 68*, 126-141.

Rüther, D. C., Mattingsdal, R., Andreassen, K., Forwick, M., & Husum, K. (2011). Seismic architecture and sedimentology of a major grounding zone system deposited by the Bjørnøyrenna Ice Stream during Late Weichselian deglaciation. *Quaternary Science Reviews, 30*(19-20), 2776-2792.

Sheriff, R. E. (1985). Aspects of Seismic Resolution: Chapter 1. In O. R. Berg & D. G. Woolverton (Eds.), *Seismic Stratigraphy II: An Integrated Approach to Hydrocarbon Exploration* (pp. 1-10): American Association of Petroleum Geologists.

Sheriff, R. E. (2002). *Encyclopedic Dictionary of Applied Geophysics* (4th ed.). Tulsa: Society of Exploration Geophysicists.

Siegert, M. J. (2001). *Ice sheets and late Quaternary environmental change*: John Wiley & Sons Inc.

Ślubowska-Woldengen, M., Koç, N., Rasmussen, T. L., Klitgaard-Kristensen, D., Hald, M., & Jennings, A. E. (2008). Time-slice reconstructions of ocean circulation changes on the continental shelf in the Nordic and Barents Seas during the last 16,000 cal yr BP. *Quaternary Science Reviews, 27*(15-16), 1476-1492.

Smelror, M., Petrov, O. V., Larssen, G. B., & Werner, S. C. (2009). *Geological history of the Barents Sea*. Trondheim: Geological Survey of Norway.

Steinsund, P. I., & Hald, M. (1994). Recent calcium carbonate dissolution in the Barents Sea: Paleoceanographic applications. *Marine Geology, 117*(1-4), 303-316.

Stokes, C. R., & Clark, C. D. (2001). Palaeo-ice streams. *Quaternary Science Reviews, 20*(13), 1437-1457.

Svendsen, J. I., Alexanderson, H., Astakhov, V. I., Demidov, I., Dowdeswell, J. A., Funder, S., Gataullin, V., Henriksen, M., Hjort, C., & Houmark-Nielsen, M. (2004). Late Quaternary ice sheet history of northern Eurasia. *Quaternary Science Reviews, 23*(11-13), 1229-1271.

Sættem, J., Poole, D. A. R., Ellingsen, L., & Sejrup, H. P. (1992). Glacial geology of outer Bjørnøyrenna, southwestern Barents Sea. *Marine Geology, 103*(1-3), 15-51.

Thiede, J., Winkler, A., Wolf-Welling, T., Eldholm, O., Myhre, A. M., Baumann, K.-H., Henrich, R., & Stein, R. (1998). Late Cenozoic history of the polar North Atlantic: results from ocean drilling. *Quaternary Science Reviews, 17*(1-3), 185-208.

Vail, P. R. (1987). Seismic stratigraphy interpretation using sequence stratigraphy: Part 1: Seismic stratigraphy interpretation procedure. *Atlas of Seismic Stratigraphy: AAPG Studies in Geology, 1*, 1-10.

Veeken, P. C. (2007). Seismic Stratigraphy, Basin Analysis and Reservoir Characterisation. In K. Helbig & S. Treitel (Eds.), *Handbook of Geophysical Exploration* (Vol. 37, pp. 509): Elsevier.

Vinje, V., Lie, J. E., Danielsen, V., Dhelle, P. E., Silliqi, R., Nilsen, C.-I., Hicks, E., & Camerer, A. J. F. B. (2017). Shooting over the seismic spread. *First Break, 35*(6), 97-104.

Vorren, T. O., Hald, M., & Lebesbye, E. (1988). Late Cenozoic environments in the Barents Sea. *Paleoceanography, 3*(5), 601-612.

Vorren, T. O., & Laberg, J. S. (1996). Late glacial air temperature, oceanographic and ice sheet interactions in the southern Barents Sea region. *Geological Society, London, Special Publications, 111*(1), 303-321.

Vorren, T. O., Lebesbye, E., & Larsen, K. B. (1990). Geometry and genesis of the glacigenic sediments in the southern Barents Sea. *Geological Society, London, Special Publications, 53*(1), 269-288.

Vorren, T. O., Richardsen, G., Knutsen, S.-M., & Henriksen, E. (1991). Cenozoic erosion and sedimentation in the western Barents Sea. *Marine Petroleum Geology, 8*(3), 317-340.

Winsborrow, M. C. M., Andreassen, K., Corner, G. D., & Laberg, J. S. (2010). Deglaciation of a marine-based ice sheet: Late Weichselian palaeo-ice dynamics and retreat in the southern Barents Sea reconstructed from onshore and offshore glacial geomorphology. *Quaternary Science Reviews, 29*(3-4), 424-442.

Winsborrow, M. C. M., Stokes, C. R., & Andreassen, K. (2012). Ice-stream flow switching during deglaciation of the southwestern Barents Sea. *Geological Society of America Bulletin, 124*(3-4), 275-290.

Worsley, D. (2008). The post-Caledonian development of Svalbard and the western Barents Sea. *Polar Research, 27*(3), 298-317.